Pontifícia Universidade Católica
do Rio de Janeiro

Alessandra Lidia Mazon

Numerical modelling of evaporites as a natural barrier for the abandonment of oil wells

Dissertação de Mestrado

Dissertation presented to the Programa de Pós-graduação em Engenharia Civil of PUC-Rio in partial fulfillment of the requirements for degree of Mestre em Engenharia Civil.

Advisor: Prof. Sérgio Augusto Barreto da Fontoura

Rio de Janeiro
April 2022

PONTIFÍCIA UNIVERSIDADE CATÓLICA
DO RIO DE JANEIRO

Alessandra Lidia Mazon

Numerical modelling of evaporites as a natural barrier for the abandonment of oil wells

Dissertation presented to the Programa de Pós-graduação em Engenharia Civil of PUC-Rio in partial fulfillment of the requirements for degree of Mestre em Engenharia Civil. Approved by the Examination Committee.

Prof. Sérgio Augusto Barreto da Fontoura
Advisor
Departamento de Engenharia Civil e Ambiental – PUC-Rio

Prof. Celso Romanel
Departamento de Engenharia Civil e Ambiental – PUC-Rio

Prof. Aldo Durand Farfán
UENF

Rio de Janeiro, April 28th, 2022

Alessandra Lidia Mazon

The author graduated in Civil Engineer at the Universidade Estadual de Ponta Grossa in 2017. She entered the master's degree in Geotechnics at the Pontifícia Universidade Católica do Rio de Janeiro in 2019, working in the research line of Petroleum Geomechanics.

Bibliographic data

Mazon, Alessandra Lidia

Numerical modelling of evaporites as a natural barrier for the abandonment of oil wells / Alessandra Lidia Mazon; advisor: Sergio Augusto Barreto da Fontoura. – Rio de Janeiro: PUC-Rio, Departamento de Engenharia Civil, 2022.

98 f.: il. ; 29,7 cm

1. Dissertação (mestrado) – Pontifícia Universidade Católica do Rio de Janeiro, Departamento de Engenharia Civil.

Inclui bibliografia

1. Engenharia Civil – Teses. 2. Sal. 3. Fluência. 4. Barreira Natural. 5. Simulação Numérica. 6. Abaqus. I. Fontoura, Sérgio Augusto Barreto da. II. Pontifícia Universidade Católica do Rio de Janeiro. Departamento de Engenharia Civil. III. Título.

CDD:624

To my eternal friend Rafael Mercer, who always taught me a lot to believe in myself.

Acknowledgements

To my advisor Prof. Sérgio Augusto Barreto da Fontoura, for the proposal of the theme, for the availability for guidance, for the contributions and for the opportunity to be part of Group of Technology and Petroleum Engineering (GTEP), which provided all the technical infrastructure for the development of the research.

To colleagues in the Group of Technology and Petroleum Engineering, the Civil Engineering Department at PUC-Rio and to the professors of the Master in Geotechnics, for the knowledge transmitted.

To my dear and beloved parents Daniel and Marta, for their love, affection, understanding and fundamental encouragement during the master's degree. You are the key pieces to my academic achievement and incessant pursuit of my life goals.

To the other members of my family and my boyfriend, for the love and support they gave me for this work could be accomplished.

My enormous gratitude to all the friends I have made throughout this period, who shared with me all the experiences, making these moments lighter and more joyful. Thank you for the friendship, companionship and love we have built all this time.

To Shell Brazil, for their financial support of research, stimulating discussion and meaningful contributions.

This study was financed in part by the Coordenação de Aperfeiçoamento de Pessoal de Nível Superior – Brasil (CAPES) – Finance Code 001.

Abstract

Mazon, Alessandra Lidia; Fontoura; Sergio Augusto Barreto da (Advisor). **Numerical modelling of evaporites as a natural barrier for the abandonment of oil wells**. Rio de Janeiro, 2022. 98p. Dissertação de Mestrado – Departamento de Engenharia Civil, Pontifícia Universidade Católica do Rio de Janeiro.

Wellbore construction through salt formation remains a great challenge in drilling engineering in many oil provinces around the world, notably offshore Brazil, due to its unique mechanical properties, in particular, its high creep mobility under downhole conditions. Initially, it is necessary to control wellbore closure during drilling in order to allow casing installation. Later, the loading of the casing in both the cemented and uncemented sections is cause of concerns to prevent issues of long-term wellbore integrity. However, the contact between the salt and the casing can provide a necessary and economically beneficial natural barrier. This work consists of extracts of the research project "*Evaluation of the potential of clayey and evaporitic formations to act as an external barrier to the casing for the abandonment of wells*", carried out by the Group of Technology and Petroleum Engineering (GTEP) at the Pontifical Catholic University of Rio de Janeiro, Brazil. The aim of this work is to model wellbore closure in salt throughout uncemented casing zones considering open annular. For this, a computational methodology was developed, using the commercial finite element code ABAQUS. As the first stage of the study, in order to validate the simulation protocol, the reproduction of studies about the formation of natural barriers in salt, reported in the literature, is presented, considering the small and large deformation modes of the ABAQUS. The comparison between the results obtained demonstrates a time difference for annular closure ranging from a few months to a few years, depending of depth and type of salt. Discussions on specific aspects of creep simulation in salt rocks are also made at this stage. In the second stage of the work, is presented an analysis to estimate the wellbore closure time under field conditions representative of the Brazilian basins, coupling the adjustments made in the previous stage. The salt constitutive behavior used to simulate the steady-state creep was double mechanism model and the parameters are representative of the Brazilian offshore scenario. As a result, it is observed the potential for the formation of natural barriers in saline layers for permanent plug and abandonment operations. In both simulations, annular closure is performed using 2D models of plane strain and axisymmetric, representing the cross section and longitudinal section, respectively. The simulation steps are divided into initial equilibrium stress field (geostatics) followed by drilling and simulated creep as a viscoelastic material.

Keywords

Creep, Salt, Natural barrier, Numerical simulation, Abaqus.

Resumo

Mazon, Alessandra Lidia; Fontoura; Sergio Augusto Barreto da. **Modelagem numérica de evaporitos para fins de barreira natural no abandono de poços de petróleo**. Rio de Janeiro, 2022. 98p. Dissertação de Mestrado – Departamento de Engenharia Civil, Pontifícia Universidade Católica do Rio de Janeiro.

A construção de poços através de formações salinas continua sendo um grande desafio na engenharia de perfuração em muitas províncias petrolíferas ao redor do mundo, notadamente *offshore* no Brasil, devido às suas propriedades mecânicas únicas, em particular, sua alta mobilidade de fluência sob condições de fundo de poço. Inicialmente, é necessário controlar o fechamento do poço durante a perfuração para permitir a instalação do revestimento. Mais tarde, o carregamento do revestimento nas seções cimentadas e não cimentadas é motivo de preocupação para evitar problemas de integridade do poço a longo prazo. No entanto, ocontato do sal com o revestimento pode fornecer uma barreira natural necessária e economicamente benéfica. Este trabalho consiste em extratos do projeto de pesquisa "Avaliação do potencial de formações argilosas e evaporíticas atuarem como barreira externa ao revestimento para o abandono de poços", realizado pelo Grupo de Tecnologia e Engenharia de Petróleo (GTEP) da Pontifícia Universidade Católica do Rio de Janeiro, Brasil. O objetivo deste trabalho é modelar o fechamento de um poço em sal ao longo de zonas de revestimento não cimentadas considerando anular aberto. Para isso, foi desenvolvida uma metodologia computacional, utilizando o código comercial de elementos finitos ABAQUS. Na primeira etapa, a fim de validar o protocolo de simulação, apresenta-se a reprodução de estudos sobre a formação de barreiras naturais em sal, reportados na literatura, considerando os modos de pequena e grande deformação do ABAQUS. A comparação entre os resultados obtidos demonstra uma diferença de tempo para o fechamento anular variando de alguns meses a alguns anos, dependendo da profundidade e do tipo de sal. Discussões sobre aspectos específicos da simulação de fluência em rochas salinas também são feitas nesta etapa. Na segunda etapa, é apresentada uma análise para estimar o tempo de fechamento do poço em condições de campo representativas das bacias brasileiras, acoplando os ajustes realizados na etapa anterior. O comportamento constitutivo do sal utilizado para simular a fluência em regime permanente foi o modelo de mecanismo duplo e os parâmetros são representativos do cenário offshore brasileiro. Como resultado, observa-se o potencial de formação de barreiras naturais em camadas salinas para operações de tampão permanente e abandono. Em ambas as simulações, o fechamento anular é feito utilizando modelos 2D de estado plano de deformação e axissimétrico, representando a seção transversal e longitudinal, respectivamente. As etapas de simulação são divididas em campo de tensão de equilíbrio inicial (geostática) seguido de perfuração e fluência simulada como um material viscoelástico.

Palavras-chave

Fluência, Sal, Barreira Natural, Simulação Numérica, Abaqus.

Table of contents

List of figures

List of tables

List of symbols

ANP	Agência Nacional do Petróleo, Gás Natural e Biocombustíveis
A, B, C, D	Structural factors
α_h, β_h, α_s, β_s	Constants of Enhanced Double-Mechanism creep law
BSEE	Bureau of Safety and Environmental Enforcement
CBL	Cement bond logs
CSB	Solidary barriers set
DHSV	Down hole safety valve
Δ	Hardening parameter
δ	Softening parameter
E	Young's modulus (static)
E_{sec}	Secant Young's modulus (static)
E_{tan}	Tangent Young's modulus (static)
ε_a	Axial Strain
ε_0	Elastic strain
ε_t^*	Intercept of the steady-state creep rate with the ordinate axis
$\dot{\varepsilon}$	Strain rate
$\dot{\varepsilon}_0$	Referente strain rate
$\dot{\varepsilon}_{total}$	Total strain rate
$\dot{\varepsilon}_i$	Partial strain rate
$\dot{\varepsilon}_{DG}$	Creep rate caused by dislocation glide mechanism
$\dot{\varepsilon}_{DCL}$	Creep rate caused by dislocation climb mechanism
$\dot{\varepsilon}_{UMC}$	Strain rate caused by undefined mechanism
$\dot{\varepsilon}_{ss}$	Steady-state creep rate
EDMT	Enhanced double-mechnism law using a transient function

EDMP	Enhanced double-mechanism law using a power law
f_i	Function
ζ	Internal isotropic hardening variable
FAB	Formation as barrier
FEM	Finite element method
F	Transient function
GTEP	Group of Technology and Petroleum Engineering
G	Shear modulus
H	Heaviside step function
IBP	Instituto Brasileiro de Petróleo, Gás e Biocombustíveis
K	Bulk modulus
K_0	Limit factor of transient creep
NORSOK	Norsk Sokkels Konkurranseposisjon
n, n_i	Stress exponent
m	Time exponent
PP&A	Permanent plug and abandonment
ρ	Density
Q, Q_i	Activation energy
R	Gas universal constant
S,MISES	Equivalent von Mises stress (Pascal)
S,S11	Normal stress in the direction 1 (Pascal) direction. Negative values denote compression
S,S22	Normal stress in the direction 2 (Pascal) direction. Negative values denote compression
S,S22	Normal stress in the direction 3 (Pascal) direction. Negative values denote compression
σ	Stress
σ_0	Reference stress
σ_c	Uniaxial compressive strength
σ_{eq}	Deviatoric stress

t	Time
T	Temperature
T_0	Reference temperature
T_m	Homologous temperature
UK	United Kingdom
USIT	Ultrasonic imaging tool
V_P	Compressional wave velocity
ν	Poisson's ratio
v	Temperature exponent
WBE	Well barrier elements

1
Introduction

1.1 Problem definition and justification

The operations carried out at the end of the useful life of any kind of well (exploration, production or injection) are called decommissioning or permanent plug and abandonment of the well (PP&A). According to Khalifeh & Saasen (2020), the PP&A operations of a well can reach up to 25% of offshore well drilling costs.

Due to the high costs of these operations and the high number of wells to be permanently plugged and abandoned in Brazil in the coming years, the oil and gas industry has increasingly invested in the development of alternative PP&A techniques.

Currently, PP&A procedures are normally performed by means of cement injection through the casing shoe, in order to establish a permanent barrier. However, voids and non-cemented failures can occur, which can compromise the operation (Fjær et al., 2016). Thus, due to the recognized characteristics of creep and great sealing capacity of some formations, the rock presents itself as an efficient technical-economic alternative for the formation of a natural barrier, and consequently, as a PP&A material.

The concept of Formation as Barrier (FAB) emerged from the finding of natural shale barriers. According to the literature, the concept was initially used in 2005 in oil and gas field of Oseberg, located in the North Sea, when a good signal of sealing in the cement bond log (CBL) and ultrasonic to imager tool (USIT) was observed in areas where the cement was not foreseen (Fredagsvik, 2017).

According Fredagsvik (2017), salt formations are not relevant to the Norwegian sector, for example, which means that many existing research and published in the literature are on shales. However, in Brazil most of the oil and gas exploration is done in the pre-salt, in which thick layers of salt are crossed during the operation, becoming relevant to this scenario.

The use of formations with high creep mobility, for annular sealing of oil and gas wells was encouraged by the regulatory agency of Norway. However, this

option of using its own natural formation in the PP&A process is currently underused (Orlic et al., 2019).

In Brazil, the Agência Nacional do Petróleo, Gás Natural e Biocombustíveis (ANP) has Resolution ANP n°. 46/2016, governed by the best practices in the sector, which takes into account the concept of Solidary Barriers Set (CSB). In this CSB, the materials used for the composition of the elements of the permanent CSB must meet certain characteristics, where it is speculated that cap-rocks, such as evaporites and shales, may be framed in the future (ANP, 2016).

As well as shale, salt is also known as a common reservoir seal for its excellent isolation capacity and the potential to heal fractures because of its mechanical properties. Thus, some authors have studied the formation of natural barriers in salt through numerical simulations (Hou et al., 2012; Orlic et al., 2019). In this work, a computational study is carried out on the formation of an annular barrier in saline layers, using finite elements method (FEM) through the ABAQUS software.

The knowledge generated by the present work contributes to the progress of research that has been carried out in Brazil, including salt as a sealing material for permanent abandonment operations of oil and gas wells. Thus, it is noteworthy that this work does not aim to exhaust the topic, but to start the discussion of the subject, aiming at the possible implementation of this methodology in the future, which may represent a significant reduction in the costs and environmental risks of these operations.

1.2 Objectives

This work has as main objective to verify the annular closure of an oil wellbore in saline zones through computer simulations using the FEM.

For the main objective to be achieved, the following specific objectives must be met:

- Develop a computational methodology to assess annular closure of the wellbore;
- Evaluate the model conditions in order to establish the closure scenario;
- Evaluate the annular closure time of the wellbore;
- After closure, evaluate the contact pressure between the casing and the salt in order to indicate the formation of a natural barrier.

1.3 Structure of the dissertation

This work is structured in 6 chapters, including this introduction, which characterizes Chapter 1 and a section of bibliographic references.

Chapter 2 presents a review of the main aspects involved in the process of permanent abandonment of wells, including the materials used, the use of salt formations as a natural barrier and the regulation for the use of salt as a natural barrier, based on international standards in force.

Chapter 3 presents the literature review on the properties of evaporites with an emphasis on creep properties, with the purpose of gathering important aspects to be considered in computational modeling. In addition, it presents the constitutive models used for modeling the creep in salt.

Chapter 4 presents the evaluation of the computational methodology through the reproduction of cases containing the elements for the analysis of a well abandonment problem, reported in the literature. This chapter presents the stress and displacement analysis of the simulations as well as discussions covering aspects such as mesh size, solution convergence, geometric linearity and nonlinearity.

Chapter 5 presents the simulation of the annular closure of the well in a syntetic scenario. It presents the plane strain and axisymmetric model, considering conditions such as stress and temperature in situ, material properties, geometry and fluid weight more realistic for the Brazilian pre-salt wells, reported in the literature. Furthermore, analyses of stresses and displacements within the context of the formation of natural barriers are presented.

Chapter 6 presents the conclusions obtained by the study and suggestions for future work.

2
Natural barriers for permanent abandonment of wells

2.1 Life cycle of oil and gas wells

In general, the life cycle of oil and gas wells can be represented by five stages: planning, drilling, completion, production and abandonment.

Well planning aims to formulate well drilling programs to achieve the necessary characteristics of safety, minimum cost, and usability. For this, many variables need to be considered and it is not always possible to meet these objectives in each well due to restrictions based on geology, drilling equipment, temperature, among others.

After the planning stage, the well is created by drilling a hole into the rock using a drilling rig that rotates a string with a bit attached, then sections of steel pipes, named casing, slightly smaller in diameter than borehole are placed in the hole.

In this process, a drilling mud with the correct physical and chemical characteristics is pumped into the inside of the drill pipe and exits the drill bit in order to stabilize the differential stresses around the hole and prevent well closure by creep and, consequently, operating losses.

Once the design well depth is reached, the formation must be tested and evaluated to determine whether the well will be completed for production, or plugged and abandoned. This phase is called completion, where the well will be enabled to safely produce oil and/or gas

The production stage starts when all the infrastructure already installed, then the field starts to produce oil and/or gas to supply the market. This stage is the longest in the entire life cycle of an oil field, and it can last for decades.

Finally, abandonment generally occurs when the well reaches its economic limit and becomes a liability, that is, when its most efficient production rate does not cover operating expenses, including taxes. This operation can be temporary when there are prospects of future return to well activities or permanent when there is no interest in re-entry.

2.2 Permanent plug and abandonment of wells

Decommissioning or permanent plug and abandonment (PP&A) of wells is the process that occurs at the end of the useful life of oil and gas exploration and production facilities, referring to the stage of dismantling and, in most cases, removing equipment from the well (Silva & Mainier, 2008).

After periods of production of more than twenty-five years, the number of wells about to reach the end of their useful life increases, mainly due to the maturation of the well, in which production decreases to the limit of its economic return. Given these conditions, the wells proceed to the permanent plug and abandon process (Vrålstad et al., 2019).

The standard NORSOK D-010 (NORSOK Standard, 2013) establishes permanent abandonment as operations in which the well or part of it will be plugged and abandoned with the intention of never being used or entered again. Thus, this operation aims to provide a seal of the annular space, which is continuous, permanent and impermeable, in order to prevent the flow of fluids from the formation and resist the pressures acting above and below by means of permanent barriers. These barriers, called security barriers, concern the physical separation made up of one or more elements that contain or isolate an unwanted event in a certain path between the system under study and the environment (Øksnes, 2017).

Vrålstad et al. (2019) presents a simplified illustration of a typical production well before and after PP&A shown by Figure 2.1. The details of a PP&A operation procedure can differ significantly from well to well, however, there are common steps in a typical operation. In this way, the three general locations for the installation of barriers are highlighted. First, the barrier positioned next to the producing zones in order to obtain an isolation of the potential source of fluid flow. Second, any formations containing over pressurized fluids, such as high pressure zones and formations containing hydrocarbons, are also isolated in order to prevent cross-flow between zones. Third, a plug from a well opened at the surface, also called an environmental barrier, is installed below the seabed, which prevents residual contamination of the fluid to the environment.

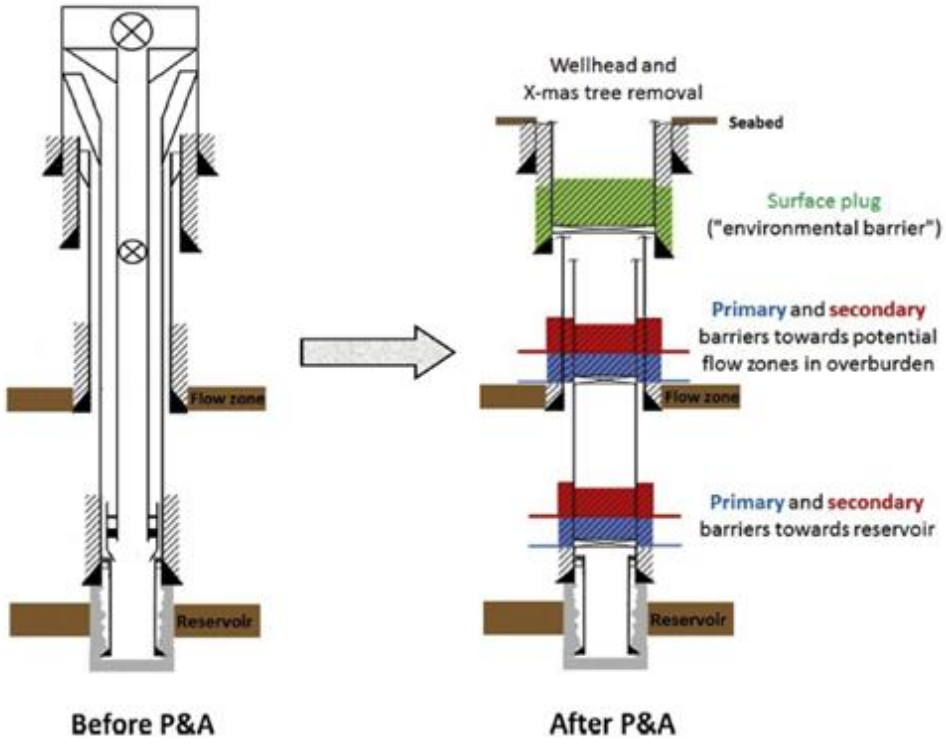

Figure 2.1 – Simplified configuration of a typical offshore production well before and after PP&A (Vrålstad et al., 2019)

Traditionally, the well abandonment process is carried out through the installation of permanent long-term sealing barriers constituted by the positioning of several plugs made by the injection of Portland cement through the casing shoe, thus being the most used material for this purpose. However, this procedure can leave large sections without cement (Williams et al., 2009).

There are records of field evidence where it is believed that some sedimentary rocks, such as evaporites and shales, can act as natural barriers at intervals without cementation, due to their creep deformation potential (Vrålstad et al., 2019).

2.3 Formation as natural barrier

The use of the formation as a barrier element is because when drilling certain formations of extremely low permeability, such as salt and shale, occasionally the rock moves inwards and begins to close the wellbore. During and after drilling this is undesirable and can cause problems in the execution of drilling and casing installation, but in the abandonment phase, it can be used to create a natural annular barrier behind the casing (Fjær et al., 2016).

In practice, creep formation has been used mainly for annular sealing of oil and gas wells in shale formations, where the concept of formation as a barrier

began (Williams et al., 2009).

In addition to shales, salt also has a noticeable tendency to creep. Unlike shales that tend to be more brittle and with a very low creep potential at greater depths because of diagenesis, the creep potential of salt is highly sensitive to temperature in the field and increases with depth. A salt formation, which has significant creep properties, can spontaneously create effective annular seals around cementless or poorly cemented parts of the casing and even create natural salt plugs for closuring and abandoning wells (Orlic & Buijze, 2014).

According to Orlic & Buijze (2014), the concept of well isolation based on the self-sealing potential of salt caps was borrowed from research on the disposal of nuclear waste in saline rocks. In addition, thousands of salt caves are being used to store hydrocarbons, being considered the safest way to store large amounts of hydrocarbons (Bérest & Brouard, 2003). Thus, some evaporites are known for their excellent isolation capacity and the potential to heal cracks and fractures because of their rheological properties.

In this way, salt is a common reservoir seal throughout the world, and the pre-salt PP&A operations in Brazil can have this same advantage, since salt formations can also be accepted as an annular barrier (Hallak, 2017). For this, research related to salt as PP&A material initiates discussions on the use of salt formations as an annular barrier in Brazil.

2.4 Evidence of formation of natural salt barriers in the field

Studies for the verification of a natural salt barrier start from the convergence and closure of the well by the creep of saline rocks. The rock salt convergence tests described by the literature are performed in holes in scale ~0.1 m, deviations and underground rooms in scale ~10 m and caves in scale ~100 m. The most relevant for this research are the field tests of borehole convergence and closure in rock salt formation.

Hou et al. (2012) describes a case study of borehole closure in the natural gas field Altmark in Germany, where a long-term well hole seal concept is developed.

The concept consists of four main sealing units, one of which is a salt plug created in the formerly reamed section of casing within the plastic Zechstein rock salt formation. The article emphasis on the development and field testing of the naturally created salt plug, as a key component of the longterm wellbore sealing concept.

In the field test, a 30 m long section of casing was reamed away in the Zechstein salt layer, at a depth of 3100 m. Subsequently, the open hole section filled with brine was monitored for 450 days. Hydraulic pressure and formation integrity test tests were performed, as well as an analysis of fluid / brine and sediment samples in order to validate the concept. In addition, the work presents a preliminary analysis of core material of the new re-crystallized rock salt, formed as a result of convergence, within the originally reamed window.

Preliminary results comprise proven convergence of the rock salt formation, a successful coring and restored integrity of Zechstein salt formation, as proven by the formation integrity test. Based on these results, the new long-term sealing concept has been successfully tested at the Altmark natural gas field and successful application of the concept on other sites with similar geological conditions is foreseen to be likely.

2.5 Regulation for the use of formation as a natural barrier

In Brazil, the regulatory agency for the activities of the oil and natural gas industry is the Agência Nacional do Petróleo, Gás Natural e Biocombustíveis (ANP) where there is still no specific regulation for permanent abandonment of wells. However, the ANP published the ANP Resolution n° 46/2016, governed by the best practices in the industry, which takes into account the concept of Solidary Barriers Set (CSB).

The CSB is defined as “a set consisting of one or more barriers capable of preventing the undesirable event considering all possible paths between the system under study and the environment” (ANP, 2016). With this, the barriers must be solidary, even preventing the failures of barriers that allow communication between independent paths, such as communication between casing and its annulus or between the well and its annulus, called "shortcuts" (Miura, 2004).

Barriers can be mapped for each path, for example, for casing, well or annular. Meanwhile, the solidarity sets are mapped for each action scenario, such as drilling, completion, restoration and others. Figure 2.2 and Figure 2.3 show the concept of barrier and CSB.

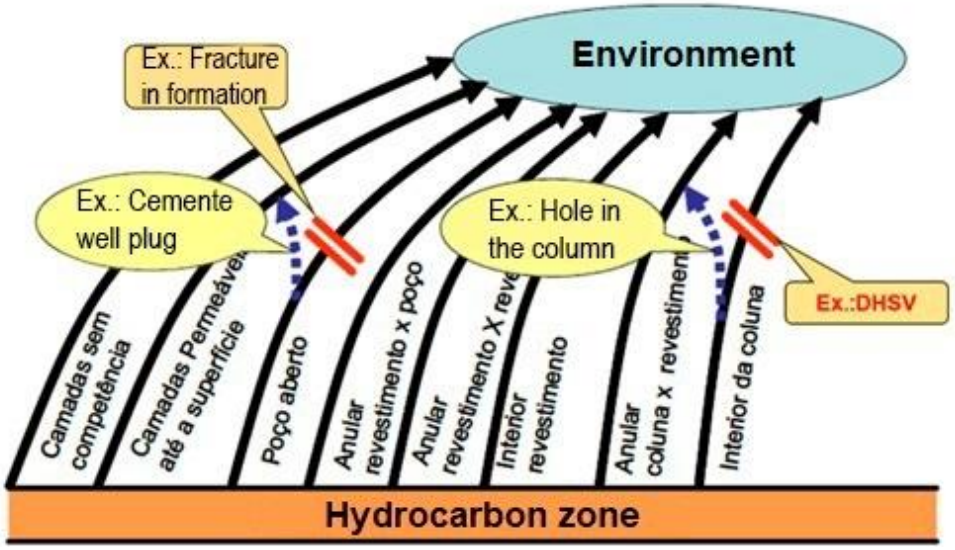

Figure 2.2 – Barrier examples. One barrier is the cement plug on the “open well” path and the other barrier is the Down Hole Safety Valve (DHSV) on the “inside column” path (modified from Miura, 2004).

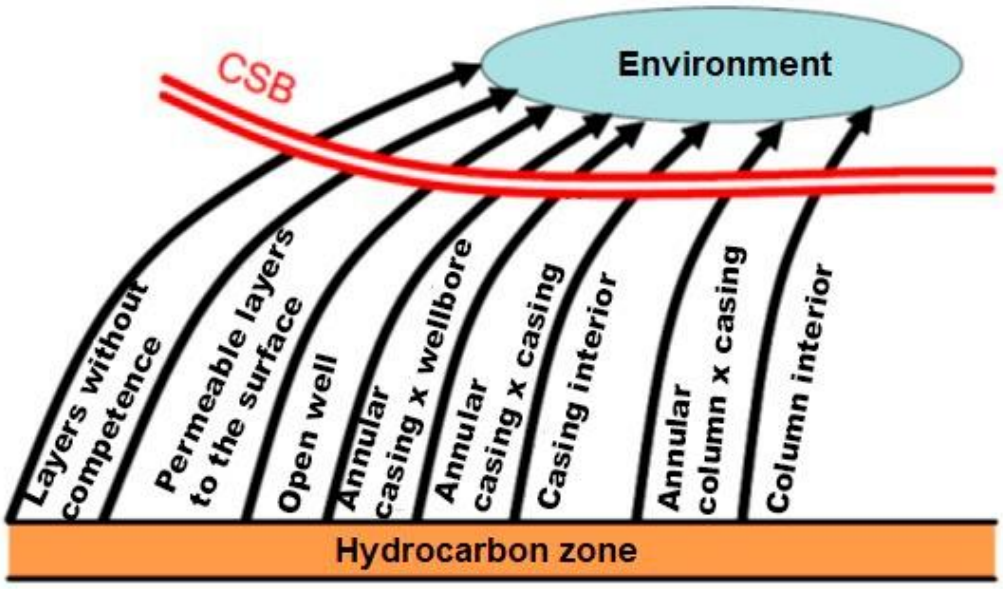

Figure 2.3 – Solidary Set of Barriers (CSB) (Modified from Miura, 2004).

ANP Resolution n° 46/2016 provides for the use of materials for the composition of the elements of the permanent CSB that meet, at least, the following criteria:

- Impermeable to fluids;
- Isolation and non-deteriorating over time;
- Resistance to formation fluids;
- Resistance adequate to support the loads to which they will be subjected;

- Do not suffer contraction that compromises its integrity; and
- Adherence to casing and formations in its surroundings.

A recognized standard that encompasses the definition and requirements for permanent barriers is NORSOK D-010 (NORSOK Standard, 2013). As well as ANP Resolution n° 46/2016, the NORSOK D-010 also describes the requirements that the permanent barrier must meet, meeting the items described above.

In addition, NORSOK D-010 states that the barrier must extend over the entire cross-section of the well, include all plugs and seal both vertically and horizontally. It must also be necessary for an annular barrier is 50 m with formation integrity at the base of the interval and a well barrier shall be placed at a depth where the formation fracture pressure is larger than the worst anticipated pressure it may be exposed to.

Ultimately, the NORSOK D-010 standard sfecifies that a bonded and impermeable in-situ formation (e.g. shale, salt) is accepted as an annulus well barrier, which allows the use of salt as a barrier element, since the salt meets its requirements such as:

- The barrier must be salt. This can be demonstrated through electrical logs or cuttings profiles made during or after drilling;
- The salt resistance must be sufficient to withstand the maximum expected pressure that can be applied to it;
- The salt displacement mechanism must be adequate to preserve the properties of the well barrier;
- The barrier must extend and seal the entire circumference of the casing and at an appropriate interval along the well. This can be verified using the ultrasonic azimuth log.

As a general rule, Skjerve (2013) postulates that the installed barriers must be located as close as possible to the potential source of entry, as well as covering all possible leakage paths. In addition, they must be placed adjacent to an impermeable formation and have an extension along the cross-section of the well, including all annuli and sea and, finally, sealing vertically and horizontally.

A methodology for establishing a comparative analysis between the main guidelines for well abandonment is presented by Teraoka (2017). Through studies of scenarios for permanent abandonment, among them, the scenario for open well and cased well, the main points evaluated are schematically summarized, for example, extension and positioning of the plug, isolated interval, barrier component material as shown in Figure 2.4 and Figure 2.2.5.

According to Teraoka (2017), about the composition of the barrier materials, the Oil & Gas UK (2015), IBP (2017) and ANP (2016) standards present the same recommendations. Among the main ones, it is noteworthy that the materials of the elements of the CSB are impermeable to fluids, resistant to formation fluids, have insulating properties and do not deteriorate over time. For NORSOK D-010, in addition, all components of the CSB or Well Barrier Elements (WBE) must support the weight and environmental conditions that will be exposed during the abandonment period. Thus, it is possible to verify that the guidelines and regulations have similar recommendations, aiming to guarantee the integrity of the elements during and after abandonment, in addition to preventing the fluid flow from inside the well.

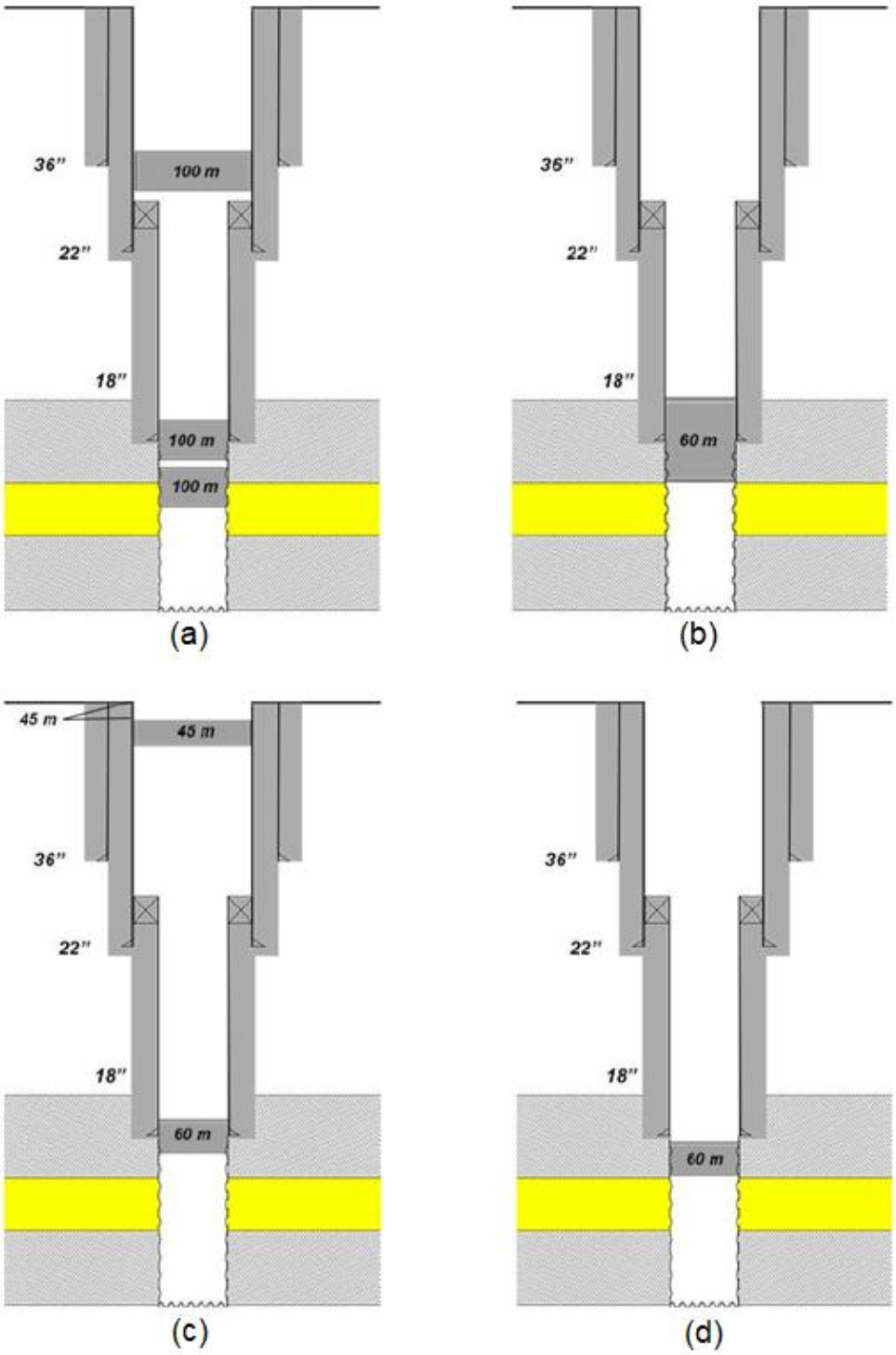

Figure 2.4 – Scheme of permanent abandonment in the open well scenario according to (a) NORSOK D-010 (b) Oil & Gas UK Guidelines (c) CFR (BSEE) and (d) IBP Guidelines (Teraoka, 2017).

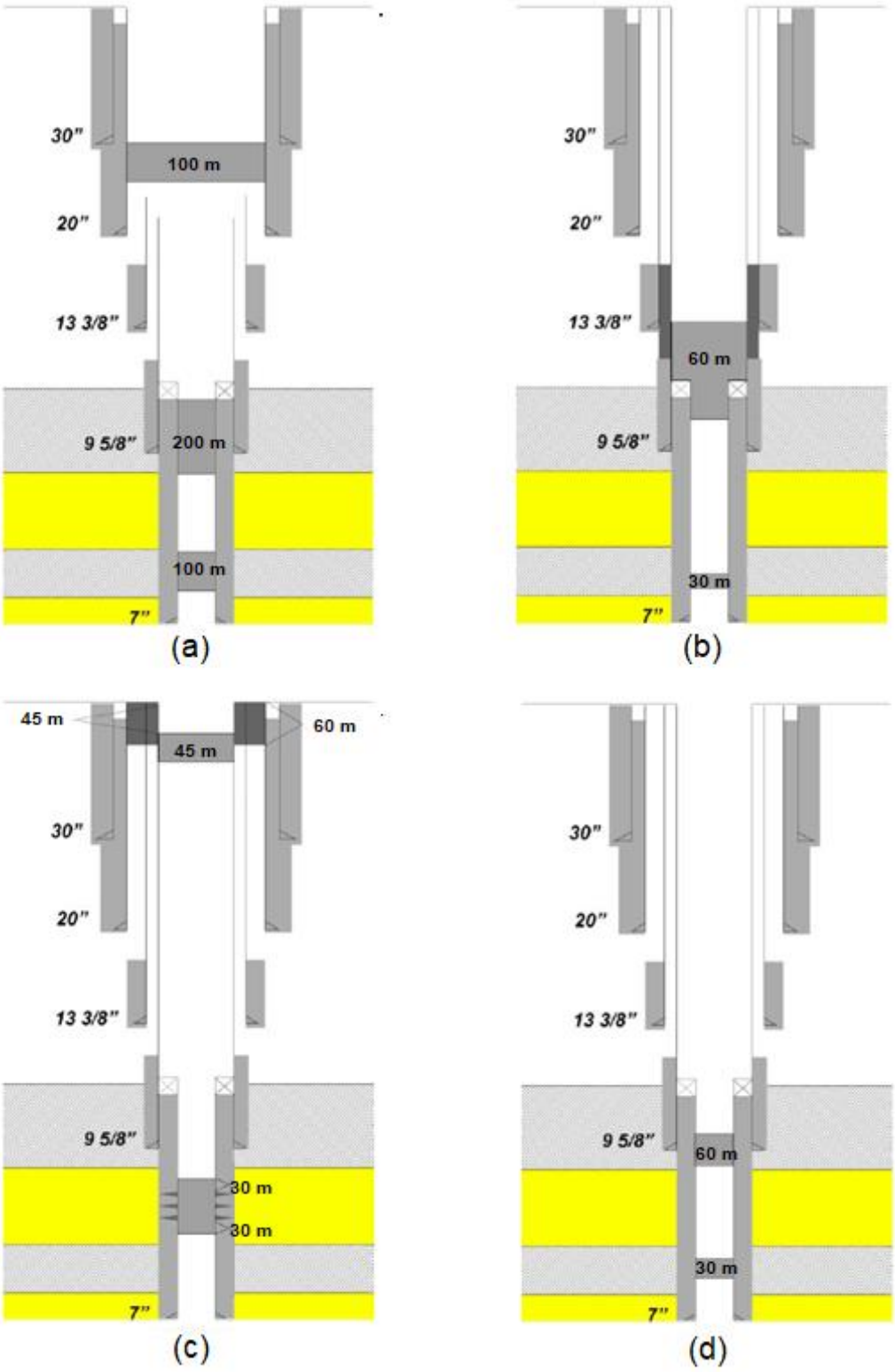

Figure 2.2.5 – Scheme of permanent abandonment in the cemented well scenario in accordance with (a) NORSOK D-010 (b) Oil & Gas UK Guidelines (c) BSEE and (d) IBP Guidelines (Teraoka, 2017).

3
Evaporites and their constituve creep models

3.1 Definition and basic properties of evaporites

Evaporites are sedimentary rocks formed from the crystallization of saline minerals, being the main one halite (NaCl), which is deposited directly from brines under conditions of strong evaporation and precipitation. Such deposits can be of continental or marine origin in which there is a periodic supply of salt water.

In most cases, the evaporite has in its composition a high percentage of halite (NaCl) in the order of 90% - 99%, in addition to other minerals and clastic sediments (Mackay, 2011).

Among the properties of evaporites, creep behavior is a phenomenon whose understanding is fundamental to the mechanics of saline rocks, being addressed in more detail in Section 3.2. However, other properties presented by the evaporites are related to the context of the formation of a natural barrier and can be mentioned.

About resistance to uniaxial compression, the evaporites are comparable with the concrete of civil construction, presenting a resistance around 35 to 40 MPa. Despite the similarity in strength, saline rocks withstand greater deformations, reaching levels of around 25% without generating irreversible cracks and fractures. Such behavior is attributed to the ability of the evaporites to self-healing (Dusseault et al., 1987). Poiate (2012) presents a laboratory testing campaign and Table 3.1 presents his results of uniaxial compression tests for Brazilian halite.

Table 3.1 – Results of uniaxial compression tests for halite (Poiate, 2012).

Specimen	V_p (m/s)	ρ (kg/m^3)	ε_a (10^{-3} m/m)	E_{sec} (GPa)	E_{tan} (GPa)	E_{lineal} (GPa)	ν_{lineal}	σ_c (MPa)
CP1	4529	2167	18.99	3.75	1.30	-	-	37.89
CP2	4473	2178	18.43	4.86	1.72	-	-	39.08
CP3	4417	2192	18.80	5.74	2.00	-	-	41.12
CP4	4385	2165	5.70	-	-	23.40	0.33	44.39
CP5	4451	2158	5.76	-	-	19.91	0.27	44.60
CP6	4341	2160	5.82	-	-	19.61	0.31	42.35
Mean	4432.67	21.70	12.25	4.78	1.67	20.97	0.30	41.57
Std. Dev.	66.58	12.85	7.11	1.00	0.31	2.11	0.03	2.75

The self-healing presented by the saline rocks is extremely desirable for the tightness in the storage of material. This property is caused due to slow deformations, leading to the natural closure of discontinuities, cracks and fractures that make the rock return to a condition of integrity. This mechanism can be consulted in more detail in Dusseault (1989).

According to Firme (2013), in relation to the evaporites porosity and permeability, functionally null properties are considered. Thus, it is idealized that there is no porepressure acting on saline rocks, in addition to suggesting a sealing capacity of the rock. Thus, jointly with the creep phenomenon, salts become prone to trapping fluids and gases and encapsulating waste materials.

Lastly, the evaporitic rocks are practically incompressible and have high thermal conductivity, which makes the geothermal gradient in a saline section to be smaller than in the other rocks above it (Poiate, 2012). Table 3.2 presents the characteristic profiling values for identifying the type of evaporites with relevant creep properties.

Table 3.2 – Properties to identify evaporites (Poiate, 2012).

Mineral	Density (g/cc)	Transit time (µs/ft)	Neutron porosity	Gamma ray
Carnalite	1.66	78	65	220
Halite	2.10	67	0	0
Tachydrite	1.57	92	60	10

It is important to highlight the difficulty of obtaining data, mainly offshore. Thus, in most cases, data are obtained from samples obtained from onshore wells and their results are extrapolated to the data from offshore wells.

3.2 Creep and creep stages in evaporites

Creep can be defined as the phenomenon of progressive plastic deformation over time, due to the state of constant stresses to which a given material is subjected.

According to materials science, the stress level at which creep occurs is below the ultimate stress of the material, undergoing deformation in order to relieve stresses, and in materials subject to high temperatures, the creep phenomenon presents itself with bigger frequency.

Being present in all materials, the occurrence of creep varies considerably depending on the crystalline structure, such as the presence of imperfections, the size of atoms or the type of connection between atoms and molecules of the various materials existing in nature (Poiate, 2012). Besides that, in the case of

evaporites, creep is significantly influenced by the thickness of the salt layer, the formation temperature, the mineralogical composition, the water content, the presence of impurities and the extent to which the differential stress is applied to the saline body (Costa et al., 2005).

Even though many studies encompassing tests on several evaporite specimens in order to understand the behavior of rock in oil wells, Oliveira et al. (1985) report that creep, strictly speaking, is uncontrollable. In this way, even if the drilling fluid backpressure is leveled with the stresses in the wellbore wall, there will be a spontaneous flow inherent to the deposit with a small deformation rate and in a preferred direction.

The development of deformations for creep over time is characterized in the laboratory following three stages of material behavior. Figure 3.1 presents a typical creep test in a specimen analyzing the behavior of material based on strain and strain rate.

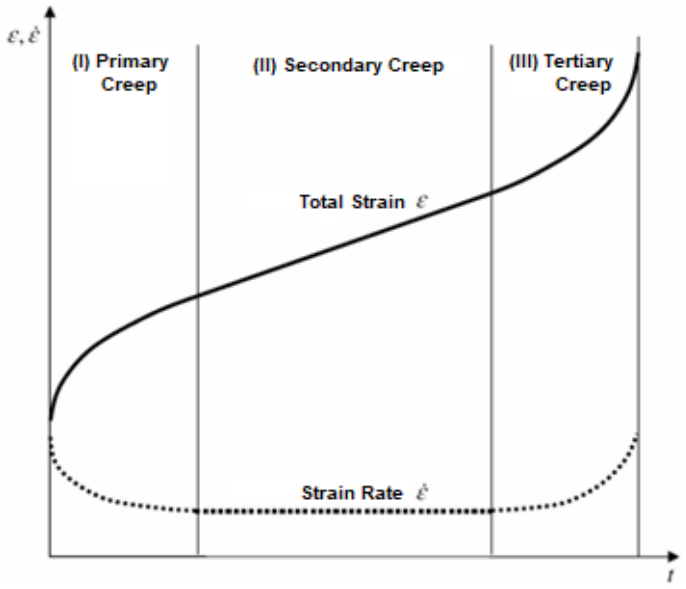

Figure 3.1 – The three creep stages analyzed by strain and strain rate.

According to Dowling (2012), when applying a constant level of stress and temperature, the material deforms almost instantly, corresponding to an elastic deformation (ε_0). Thereafter, the strain rate or creep speed decelerates over time, corresponding to the stress distribution applied, only partially accommodated in the initial elastic strain, reaching a constant strain rate. This phase is called transient or primary creep, characterized by a high deformation rate.

According to Costa et al. (2010), because the primary creep developed in well drilling is quickly and completely dissipated, this phase can be considered included in the initial elastic deformations of the numerical simulations, not being

approached as an isolated creep stage.

Given the constant deformation rate, the second stage begins, also known as permanent or stationary regime, as well as secondary creep. According Benitz (2012), the strain rate maintains a constant value because the recovery of the microstructure occurs together with the deformation. In this region, the thermal energy activates the sliding and scaling, which are displacements that change the planes of the crystalline network in order to circumvent the obstacles, allowing the recovery of the material to balance with its hardening capacity. Both sliding and scaling increase the degree of freedom of movement. This stage is characterized by a constant strain rate over time.

Secondary or steady-state creep is predominant in the field creep behavior of saline rocks, and is also evidenced by the formation of glaciers and saline domes (Dusseault et al., 1987).

Finally, in the third stage, known as tertiary creep, there is an acceleration of the deformation speed, which quickly leads to the rupture of the material. This is due to the fact that micro fracturing occurs in a preferential plan leading to the formation of macro fractures.

3.3 Constitutive creep models and their parameters

Over time, many constitutive models developed to describe the behavior of metals have been adapted to rock mechanics, in order to represent creep behavior in rock masses. Analogies between the micromechanical mechanisms of metals and saline rocks were made, in addition to other particular mechanisms of saline rocks.

These models commonly address the creep stages separately or the union of two of them, thus representing only a part of the typical creep curve, as presented by Figure 3.1. In this way, they can be divided into three large groups named as rheological, empirical and physical creep models.

3.3.1 Rheological models

The rheological models, introduced by Bingham (1928) apud Jeremic (1994), which presents rheology as a science that studies deformability in general and not just fluids.

Such models are composed of springs and dashpots, arranged in series and/or parallel and are capable of simulating the stresses and deformations of

linear and homogeneous viscoelastic materials subjected to uniaxial loading. The springs simulate the elastic portion and the dashpots the viscous portion of the deformation.

According to Gravina (1997), the rheological models do not explicitly consider temperature as a creep variable, considering the thermal effect implicitly in the model constants. However, it is known that in saline rocks the influence of temperature is of great relevance, making the results obtained by rheological models not definitive, being considered as reference values.

Thus, the rheological models typically employed in rock mechanics, such as Maxwell, Kelvin and Burgers models, are not part of the scope of this work and can be consulted in detail in Goodman (1989) and Jeremic (1994).

3.3.2 Empirical models

The empirical models present mathematical equations derived from the observation and adjustment of a typical creep curve in relation to the experimental result of a problem according to the uniaxial state of stresses and strains.

Classically, creep modeling by empirical methods was developed by Norton (1929), known as the Power Law. The model considered only the influence of applied stress to estimate creep strain rates, subsequently assuming time and temperature as governing variables of the phenomenon.

3.3.2.1 Power Law

The Power Law is applied to the transient phase of the creep strain curve. In addition, it comprises three functions (f) that determine the influence of the deviatoric stress (σ_{eq}), the time (t) and the temperature (T) (Yao et al., 2007). The general equation of Power Law model is presented by Equation (3.1).

$$\varepsilon = f_1(\sigma)\, f_2(t)\, f_3(T) \tag{3.1}$$

Where, ε is the creep strain, $f_1(\sigma)$ is the contribution of stress given by $f_1(\sigma) = B\sigma_{eq}^n$, $f_2(t)$ is the contribution of time given by $f_2(t) = Ct^m$ and $f_3(T)$ is the contribution of temperature given by $f_3(T) = D \exp\left(\frac{-Q}{RT}\right)$ or $f_3(T) = DT^v$. In this way, B, C and D are the structural factors and n, m and v the exponents, both determined empirically, Q is the energy activation associated with the mechanism and R is the universal gas constant.

The implicit structural factor in Equation (3.1), B, C and D can be encompassed in a general factor named A, where $A = BCD$.

Thus, the creep strain as a function of time ($\varepsilon(t)$) is expressed by the superposition of the three effects mentioned above, resulting in the Equation (3.2).

$$\varepsilon(t) = A\,\sigma_{eq}^{n}\,t^{m}\,exp\left(\frac{-Q}{RT}\right)\,ou\,\varepsilon(t) = A\,\sigma_{eq}^{n}\,t^{m}\,T^{v} \tag{3.2}$$

In case of constant temperature, the temperature contribution portion can be encompassed by coefficient A. Thus, the equation that describes creep deformation over time is presented by Equation (3.3).

$$\varepsilon(t) = A\,{\sigma_{eq}}^{n}\,t^{m} \tag{3.3}$$

Where, A is the structural factor of mechanism, σ_{eq} is the deviatoric stress, t is the time and n and m are the exponents determined empirically.

From this, for this model the parameters adopted for Brazilian halite are those used for the Salt Vault Mine, being a nuclear waste repository in Kansas (USA). These data are presented by Lomenick & Bradshaw (1969) and previous work in the area such as Botelho (2008) and Firme (2013). In this way, the Power Law is given by Equation (3.4).

$$\varepsilon(t) = 1{,}3(10^{-37})T^{9{,}5}{\sigma_{eq}}^{3{,}0}t^{0{,}3} \tag{3.4}$$

Where, σ_{eq} is the deviatoric stress given in psi, T is the temperature in Kelvin and t is the time expressed in hours. Thus, applying the respective conversion factors for Pascal (1 psi ≅ 6896,55 Pa) and seconds (1 h = 3600 s) in stress and time units, as well as considering the reference temperature of 86 °C (≅ 359,15 K), the values of the parameters for the Brazilian halite presented by the Table 3.3.

Table 3.3 – Power law – Parameters of Brazilian halite.

Power law – Parameters of Brazilian halite		
A	Power law multiplier (T = 86 °C)	6.40673(10^{-26})
n	Stress exponent (stress in Pa)	3.0
m	Time exponent (time in s)	0.3

It should be noted that parameter A refers to the temperature of 86 °C. For other temperatures, this value changes, although the procedure for determining it is the same. The remaining variables do not change.

The Power Law is implemented in ABAQUS encompassing two theories for

time-varying stress analysis, namely the time hardening theory and the strain hardening theory.

According to Baar (1977), the creep deformation in saline rocks under in-situ conditions is not affected by strain hardening. Although this mechanism is observed in conventional laboratory creep tests, the non-occurrence of long-term strain hardening is evidenced by constant creep rates under constant conditions.

Thus, the time hardening theory is more representative for the wellbore closure analysis, being obtained directly from the derivative of Equation (3.3) as a function of time, that is, the creep strain equation by the Power Law as a function of time. In this way, we have the Equation (3.5).

$$\dot{\varepsilon} = Am\ {\sigma_{eq}}^{n}\ t^{m-1} \tag{3.5}$$

It is possible to observe that temperature is not an explicit variable in this formulation, being implicitly encompassed by parameter A and considered constant.

In addition, the terms of Equation (3.6) can be included in $\bar{A} = Am$ and $\bar{m} = m - 1$. Thus, the expression of the creep strain rate by ABAQUS is given by Equation (3.6).

$$\dot{\varepsilon} = \bar{A}\ {\sigma_{eq}}^{n}\ t^{\bar{m}} \tag{3.6}$$

Therefore, Table 3.4 presents the parameters for Brazilian halite to be used in ABAQUS.

Table 3.4 – Power law – Parameters of Brazilian halite in ABAQUS.

Power law – Parameters of Brazilian halite in ABAQUS		
$\bar{A}$	Power law multiplier ($T = 86$ °C)	1.92202(10^{-26})
n	Stress exponent (stress in Pa)	3.0
$\bar{m}$	Time exponent (time in s)	-0.7

3.3.2.2 Double Power Law

The Double Power Law is a modification of the conventional Power Law and considers the creep rate constant over time, modeling the secondary or steady-state stage of the creep curve. The steady-state creep rate is given by the constitutive equation for creep of the Power Law presented by Equation (3.7).

$$\dot{\varepsilon} = A\ \left(\frac{\sigma_{eq}}{\alpha}\right)^{n} \exp\left(\frac{-Q}{RT}\right) \tag{3.7}$$

Where, A is the structural factor of mechanism, σ_{eq} is the deviatoric stress, α is the reference stress, n is the stress exponent, Q is the activation energy, R is the gas universal constant and T is the temperature.

According to Benitz (2012), this law takes into account a regime of mixed dominance that considers two deformation mechanisms acting in parallel. In this way, the total strain rate is the sum of the individual mechanisms, with the greater rate giving the net creep rate. Equation (3.8) presents the total strain rate of creep by the Double Power Law.

$$\dot{\varepsilon}_{total} = \dot{\varepsilon}_1 + \dot{\varepsilon}_2 \quad \dot{\varepsilon} = A_1 \left(\frac{\sigma_{eq}}{\alpha}\right)^{n_1} \exp\left(\frac{-Q}{RT}\right) + A_2 \left(\frac{\sigma_{eq}}{\alpha}\right)^{n_2} \exp\left(\frac{-Q}{RT}\right) \tag{3.8}$$

Changing the two stress exponents provides the ability to model regimes occurring simultaneously in a same sample such as Nabarro-Herring and Coble creep ($n = 1$) at lower stresses and mechanisms of dislocation climb or dislocation glide at moderate stresses (n greater than 1) (Benitz, 2012).

The Double Power Model gives the steady-state creep behavior with two regions with differing slopes on a plot of log stress versus log strain, where the slopes are equivalent to the stress exponents.

The parameters of Brazilian halite for this model are not presented in the current literature until the publication of this work.

3.3.3 Physical models

Munson published studies, such as Munson & Dawson (1979) and Munson & DeVries (1991), presenting the constitutive physical laws for secondary creep through strain mechanism maps based on temperature ranges and differential stress. In this way, the combination of temperature and stress structures specific micromechanical mechanisms, acting at the level of crystals and granular aggregates, which control the creep deformation of the salt for such an arrangement.

The dislocations spread in different ways through the creep, and this occurs according to the conditions of loading and temperature, leading to different governing creep mechanisms in certain conditions. Figure 3.2 presents a scheme of strain mechanisms for saline rocks.

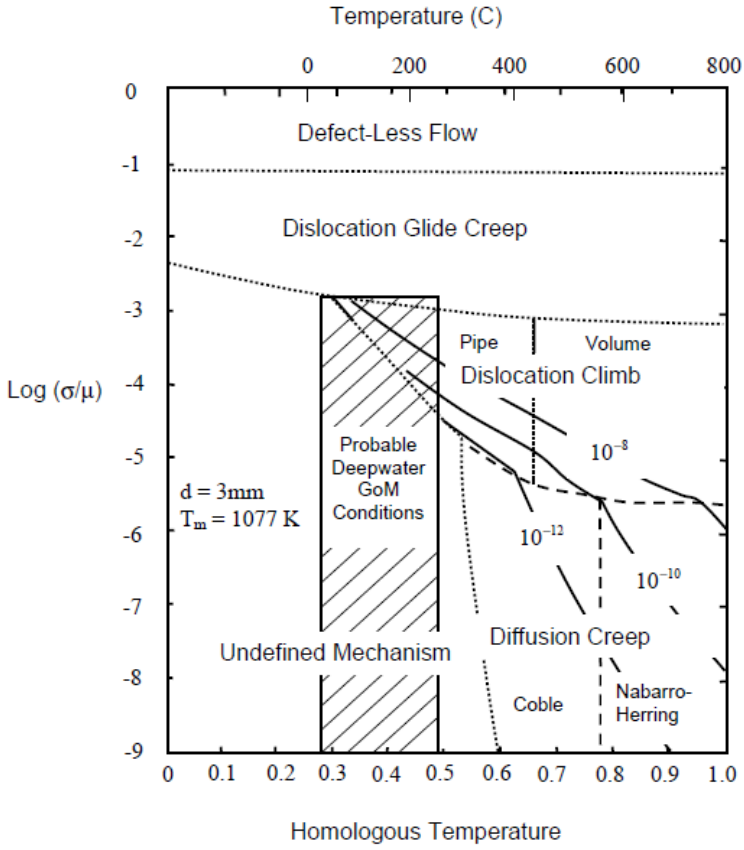

Figure 3.2 – Strain mechanisms map for saline rocks (Munson & Dawson, 1979).

In this map, the predominant creep mechanism can be observed for a set of conditions such as the deviatoric stress (σ_{eq}), the material shear modulus (μ) and the temperature presented as the homologous temperature of material (T/T_m), being considered $T_{m,sal} = 1077\ K$ (Fossum & Fredrich, 2002).

Predominantly, the consolidated laws of steady-state creep include both the effects of temperature and the maximum stress differential ($\sigma_1 - \sigma_3$), with an evident dependence between the rate of deformation and temperature, due to thermally activated micro mechanisms, in addition to a strongly nonlinear relationship with the differential stress or the effective plastic stress. The general form of the equation for each mechanism is presented by Equation (3.9).

$$\dot{\varepsilon} = \left[A \exp\left(\frac{-Q}{RT}\right)\left(\frac{\sigma_{eq}}{\sigma_0}\right)^n\right] \tag{3.9}$$

Where, A is the structural factor of mechanism, Q is the energy activation associated with the mechanism, R is the universal gas constant, T is the temperature, n is the gradient obtained by diagram $\ln(\varepsilon)$ versus $\ln(\sigma_{eq})$, σ_{eq} is the deviatoric stress, σ_0 can be the shear modulus (G), or the predetermined limit stress that denotes the beginning of a specific mechanism or the passage from

one mechanism to another (Dusseault & Fordham, 1995).

The discussion of the deformation mechanisms is the subject of numerous studies and researches about the creep of saline rock and other types of rock. The conceptual discussion of some important types of deformation by creep, by mass diffusion and the two dominant types of distortion, dislocation glide and dislocation climb, can be found in Turcotte & Schubert (1982) and Dusseault & Fordham (1995).

3.3.3.1 Multi-mechanism deformation model

The model that incorporates all the deformation mechanisms that are active and relevant to the oil industry is the multi-mechanism model (Multimechanism Deformation - MD), developed by Munson & Dawson since 1979 in the Sandia research group.

Five micro-mechanical deformation mechanisms underlie this law, but only three are of interest to the oil industry, namely the dislocation glide, dislocation climb and an undefined mechanism presented by Equation (3.10), Equation (3.11) and Equation (3.12), respectively.(3.12)

$$\dot{\varepsilon}_{DG} = \left[A_1 \exp\left(\frac{-Q_1}{RT}\right)\left(\frac{\sigma_{eq}}{2K}\right)^{n_1}\right] \tag{3.10}$$

$$\dot{\varepsilon}_{DCL} = H(\sigma - \sigma_0)\left[B_1 \exp\left(\frac{-Q_1}{RT}\right) + B_2 \exp\left(\frac{-Q_2}{RT}\right)\right]\sinh\left[\frac{q(\sigma_{eq} - \sigma)}{G}\right] \tag{3.11}$$

$$\dot{\varepsilon}_{UMC} = \left[A_2 \exp\left(\frac{-Q_2}{RT}\right)\left(\frac{\sigma_{eq}}{G}\right)^{n_2}\right] \tag{3.12}$$

Where, $\dot{\varepsilon}$ is the creep strain rate, A_i e B_i are the constants of mechanism, n_i are the stress exponents, Q_i are the activation energies associated with the mechanisms, R is the universal gas constant, T is the temperature, σ_{eq} is the deviatoric stress, σ_0 is the limit stress of deformation mechanism, K is the Bulk modulus, G is the shear modulus and H is the Heaviside step function.

Thus, the steady-state creep rate for this model is given by the sum of the three deformation mechanisms presented by the Equation (3.13).

$$\dot{\varepsilon}_{ss} = \dot{\varepsilon}_{DG} + \dot{\varepsilon}_{DCL} + \dot{\varepsilon}_{UMC} \tag{3.13}$$

The greatest contribution of one or the other mechanism depends on the temperature and deviatoric stress conditions to which the evaporite rock is

subjected.

The contribution of transient creep is inserted into the model based on retroanalysis with a secondary creep rate as presented by Equation (3.14).

$$\dot{\varepsilon} = F\dot{\varepsilon}_{ss} \tag{3.14}$$

Where, $\dot{\varepsilon}$ is the transient/steady-state creep rate, $\dot{\varepsilon}_{ss}$ is the steady-state creep rate calculated by Equation (3.13) and F is the transient function given by Equation (3.15).

$$F = \begin{cases} \exp\left[\Delta\left(1 - \dfrac{\zeta}{\varepsilon_t^*}\right)^2\right] & \rightarrow \zeta < \varepsilon_t^* \\ 1 & \rightarrow \zeta = \varepsilon_t^* \\ \exp\left[-\delta\left(1 - \dfrac{\zeta}{\varepsilon_t^*}\right)^2\right] & \rightarrow \zeta > \varepsilon_t^* \end{cases} \tag{3.15}$$

Where, Δ and δ are the hardening and softening parameters, respectively, and ζ is an internal isotropic hardening variable subjects to evolution law given by Equation (3.16).

$$\dot{\zeta} = (F - 1)\dot{\varepsilon}_{ss} \tag{3.16}$$

The hardening and softening parameters are presented by Equations (3.17) and (3.18), respectively.

$$\Delta = \alpha_h + \beta_h \log\left(\frac{\sigma_{eq}}{G}\right) \tag{3.17}$$

$$\delta = \alpha_s + \beta_s \log\left(\frac{\sigma_{eq}}{G}\right) \tag{3.18}$$

Where, α_h, β_h, α_s and β_s are constants.

In general, softening is not considered in the main geomechanical problems of saline rocks.

Considering that the formulation of the steady-state creep is independent of the transient one, it is necessary to determine, in the experimental creep curve, the value of the intercept of the line that corresponds to the secondary phase of creep in the ordinate axis (ε_t^*). This intercept is necessary to determine the K_0 parameter, in the primary stretch estimate, based on the empirical relationship presented by the Equation (3.19) by Munson & DeVries (1991).

$$\varepsilon_t^* = K_0 \exp(cT) \left(\frac{\sigma_{eq}}{G}\right)^l \quad (3.19)$$

Thereby, the multi-mechanism model is one of the most sophisticated physical models available for numerical creep simulations in saline rocks. However, this fact reflects a large number of parameters required by the model, totaling 16 parameters and more those of elasticity. Thus, due to the lack of laboratory tests under various conditions of temperature and stress, the use of this model becomes limite (Firme, 2013).

Table 3.5 presents the parameters of Multi Mechanism Model determined for the Brazilian halite.

Table 3.5 – Multi Mechanism Model – Paramenters of Brazilian halite.

Multi Mechanism Model – Paramenters of Brazilian halite		
Dislocation Climb		
A_1 (s^{-1})	Structure factor of DCL	1.638(10^{27})*
Q_1 (J/mol)	Activation energy of DCL	104500.0***
n_1	Stress power of DCL	7.2*
Undefined Mechanism		
A_2 (s^{-1})	Structure factor of UMC	1,924(10^{6})*
Q_2 (J/mol)	Activation energy of UMC	41800.0***
n_2	Stress power of UMC	3.2*
Dislocation Glide		
σ_0 (MPa)	Reference stress of DGL	20.57***
q	Stress constant	5335.0***
B_1 (s^{-1})	Structure factor of DGL	9,981(10^{6})**
B_2 (s^{-1})	Structure factor of DGL	4,976(10^{-2})**
Primary creep		
l	Theoretical constant	3.0***
K_0	Limit factor of transient creep	7.750(10^{4})*
c (K^{-1})	Constant related to the activation process	9.198(10^{-3})***
Hardening and Softening		
α_h	Fitting parameters for hardening	-17.37***
β_h		-7.738***
δ	Softening parameter**	0.58***

Universal gas constant (K) = 8.314 J/mol.K
* Calibrated by Firme (2013) from experimental data presented by Poiate (2012);
** Big Hill Salt, from Fossum & Fredrich (2002);
*** WIPP standard, from Fossum & Fredrich (2002).

3.3.3.2 Double mechanism model

The double mechanism model is based on the multi-mechanism model, where both assume the dominance of one mechanism over the others according to the level of deviatoric stress. However, this model restricts the application of the multi-mechanism law to the stationary creep interval, disregarding the dislocation climb mechanism. Thus, the constitutive equation of double mechanism is presented by the Equation (3.20).

$$\dot{\varepsilon}_{total} \quad \dot{\varepsilon} = \dot{\varepsilon}_0 \left(\frac{\sigma_{eq}}{\sigma_0}\right)^n \exp\frac{Q}{R}\left(\frac{1}{T_0} - \frac{1}{T}\right) \tag{3.20}$$

Where, $\dot{\varepsilon}$ is the creep strain rate in the steady-state, $\dot{\varepsilon}_0$ is the reference creep strain rate, σ_{eq} is the deviatoric stress, σ_0 is the reference deviatoric stress, Q is the activation energy, R is the universal gas constant, T_0 is the reference temperature, T is the absolute temperature of rock at the analyzed depth, n is the stress exponent.

Considering the change in the mechanism acting on creep, n assumes its value from the level of applied stresses, according to the Equation (3.21).

$$n = \begin{cases} n_1 & ; \quad \Delta\sigma < \sigma_0 \\ n_2 & ; \quad \Delta\sigma > \sigma_0 \end{cases} \tag{3.21}$$

The reference strain creep rate ($\dot{\varepsilon}_0$) corresponds to the steady-state strain rate achieved in a test performed at the reference temperature (T_0) under the reference stress (σ_0), which marks the change between the creep regimes deformation, that is, the pair of values (σ_0, $\dot{\varepsilon}_0$) corresponds to the intersection of two lines adjusted in a deformation versus applied deviatoric stress graph, on the log(ε) x log(σ_{eq}) (Poiate, 2012).

The thermal activation factor, represented by the term $\exp\frac{Q}{R}\left(\frac{1}{T_0} - \frac{1}{T}\right)$, can be considered as a constant defined as a function of temperature, acting as a multiplication factor of the reference deformation speed. In addition, the parameters $\dot{\varepsilon}_0$, σ_0, n_1 and n_2 are obtained through laboratory creep tests under controlled conditions of temperature and differential stress (Poiate, 2012).

Poiate (2012) presents triaxial creep tests obtained in salt specimens with confinement pressures of 10 MPa, axial pressures of 16 to 30 MPa and a range of temperatures.

Figure 3.3 shows on a log-log scale the relationship between the creep strain rate and the differential stress applied in the tests, varying from 6 to 20 MPa, for the temperature of 86 °C for halite (Poiate, 2012).

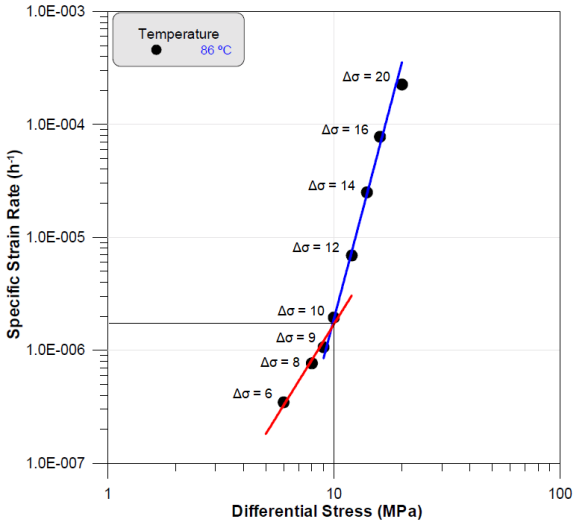

Figure 3.3 – Creep deformation rate in steady state as a function of the differential stress at a temperature of 86 ºC for halite (Modified from Costa et al., 2005).

For the tests with a temperature of 86 °C, 9.91 MPa of applied deviatoric stress and 1.888x10^{-6} deformation rate are found to have a threshold for changing the deformation regime of the halite, in which the slope (n) goes from 3.36 to 7.55. Therefore, the constitutive equation for halite at a temperature of 86 °C is given by Equation (3.22).

$$\dot{\varepsilon} = 1.888 \times 10^{-6} \left[\frac{\sigma_{eq}}{9.91}\right]^{n} \tag{3.22}$$

Where, $n = 3.36$ for $\sigma_{eq} \leq 9.91$ MPa or $n = 7.55$ for $\sigma_{eq} > 9.91$ MPa.

Table 3.6 summarizes the properties adopted for Brazilian halite.

Table 3.6 – Double Mechanism Model – Parameters of Brazilian halite (Poiate, 2012).

Double Mechanism Model – Parameters of Brazilian halite		
σ_0 (kPa)	Mechanism change stress (Prandtl limit)	9910.0
$\dot{\varepsilon}_0$(h^{-1})	Strain rate of mechanism change	1.888(10^{-6})
T_0 (°C)	Mechanism change temperature	86.0
n_1	Stress exponent for dislocation glide	3.36
n_2	Stress exponent for pressure solubilization (undefined mechaninsm)	7.55
Q (kcal/mol)	Activation energy for both mechanisms	12.0
R (kcal/mol.K)	Universal gas constant	1.9858(10^{-3})

3.3.3.3 Enhanced double-mechanism creep laws

Enhanced double-mechanism models present a way to encompass deformation due to transient creep in the double-mechanism model, which presents good performance in steady-state creep prediction. In this way, enhanced double mechanism considers that the standard version of the double mechanism model is already validated and open for improvement.

Firme et al. (2018) present two alternatives to account the transient creep in the double mechanism model , the first by coupling the transient function of Sandia's multi-mechanism deformation model (EDMT model) as presented by the item 3.3.3.1 and the second by coupling the empirical model of the power law (EDMP model) as presented by the item 3.3.2.1. According the author, both methods were successful in treating transient creep and in simulating experimental results.

The improvement of the double mechanism law is especially important in short-term creep analyses or long-term analyses subject to significant deviatoric stress over time, that is, whenever the transient creep is active and needs to be monitored, as in tests of triaxial fluency, maintenance of the well and integrity of the salt caverns throughout the period of operation.

According Firme et al. (2018), the choice between EDMT and EDMP depends on the data available. In cases of availability of primary creep curves until the start of secondary creep, the necessary transient parameter for this model can be determined. In this case, since it simulates the transient creep in a more intrinsic way, EDMT model is preferable. However, in the absence of experimental curves, the EDMP model can be adopted, showing itself capable of providing good estimates of primary or transient creep.

A greater level of detail on enhanced double-mechanism creep laws can be found in Firme et al. (2018).

4
Computational methodology

4.1 Introduction

The computational methodology developed is based on a set of processes that aim to simulate the annular closure of a well and to study the formation of natural barriers for permanent abandonment of oil wells at the end of their useful life.

For this, the simulation process is divided into steps that simplify simulating the stages of a well throughout its useful life using the finite element computational program Abaqus FEA as a calculation tool, called ABAQUS in this work.

The ABAQUS is a software suite utilized for finite element analysis and computer aided engineering. This software provides an interface for creating, submitting, monitoring, and evaluating results from simulations, using an implicit and/or explicit integration scheme (ABAQUS, 2017).

In addition, the user can make use of subroutines that are provided to increase the functionality of several software features for which the usual data input methods alone can be very restrictive (ABAQUS, 2017).

ABAQUS interface is divided into modules, where each module defines a logical aspect of the modeling process. In the case of simulation of annular closure problems, the process can be summarized in the definition of geometry, definition of material properties, generation of a mesh, definition of simulation steps, definition of boundary conditions, application of loads and result analyses. Figure 4.1 presents the general flowchart of the numerical simulation procedure proposed for the evaluation of the formation of an annular salt barrier.

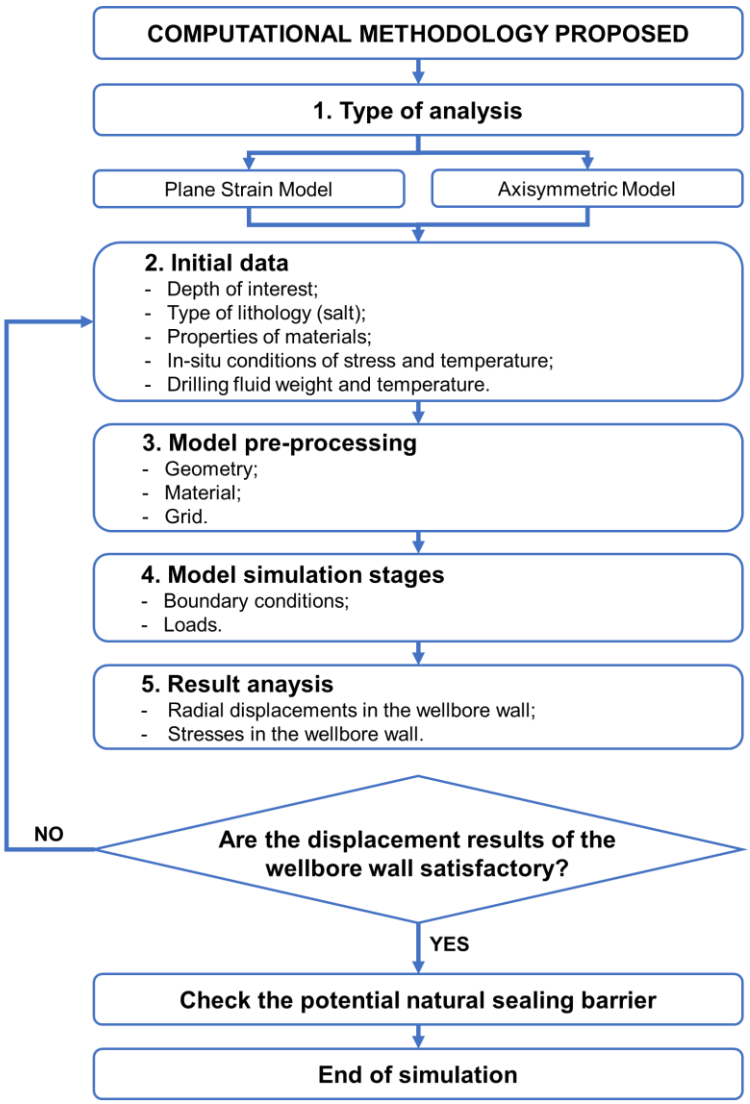

Figure 4.1 – Flowchart of the numerical simulation protocol.

Modeling for well closure analyses can be performed using 2D models for situations where there is a symmetry condition of one or two axis. These two-dimensional models represent a great computational economy and, if well used, usually lead to good results, being conservative, but maintaining the same order of magnitude as the results obtained by three-dimensional models (Firme, 2013).

Evidently, two-dimensional models are limited to a set of possible scenarios of wells, lithology and construction conditions. In the case of simulating inclined, directional or bilateral wells, as well as certain imperfections, it is necessary to use three-dimensional models. However, for general understanding of the study, global analyses, design estimates and validations, 2D models are extremely useful and fast (Firme, 2013).

Thus, the study carried out in this work assumes a vertical well crossing the salt layer thickness and makes use of two types of two-dimensional models

considering a cross-section and longitudinal section of a well through an axisymmetric model and a plane strain model, respectively.

The cross-section is simulated by a plane strain model that adopt the simplifying hypothesis of a plane state of deformations, considering the transversal symmetry, perpendicular to the axis of the well. This analysis takes into account only one type section at a given depth, not taking into account the general well behavior in the lithology.

In the case of the longitudinal section of the well, the simulation is done using an axisymmetric model, considering the symmetry around the axis of the well, that is, the longitudinal symmetry. Thus, the analysis encompasses loading and geothermal conditions that vary with depth.

Considering the axis of symmetry, the modeling will be reduced to a quarter of the section in plane strain model, and half in the axisymmetric model in order to reduce computational costs.

In order to implement and evaluate the computational methodology elaborated, part of the cases presented in Orlic et al. (2019) were reproduced. This work was chosen as a reference work because it presents the simulation components of well abandonment operation and formation of a natural barrier since the conceptual approach followed was the removal of a casing section, causing the unbalance of the stresses and, consequently, the salt creep to the uncased section of the wellbore, thereby reinstating the original natural salt seal.

The analyses were made at three depths in the reference work: 2000 m, 2500 m and 3100 m. These cases were reproduced by the project to evaluate the formation of natural barriers in shale and salt developed by the Technology and Petroleum Engineering Group (GTEP) at the Pontifical Catholic University of Rio de Janeiro (PUC-Rio). However, in this work only the results obtained for the depth of 3100 m are presented, as it is a critical modeling case.

Thus, the modeling parameters and conditions used are presented, as well as the results obtained comparing them with the results published in the reference work.

It should be noted that in this work, the simulator adopted was ABAQUS, while in Orlic et al. (2019) the calculation tool used was the Diana (DIANA FEA, 2018). However, both use the finite element method and, therefore, their results of simulations are compared in this work.

4.1.1 Linearity and nonlinearity

The present study is based on numerical simulations using the finite element method. In this way, some approaches used can influence the results obtained, such as the consideration or not of sources of nonlinearity.

The analyses carried out by ABAQUS consider that the initial condition for each step is the final condition of the last simulated step, causing the model state to evolve along the history of the analysis steps. This evolution occurs as the model responds to the loading history of the simulation stages, which may result in a linear or nonlinear response.

Thereby, nonlinear stress analysis problems can contain up to three sources of nonlinearity: material nonlinearity, geometric nonlinearity, and boundary nonlinearity. In the case of modeling the well abandonment problem the three sources can be identified.

With regard to the material, nonlinearity is considered through the constitutive law adopted for the simulation. For the creep modeling in salt rocks, the constitutive models presented in item 3 of this work demonstrate the equations that predispose the nonlinear behavior of the material considered by ABAQUS.

Boundary nonlinearity occurs when boundary conditions change during analysis. In the case of the annular closure of an oil well, the change in the boundary condition occurs at the moment of contact between the salt and the casing. When contact occurs during the simulation, there is a large and instantaneous change in the response of the assembly, as displacement in the wellbore wall is prevented, and thus the rock response is no longer linear.

This condition was applied in order to recognize the contact between the two parts of the model: salt and casing. However, in a finite element analysis, contact conditions are a special class of discontinuous constraint, allowing forces to be transmitted from one part of the model to another. The constraint is discontinuous because it is applied only when the two surfaces are in contact. When the two surfaces separate, no constraints are applied.

Finally, geometric nonlinearity is related to changes in the geometry of the model during the analysis. Geometric nonlinearity occurs whenever the magnitude of the displacements affects the response of the structure. In this way, it is inferred that the creep problem in salt is susceptible to this condition due to its high strain rate.

However, this is a single source of nonlinearity chosen optionally in the analyses. ABAQUS geometrically divides its analyses into small- and large-displacements. The problem defined as an analysis of small displacements

disregards the geometric nonlinearity in the calculations of the element, causing the kinematic relations to be linearized.

The elements in a small displacement analysis are formulated using the original nodal coordinates. The errors in such an approximation are in the order of deformations and rotations compared to the unit. The approach also eliminates the possibility of capturing the reduction in the deformation rate, which is a relevant aspect of this study.

On the other hand, in an analysis that includes the effects of large-displacement, most elements are formulated in the current configuration using the current nodal positions. In this case, the stiffness matrix is changed at each integration according to the deformation of the element, updating the nodal position. The elements, therefore, distort from their original forms as the deformation increases. With sufficiently large deformations, the elements can become so distorted that they are no longer suitable for use, as is the case with high creep strain rates in an extended annular.

Importantly, all physical structures exhibit nonlinear behavior. However, linear analysis is a convenient approach due to the reduction of computational costs involved, being generally suitable for design purposes that aim to reduce problems involving numerical instability and costs. This is because, in a nonlinear implicit analysis, the stiffness matrix of the structure must be assembled and inverted several times during the course of the analysis, making it much more expensive to solve than a linear implicit analysis. In the case of an explicit analysis, the increase in cost of a nonlinear analysis is due to reductions in the stable time increment, which must be very small for the solution to converge.

Therefore, these questions must be considered when choosing and interpreting the results of each type of analysis.

4.2 Initial Data

Following Orlic et al. (2019), simulation scenarios considered are characteristics of the Zechstein evaporate cap-rocks that cover many Rotliegend hydrocarbon reservoirs in Northwestern Europe.

Halite creep properties are based on the data previously reported in the salt mining industry and salt deformation is modeled taking into account the steady-state creep deformation mechanism driven by deviatoric stresses in the drilling and creep phases. The constitutive model for the steady-state creep used in simulations is the Double Power that combines two different terms: a power-law

(nonlinear) creep branch and a linear creep branch. Equation (3.8) presents the constitutive model of creep.

However, for the cases chosen for this study, only the first part of the equation is used, considering that the second part is not representative of the studied formations. Table 4.1 presents the creep parameters for halite.

Table 4.1 – Salt (halite) creep properties (Modified from Orlic et al., 2019).

Salt type	A_1 (1/day)	n_1	Q_1/R (K)	A_2 (1/day)	n_2	Q_2/R (K)
Zwd (base case) [1)]	0.053	5	6495	-	-	-
Bas-HNC [2)]	2.12	3.6	6495	-	-	-
Bas-LNC [3)]	0.82	3.6	6495	-	-	-

[1)] Zoudwending salt
[2)] Barradeel-HNC – High Nonlinear Creep parameters
[3)] Barradeel-LNC – Low Nonlinear Creep parameters

Physical and elastic properties of halite were the same in all simulations: density $\rho =$ 2180 kg/m³, Young's modulus $E =$ 30 GPa and the Poisson's coefficient $\nu = 0.3$.

Casing is modeled as pure elastic steel with Young's modulus $E = 200$ GPa and Poisson's coefficient $\nu = 0.27$.

The fluid type used in the drilling phase is a heavy mud with a density considered equal to 16 ppg that leads to pressures of 58.31 MPa to depth 3100 m, and then it is replaced by brine with N_2 above it, which leads to a pressure of 1 MPa.

Considering that the salt layer is located from 2 to 3.1 km, the in-situ isotropic state of stress in rock salt with the stress magnitude is dependent on the depth and average density of overlying rock formations, considered as $\rho =$ 2369 kg/m³ as shown in Figure 4.1. Thus, the scenario considered as critical in terms of computer simulation and reproduced by this work is the depth of 3100 m in which its geostatic conditions are presented in Table 4.2.

The contact between rock and casing considers mechanical interaction properties of frictionless as tangential behavior and "hard" contact as normal behavior.

Simulations are carried out by activating and deactivating the large deformation mode available in ABAQUS. This implies conditioning the solution in geometrically nonlinear and linear, respectively.

It is important to emphasize that the temperature of the fluid in the annular space is considered equal to the temperature of the formation, not considering heat exchanges and temperature changes during the simulation. Thus, the type of

analysis used in the simulation stages does not have thermal coupling.

Figura 4.1 – Simplified stratigraphy.

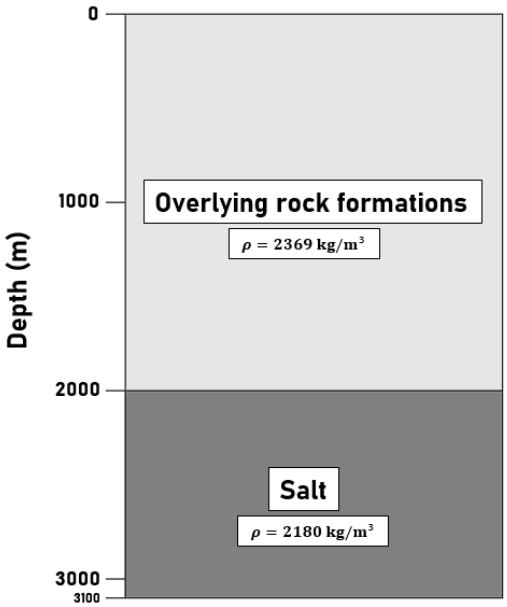

Table 4.2 – Input data for simulation scenarios (Modified from Orlic et al., 2019).

Depth (m)	In-situ isotropic stress (MPa)	In-situ temperature (°C)
3100	70	120

4.3 Model pre-processing

4.3.1 Plane strain model

The geometry of the two-dimensional numerical model of the near-well area is developed along a horizontal cross-section normal to the wellbore axis in the depth of 3100 m.

Following Orlic et al. (2019), the numerical models are considered the set-up with a small diameter casing for monitoring and testing introduced in an enlarged interval. Thus, the well diameter is 27.9 cm (11 inches) and the internal and external diameter of the casing is 6 cm (2.4 inches) and 7.6 cm (3 inches), respectively, generating an annular of approximately 10 cm. The outer model boundary was set at a radial distance of 50 m from the well axis.

Plane strain elements are used to allow the formulation of full three-dimensional stresses in the rock salt. Quadratic eight-node quadrilateral elements (with mid-nodes) and reduced integration are used for the solution.

The model was reduced to one quarter of the near-well area due to

symmetry considerations to reduces computational costs.

The distribution of elements and mesh refinement took into account the greater importance of the area close to the wellbore wall and the direction of greatest deformation of the elements, given the critical condition of the simulation that considers an enlarged annular subject to a high rate of salt creep.

In this case, as the creep occurs in an anisotropic way, the elements are deformed much more in the radial direction than in the tangential direction, presenting great distortion over time that can lead to numerical errors.

In order to avoid distortion of the element, the dimension of the element was reduced in the radial direction, making it more elongated in the tangential direction of the well. Thus, with the greater deformation in the radial direction of the element throughout the simulation, the difference between the size of the element faces tends to disappear, decreasing the distortion. Figure 4.2 presents the numerical model and mesh distribution.

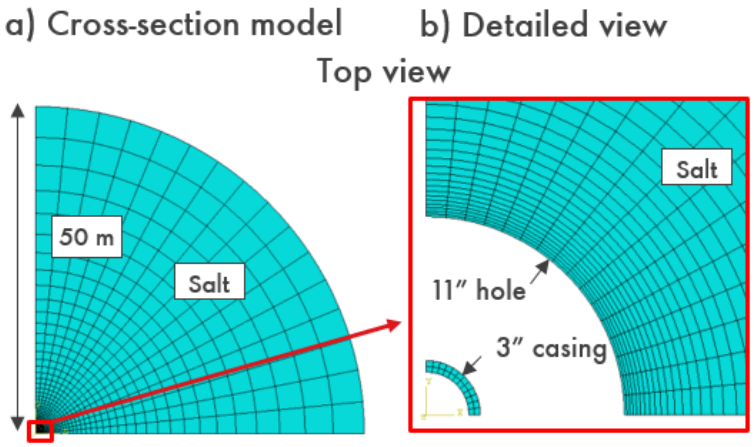

Figure 4.2 – (a) Mesh for a plane strain model of wellbore cross-section normal to the well axis, located in the middle of the reamed interval and (b) detailed view of the same model around the wellbore (Modified from Orlic et al., 2019).

4.3.2 Axisymmetric model

The axisymmetric model of the area close to the well is developed around the vertical axis of a well, modeling a longitudinal section that crosses a layer of salt.

The model is shaped like a 90 m high cylinder with a 50 m radius. The external limit of the model was defined in the same radial distance adopted for the model of the cross-section of the well. The concept of the study is the same as that of the plane strain model which consists of the removal of a section of the casing and the insertion of a small diameter casing (3 inches) for the purpose of monitoring and control.

Due to the removal of the casing, which was initially 7 inches, a reamed interval is obtained with 11 inches of wellbore diameter, generating an annular of approximately 10 cm. The reamed interval adopted by the authors is positioned in the middle of the model at a depth of 3100 m and has the magnitudes of 1 m and 10 m. The overload load is applied on top of the model to balance the system against in-situ stresses.

Axisymmetric elements are used to allow the formulation of complete three-dimensional stresses in rock salt. Quadratic quadrilateral elements of eight nodes (with mid-nodes) and reduced integration are used for the solution.

The model was reduced to half the area close to the well due to symmetry considerations to reduce computational costs.

The distribution of elements and mesh refinement was determined in the same way as in the plane strain model, which considers the greater importance of the area close to the wellbore wall and the direction of greater deformation of the elements throughout the simulation. Figure 4.3 shows the numerical model, as well as its mesh.

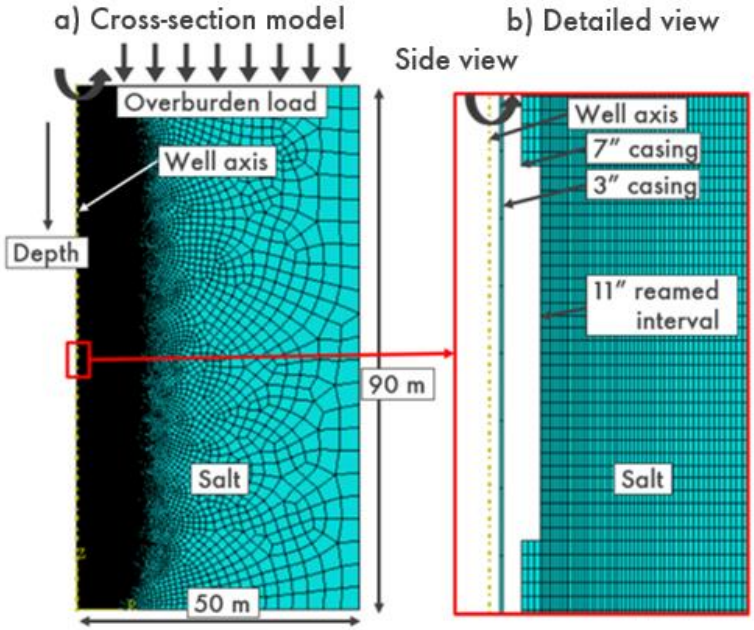

Figure 4.3 – (a) Mesh for an axisymmetric model around the axis of a wellbore and (b) detailed view of the reamed interval of the wellbore at the level of rock salt. Modified from (Orlic et al., 2019).

4.4 Model simulation stages

Three stages of analysis are conducted: geostatic, drilling and annular closure.

In the geostatic stage is inserted the field conditions of stress and temperature in the model. Boundary conditions are prescribed to restrict displacement in the normal direction to the outer limits of the models with a few exceptions mentioned below. For the plane strain model, the wellbore wall and the outer limit of the model are restricted on the x and y axes. In this way, zero horizontal and vertical displacement is guaranteed in this stage. In the axisymmetric model, the boundary condition of the upper limit of the model is not made with displacement restriction, but by applying the load referring to the layers overlying the top of the model. Figure 4.4 and Figure 4.5 present the boundary conditions in the first stage of simulations in the plane strain and axisymmetric model, respectively.

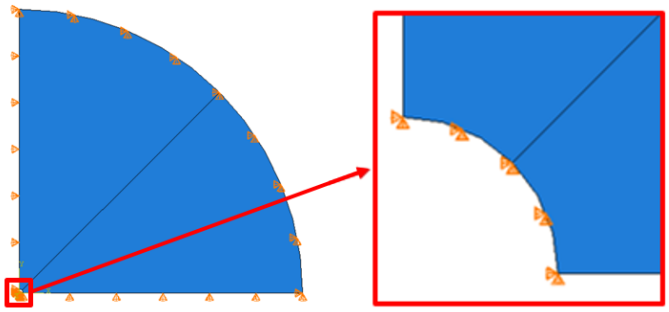

Figure 4.4 – Boundary conditions of geostatic stage in plane strain model.

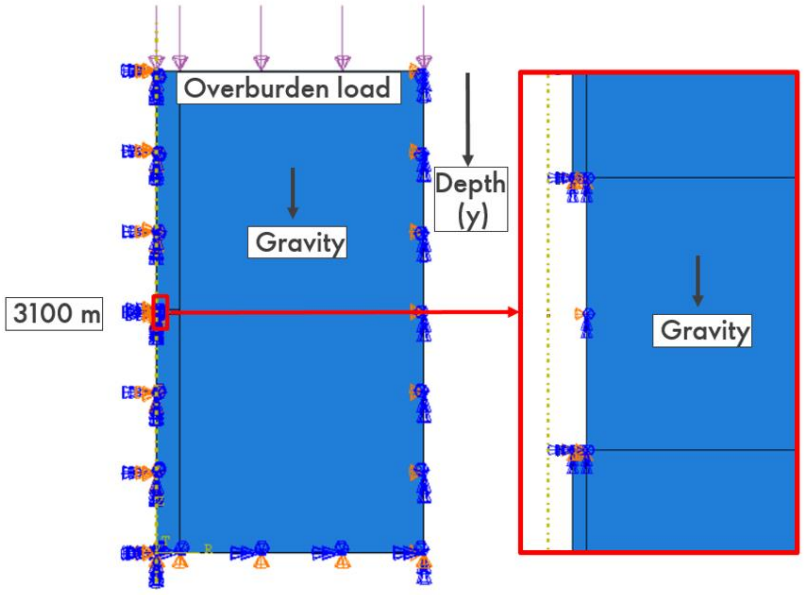

Figure 4.5 – Boundary conditions of geostatic stage in axisymmetric model.

The in-situ temperature is considered constant at each depth in the plane strain model. However, in the axisymmetric model, the temperature has a constant variation with the depth being equal to the temperature at depth of 3100 m,

reported in Table 4.2, in the middle of the model. Figure 4.6 presents the distribution of temperature in the axisymmetric model.

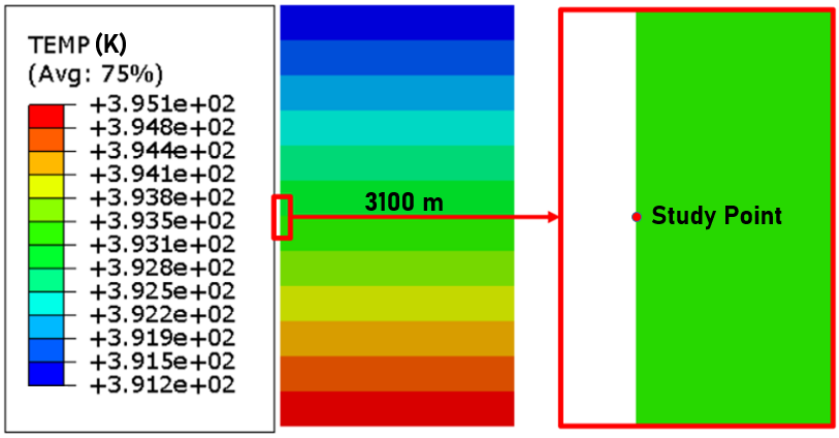

Figure 4.6 – Constant gradient of in-situ temperature in axisymmetric model.

In terms of in-situ isotropic stress, the procedure is given in a similar way to temperature, being constant in the plane strain model and varying according to the multiplication between the depth, density of the halite and gravity (g = 9.81 m/s²). Thus, the in-situ stress in the middle of the axisymmetric model is equal to the stress reported in Table 4.2 at the depth of 3100 m. Figure 4.7 presents the distribution of stress in the axisymmetric model.

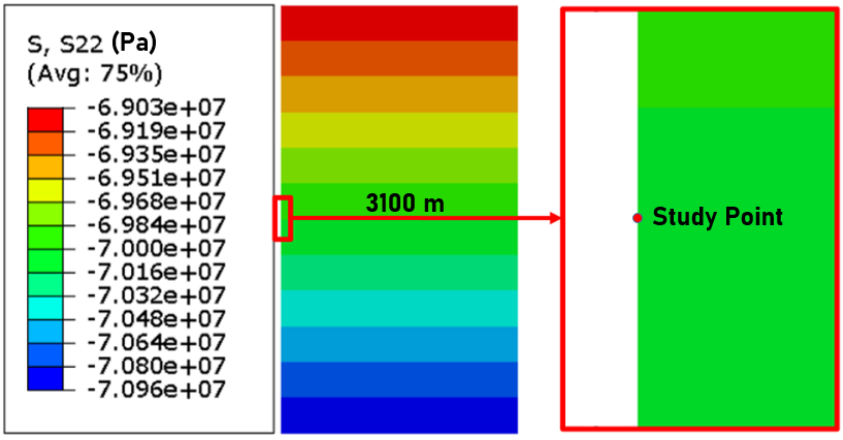

Figure 4.7 – Constant gradient of in-situ isotropic stress in axisymmetric model.

The drilling stage is divided into three sub-stages where the excavation of the well is simulated by removing the restrictions of the wellbore wall and a redistribution of stress that causes the displacement due to this disturbance in the formation.

In the first sub-stage, named drilling (1), the stress of the weight of the overload sediments inserted in the geostatic stage is reduced until reaching the

mud weight pressure, considered as 16 ppg, this procedure is made in 2 days of simulation time.

In the second sub-stage, drilling (2), the pressure caused by the weight of the mud on the borehole is held constant during 3 days.

Finally, in the sub-stage drilling (3), the pressure is reduced to 1 MPa in 2 days due to the replacement of mud by brine in the reamed interval with N_2 above it. Table 4.3 presents the fluid pressure in drilling sub-stage and Figure 4.8 and Figure 4.9 present the boundary conditions in the drilling stage of simulations in plane strain and axisymmetric model, respectively.

Table 4.3 – Drilling sub-stages (Modified from Orlic et al., 2019).

Sub-stages	Time (day)	Fluid pressure
Drilling (1)	0-2	Lithostatic pressure decreased to the pressure of heavy mud considered as 16 ppg
Drilling (2)	2-5	Heavy mud pressure
Drilling (3)	5-7	Heavy mud pressure decreased to 1 MPa

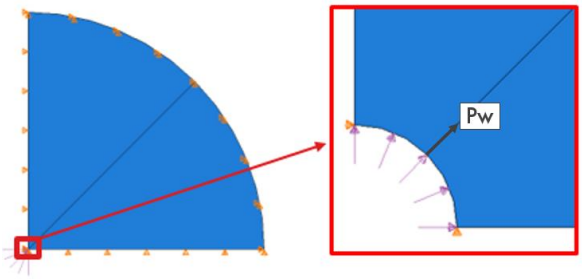

Figure 4.8 – Boundary conditions of drilling phase in plane strain model.

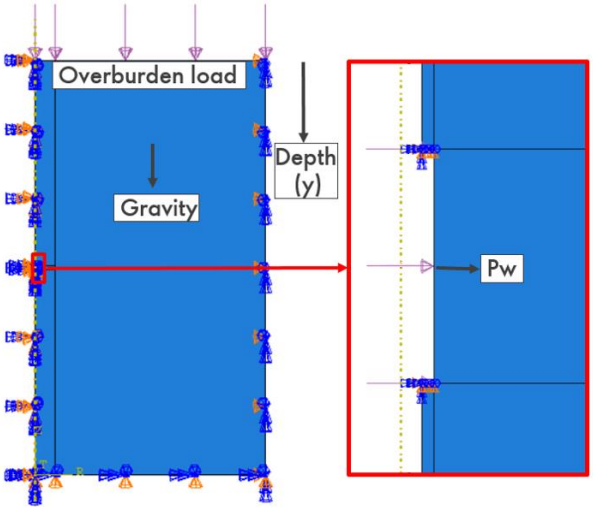

Figure 4.9 – Boundary conditions of drilling phase in axisymmetric model.

The last stage of simulation is called annular closure where is inserted the casing. The pressure of 1 MPa is held constant until the end of 70 days of simulation.

In this stage, boundary conditions are the same as the drilling stage plus the contact boundary condition that corresponds a special class of discontinuous constraint because it is applied only when the two surfaces are in contact. This contact condition allows the analysis detects when the two surfaces come into contact and apply the contact constraints accordingly, allowing forces to be transmitted from one part of the model to another.

4.5 Result analysis – Plane strain model

4.5.1 Stress analysis

The reference work does not present the analysis of the stresses acting on the model. However, such analysis is an important indication of the correct behavior of the model and the results obtained. Thus, the analysis of stresses is done autonomously in this work, without comparison with the reference work.

Initially, the stresses are analyzed in order to verify the values applied as input data due to the steps used for the simulation, where the pressure exerted by the fluid on the wellbore wall varies in specific stages.

The critical analysis takes place at a depth of 3100 m because of the higher stress and temperature in-situ compared to other depths, causing high deviatoric stress and, consequently, a high deformation rate making the stresses imposed on the wellbore wall unstable. This instability is mainly verified when the analysis considers the mode of large deformations of the software, generating numerical instability in the simulation.

Figure 4.10, Figure 4.11 and Figure 4.12 present the behavior of the stresses over time until the closure of wellbore wall at depth of 3100 m for the three types of salt Zoudwending, Barradeel-HNC and Barradeel-LNC, activating and deactivating the mode of large deformations, that is, considering the geometric nonlinearity and linearity of the solution, respectively.

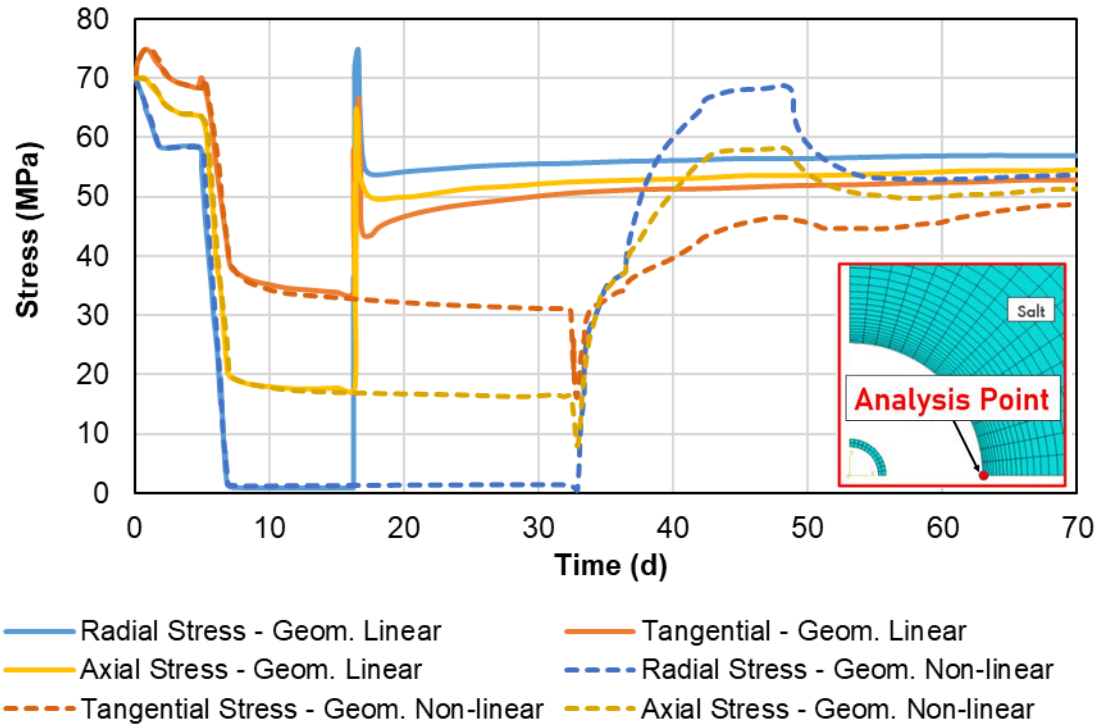

Figure 4.10 – Plane Strain Model – Stress behavior throughout the time of simulation at depth 3100 m in Zwd (base case).

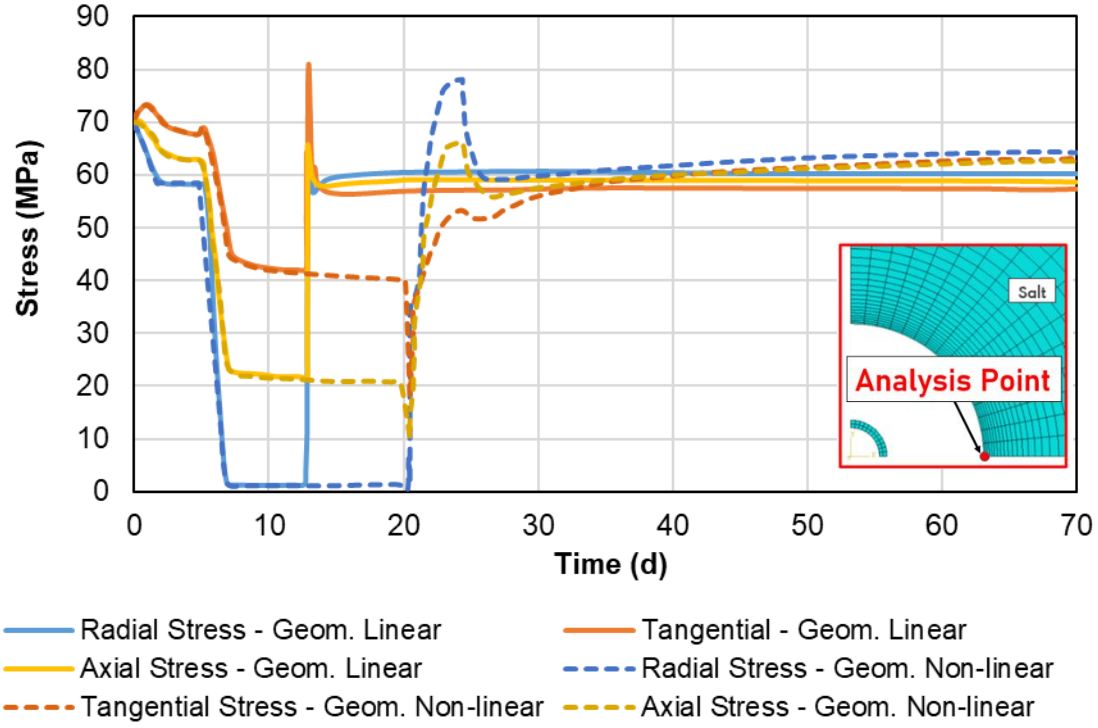

Figure 4.11 – Plane Strain Model – Stress behavior throughout the time of simulation at depth 3100 m in Bas-HNC case.

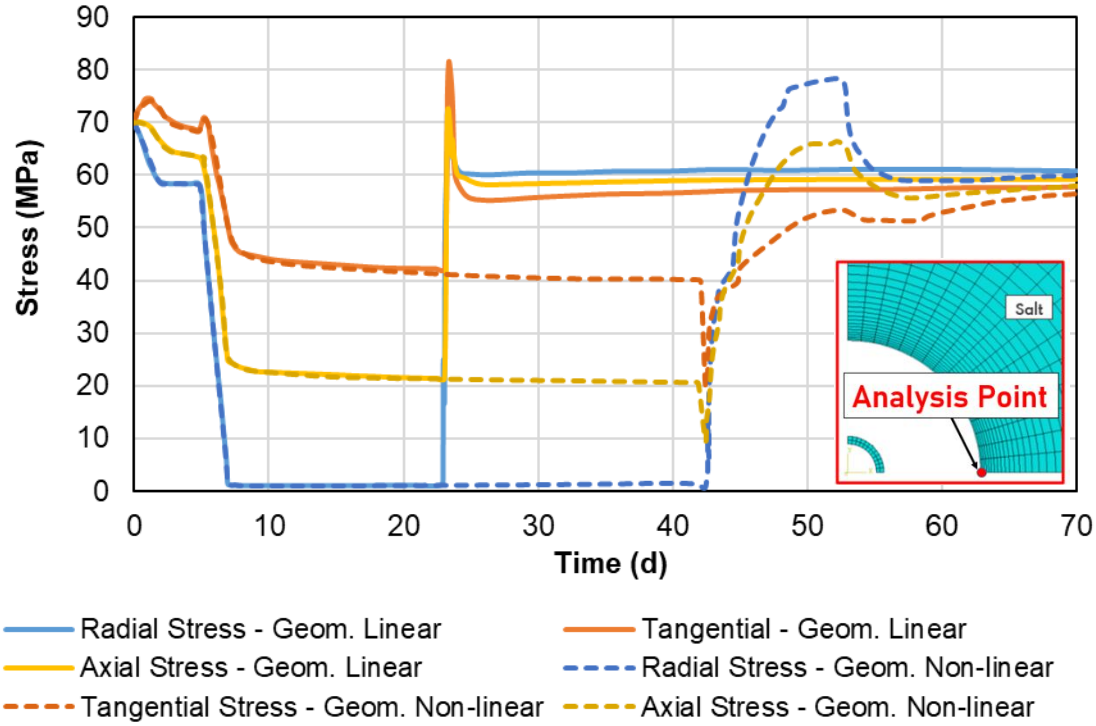

Figure 4.12 – Plane Strain Model – Stress behavior throughout the time of simulation at depth 3100 m in Bas-LNC case.

From the above, it is possible to notice that in all cases the model presents the radial stress congruent with the imposed stress as input data. However, when the formation reaches the casing, displacement is prevented and, consequently, stresses increase, including radial stress.

In this context, in the large strain mode, there is a drop in stress when the formation reaches the casing. This fact is attributed to a numerical instability caused by the distortion of the wellbore wall elements due to the large change in stresse state that occur instantly at this point which caused the stresses to drop. After the contact and stresses drop, it is likely that there will be a compensation for the ABAQUS error caused by numerical instability, raising the stresses again.

In both geometric linearity and nonlinearity approaches, it is possible to observe an unstable behavior of the stresses after contact and in most cases reaching levels higher than the in-situ formation stresses at the peak of the curve, which could lead to a fracture of the salt, being an unacceptable behavior for the formation of a natural barrier, since the rock fracture would open the way for the fluid to flow.

However, stresses tend to converge after a certain time, and in large strain mode this convegence occurs considerably slower, approximately after 10-15 days, while in small strain mode the convegence occurs in about 1 day. This is

because, considering the geometric nonlinearity, the mesh is more deformed throughout the simulation, making the model take more increments until it reaches convergence, as presented by Figure 4.13.

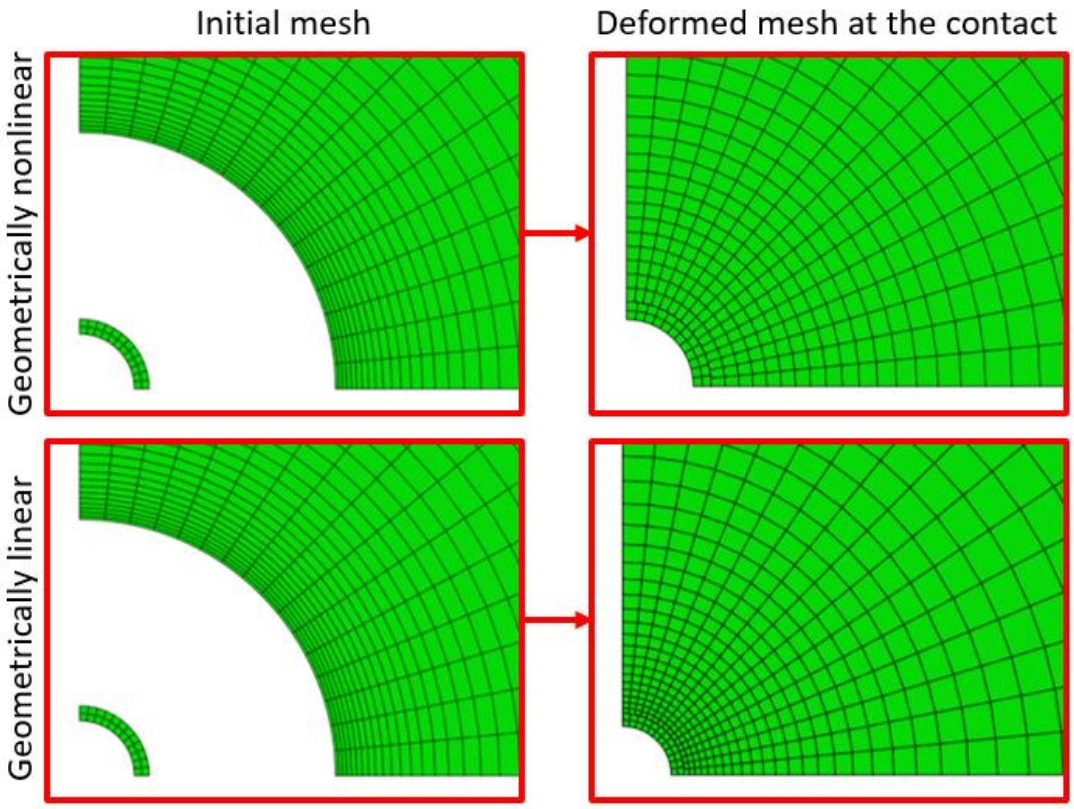

Figure 4.13 – Plane Strain – Deformation of the meshes at the moment of contact.

It is interesting to verify that after the instabilities, the rock stresses on the casing converge to similar values, around 55 MPa for Zwd salt and 60 MPa for Bas-LNC and Bas-HNC salt, that is, approximately 10-15 MPa below the in-situ stresses, with a slight upward trend of convergence to the in-situ stresse values. Thus, it is speculated that over time the rock will reach the initial stress value, before the disturbance due to drilling, returning to act as a natural seal for the reservoir.

All the observed instabilities can be attributed to the high deformation rate of the rock and the large annular dimension of about 10 cm, which is adopted by the concept used in the analysis of the reference work and aims to restore the natural salt seal, closing the entire space annular of an enlarged section. Such a concept creates a critical simulation condition with an unusual dimension in oil wells, generating the reported instabilities.

4.5.2 Displacement analysis

Due to the initial isotropic stress in rock salt and a perfectly circular shape of the section of study, the total radial displacement of all nodes at the wellbore wall is identical. Thus, Figure 4.14, Figure 4.15 and Figure 4.16 show the displacements obtained by the simulations in ABAQUS compared with results presented by Orlic et al. (2019) for the case at depth 3100 m. The caption *Nlgeom* refers to the activation or non-activation of the geometric nonlinearity of the solution.

Considering the results obtained with the ABAQUS large-deformation mode, the estimated closure times of the open-hole section in rock salt for the maximum achievable underbalanced in the section of study are in the range of 20-42 days for a depth of 3100 m as shown in Figure 4.14, Figure 4.15 and Figure 4.16. In the other hand, for the ABAQUS small-deformation mode, the estimated closure time in the study section is in the range of 13-23 days for a depth of 3100 m.

It is possible to observe that the closing times of the well presented in Orlic et al. (2019) are compatible with those chosen by the models that classify the small deformation mode. Small differences between displacements are observed, indicating divergences between the data used that are not present in the reference work.

However, the large-deformation mode has longer closure times than those observed in the reference work and in the small-deformation mode.

This difference generated by the consideration of geometric nonlinearity, refers to the fact that the geometrically nonlinear analysis updates the stiffness matrix at each iteration. This implies a great mesh deformation during the simulation and the stress redistribution over time, which generate less differential stresses in a larger and more deformed element and, consequently, a lower rate of deformation over time (Figure 4.13).

This fact is not captured by the geometrically linear analysis, preventing the model generated in the small-deformation mode from reproducing the behavior of decreasing strain rate due to salt creep over time.

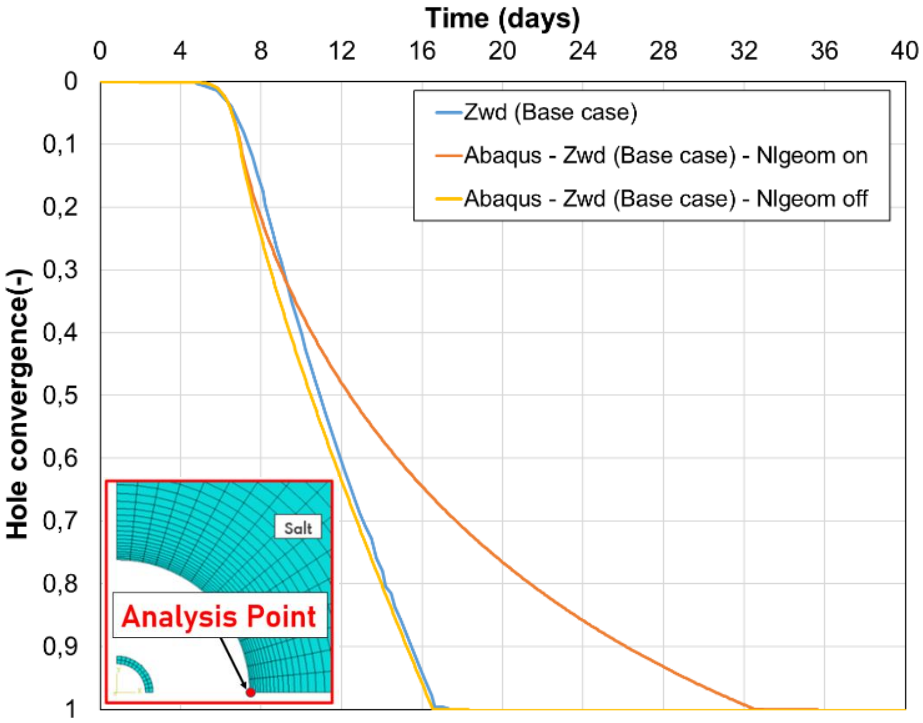

Figure 4.14 – Plane Strain Model – Displacements obtained by the simulations in the ABAQUS compared with results presented by Orlic et al. (2019) at depth of 3100 m in the Zwd (base case)

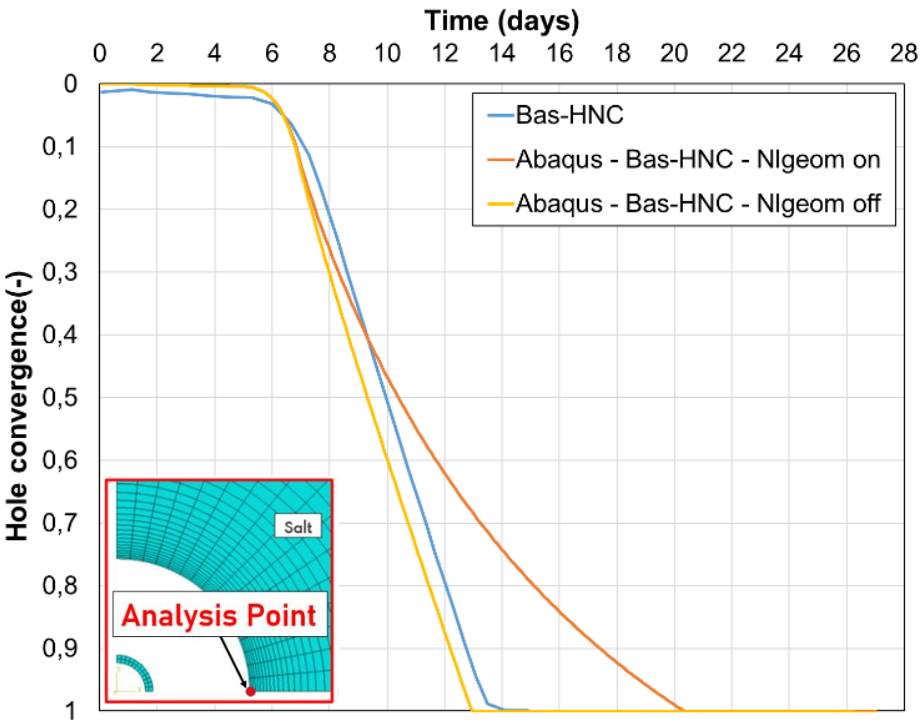

Figure 4.15 – Plane Strain Model – Displacements obtained by the simulations in the ABAQUS compared with results presented by Orlic et al. (2019) at depth of 3100 m in the Bas-HNC case

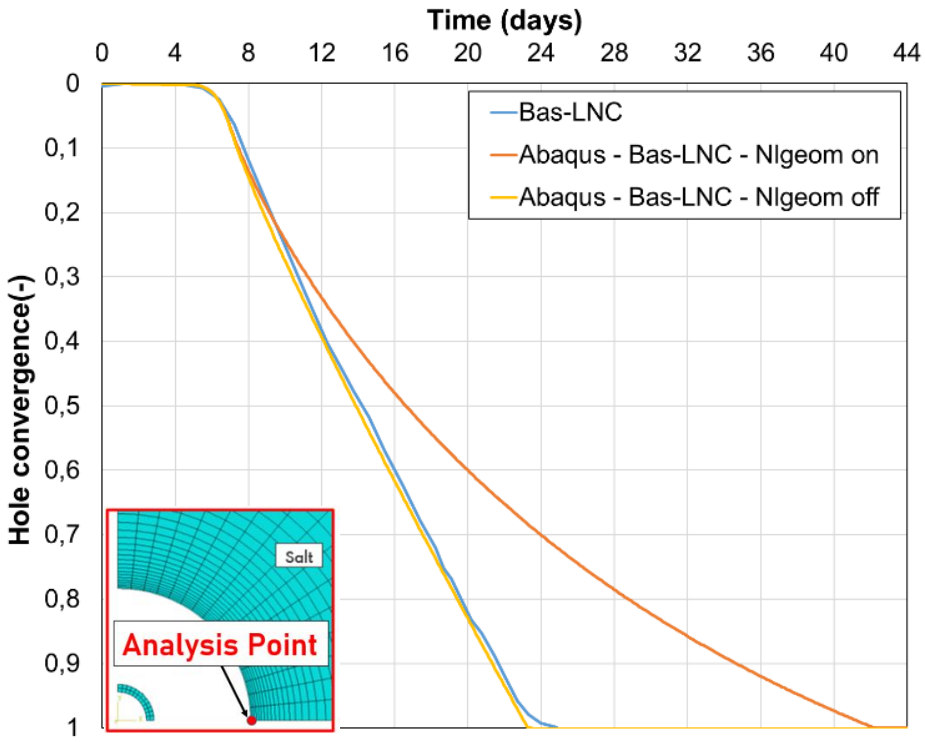

Figure 4.16 – Plane Strain Model – Displacements obtained by the simulations in the ABAQUS compared with results presented by Orlic et al. (2019) at depth of 3100 m in the Bas-LNC case

4.6 Result analysis – Axisymmetric model

4.6.1 Stress analysis

Figure 4.17 and Figure 4.18 show the behavior of the stresses of Zoudwending salt over time until the closure of wellbore wall at middle of the model with the reamed interval of 10 m and 1 m, activating and deactivating the mode of large deformations, that is, considering the geometric nonlinearity and linearity of the solution, respectively.

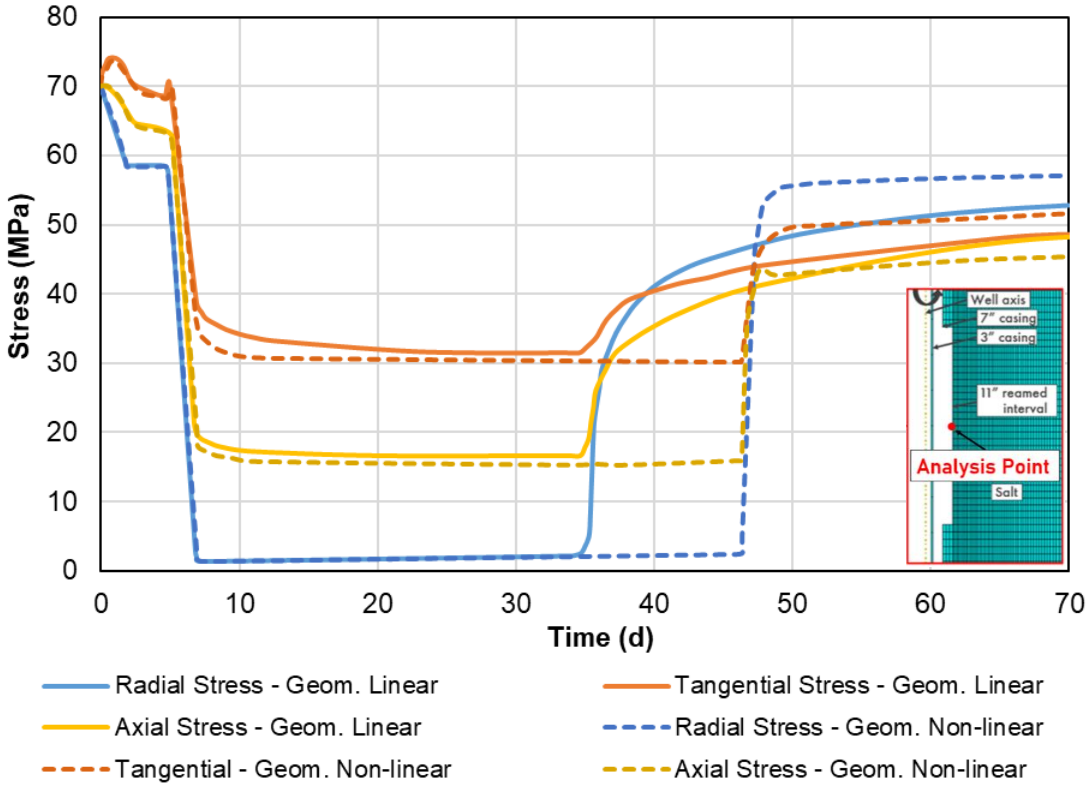

Figure 4.17 – Axisymmetric Model – Stress behavior throughout the time of simulation in Zoudwending salt in 1 m-long reamed interval case.

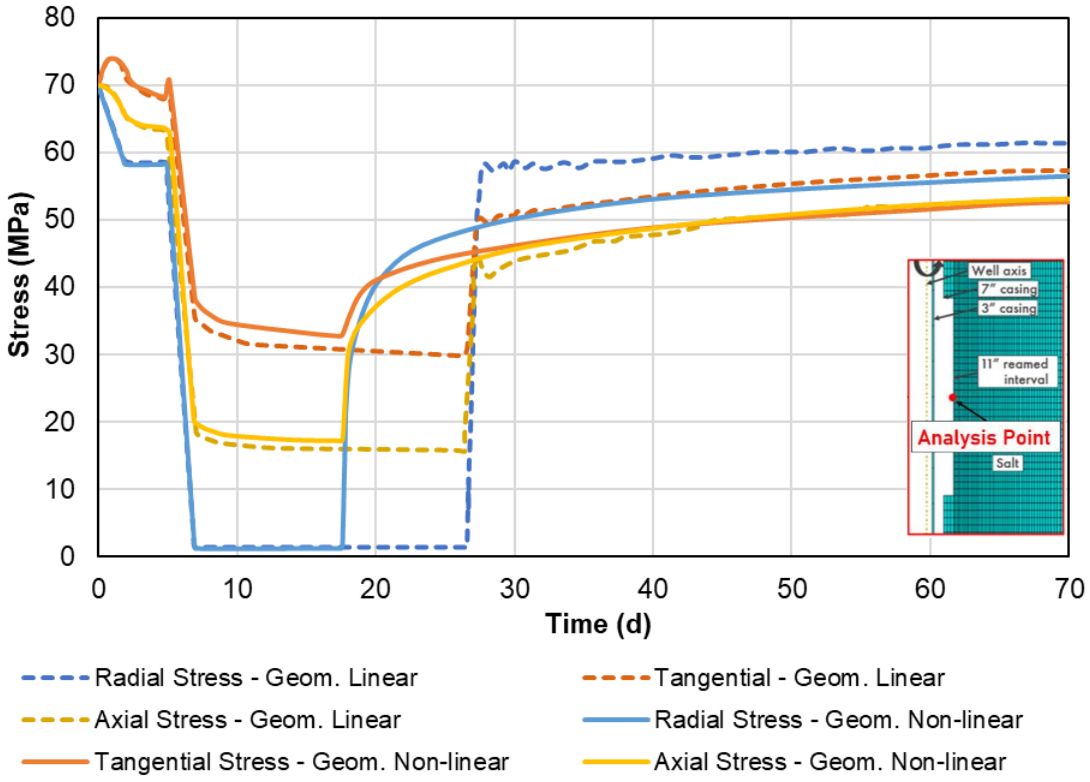

Figure 4.18 – Axisymmetric Model – Stress behavior throughout the time of simulation in Zoudwending salt in 10 m-long reamed interval case.

From the above, it is possible to notice that the model presents the radial stress congruent with the imposed stress as input data. However, just like in the plane strain model, when the formation reaches the casing, displacement is prevented and, consequently, stresses increase changing the radial stress from input data to a model response.

After annular closure, there is no drop or peak in the stresses as seen in the plane strain model. However, it is possible to observe an unstable behavior of the stresses after contact in the geometric nonlinearity approach, being treated as a numerical instability of the model.

It is also verified that the stresses after the contact between the salt and the casing converge to values of the same magnitude in the two approaches, being around 50 MPa for the case of the reamed interval of 1 m and between 50 MPa and 60 MPa for the reamed interval of 10 m, that is, approximately 10-20 MPa below the in-situ stresses.

Such stresses are lower than in-situ stresses with a slight upward trend. Thus, as in the plane strain model, it is speculated that over time the rock will reach the initial stress value, before the disturbance due to drilling, returning to act as a natural seal for the reservoir.

In addition, the stresses do not reach the level of in-situ stresses, demonstrating that there is no fracturing of the salt and indicating the possible barrier efficiency.

As in the plane strain model, all observed instabilities can be attributed to the critical conditions adopted for the simulation, which include the high rate of rock deformation and the large annular dimension of about 10 cm, causing high distortion in the elements of the wellbore wall.

4.6.2 Displacement analysis

The displacements obtained in the middle of the axisymmetric model are shown by Figure 4.19 and Figure 4.20, comparing with the results presented by Orlic et al. (2019). As it was presented before, the caption *Nlgeom* refers to the activation or non-activation of the geometric nonlinearity of the solution.

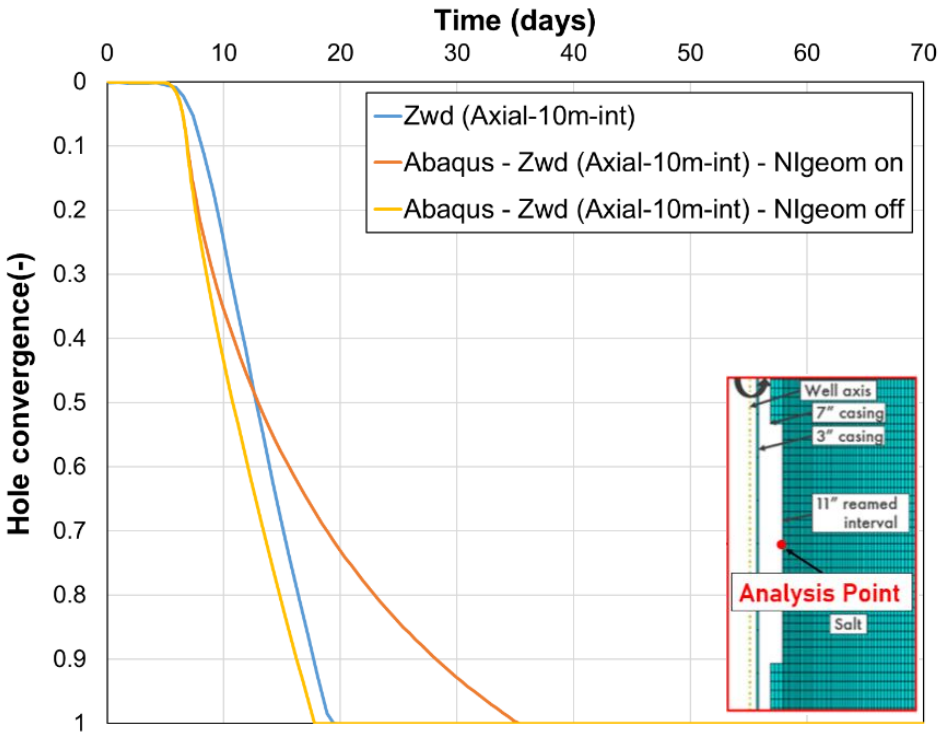

Figure 4.19 – Axisymmetric Model – Displacements obtained by the simulations in the ABAQUS compared with results presented by Orlic et al. (2019) around the 10 m-long reamed interval at a depth of 3100 m in the Zwd (base case).

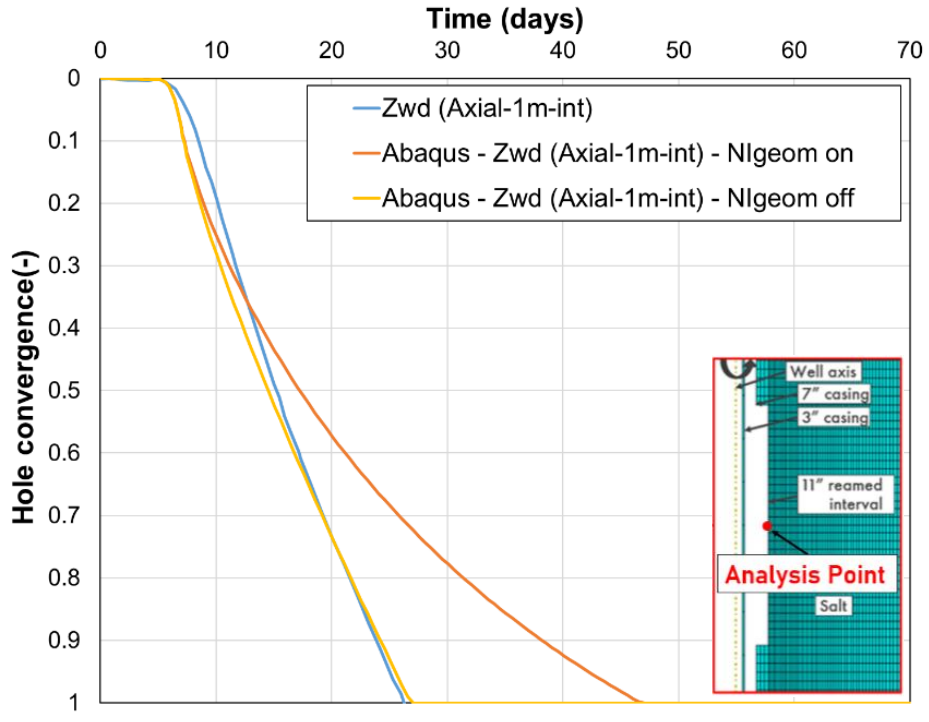

Figure 4.20 – Axisymmetric Model – Displacements obtained by the simulations in the ABAQUS compared with results presented by Orlic et al. (2019) around the 1 m-long reamed interval at a depth of 3100 m in the Zwd (base case).

As a result obtained by simulations of the axisymmetric model, the estimated closure times of the open-hole section in rock salt for the maximum imbalance attainable at a depth of 3100 m are in the range of:

- 35-47 days for the geometrically nonlinear analyses;
- 20-26 days for the geometrically linear analyses.

The axisymmetric model in terms of large and small deformation modes repeats the behavior achieved by the plane strain model.

Thus, it is possible to observe that the well closure times presented in Orlic et al. (2019) are smaller than estimated in a nonlinear solution, indicating that the closure occurs around 2 weeks earlier than the closure times indicated by the model that considers geometric nonlinearity. In addition, it is possible to notice the tendency of creep rate decrease over time demonstrated by the geometrically nonlinear model, which is not captured by the linear geometric model.

However, in the results obtained by linear geometric solution, or in the small deformation mode, the annular closure rates present results very close to those reported in the reference work. The differences observed between the results obtained by the simulations and the literature refer to the adopted data that are not found in the article, representing the uncertainties of model reproduction.

4.7 Uncertainties

In Orlic et al. (2019) the calculations are developed by the simulator Diana (DIANA FEA, 2018) while the presented analyses are developed by the simulator ABAQUS, both being finite element simulators. In addition, certain uncertainties that may be the cause of the divergence found between the simulations.

The specified drilling fluid weight as a heavy mud can be listed as uncertainty. The value adopted for the simulation was 16 ppg becoming 58.31 MPa for 3100 m, approximately.

Futhermore, the hole convergence used by the author to present the closure times of the wellbore is not specified. Thus, it is assumed as a relationship between the displacement of the wellbore wall and the annular space given by Equation (4.1).

$$HC = u/(w_r - c_r) \tag{4.1}$$

Where, HC is the hole convergence (-), u is the displacement of wellbore wall (m), w_r is the wellbore radius (0.1397 m) and c_r is the casing radius (0.0381 m).

Another uncertainty of the model is the mesh and its influence on the results. Even with the type of element specified by Orlic et al. (2019) the quantity and distribution of the elements is not mentioned and it is not possible to reproduce exactly the mesh used by the author.

Finally, stress analysis is not published in the reference paper. Taking into account that due to the high temperature and pressure conditions that cause a high degree of deformation in the simulations, the stresses can suffer oscillations. Thus, it is not possible to say that the simulations in Orlic et al. (2019) follow the stresses specified by the authors throughout the simulation, becoming another model uncertainty.

4.8 Analysis with new geometry

A new geometry was considered for the simulations in order to verify the occurrence of numerical instability in a more realistic geometry even under conditions of high temperature and high pressure.

In this way, the simulations take into account the critical condition of temperature and pressure given by the depth of 3100 m, according to Table 4.2. The creep parameters adopted are those of the base case (Zoudwending salt) presented in Table 4.1.

The other physical and elastic properties of the rock and casing, the constitutive model, the pressure caused by the weight of the drilling mud, element types and the simulation stages are the same as described in Sections 4.2 and 4.4.

In the plane strain model, the wellbore diameter is 37.5 cm ($14^3/_4$ inches) and the internal and external diameter of the casing is 23.5 cm ($9^1/_4$ inches) and 27.3 cm ($10^3/_4$ inches), respectively, generating an annular of approximately 5 cm. The outer model boundary was set at a radial distance of 50 m from the well axis.

The axisymmetric model is shaped like a 90 m high cylinder with a 50 m radius. The external limit of the model was defined in the same radial distance adopted for the plane strain model. To follow the concept of simulation used in Orlic et al. (2019), which consists of removing a section of the casing and inserting a small diameter casing for monitoring and control, the model consists of an initial casing of 32.4 cm ($12^3/_4$ inches) of diameter. Due to its removal, a reamed interval is obtained with a 37.5 cm ($14^3/_4$ inches) diameter of the wellbore and a 27.3 cm ($10^3/_4$ inches) diameter casing is inserted, generating an annular of approximately 5 cm. The reamed interval of 10 m is positioned in the middle of the model and has

the same dimensions as the plane deformation model.

Figure 4.21 and Figure 4.22 present the new geometry of simulations and mesh distribution of plane strain and axisymmetric models, respectively.

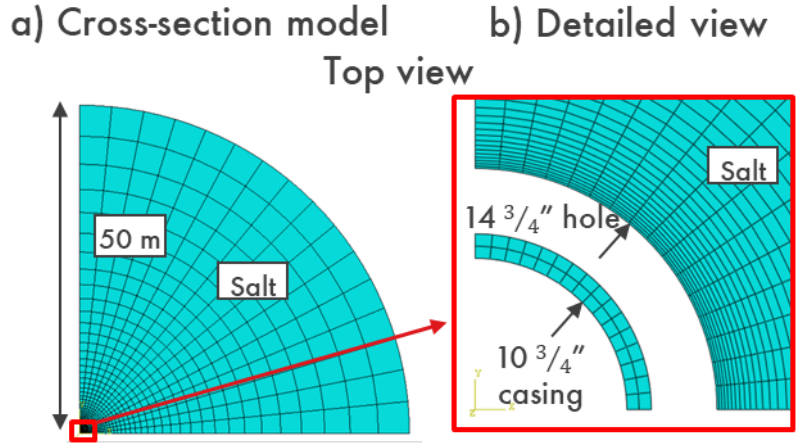

Figure 4.21 – (a) Mesh for a plane-strain model considering the new geometry and (b) detailed view of the same model around the wellbore.

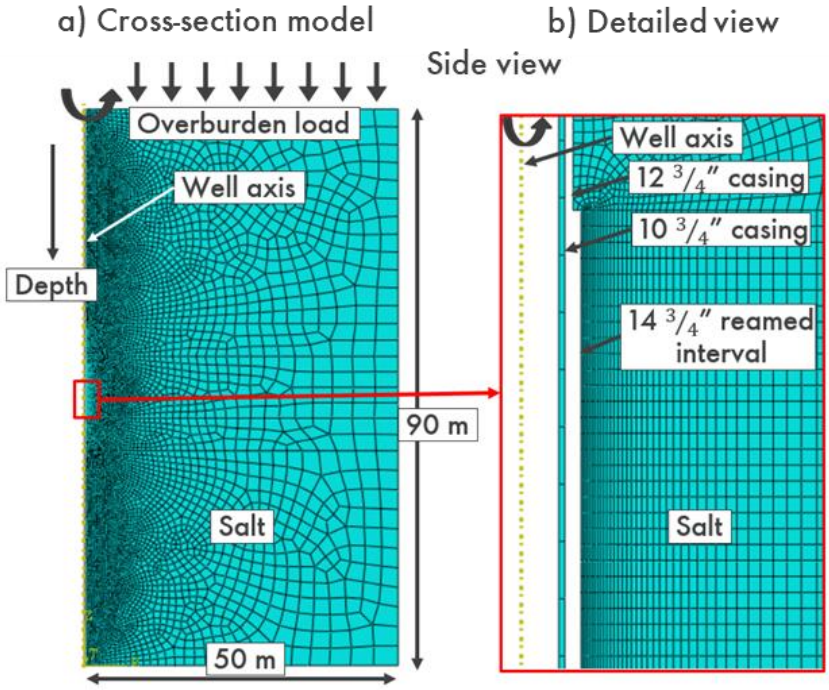

Figure 4.22 – (a) Mesh for an axisymmetric model considering the new geometry and (b) detailed view of the reamed interval of the wellbore at the level of rock salt.

4.9 Results analysis – New geometry

4.9.1 Stress analysis

Figure 4.23 and Figure 4.24 present the results of the simulations in stress

terms with the new geometry for the plane strain and axisymmetric models. The geometric nonlinearity and linearity of the solution are considered by activating and deactivating the mode of large deformations of the ABAQUS, respectively.

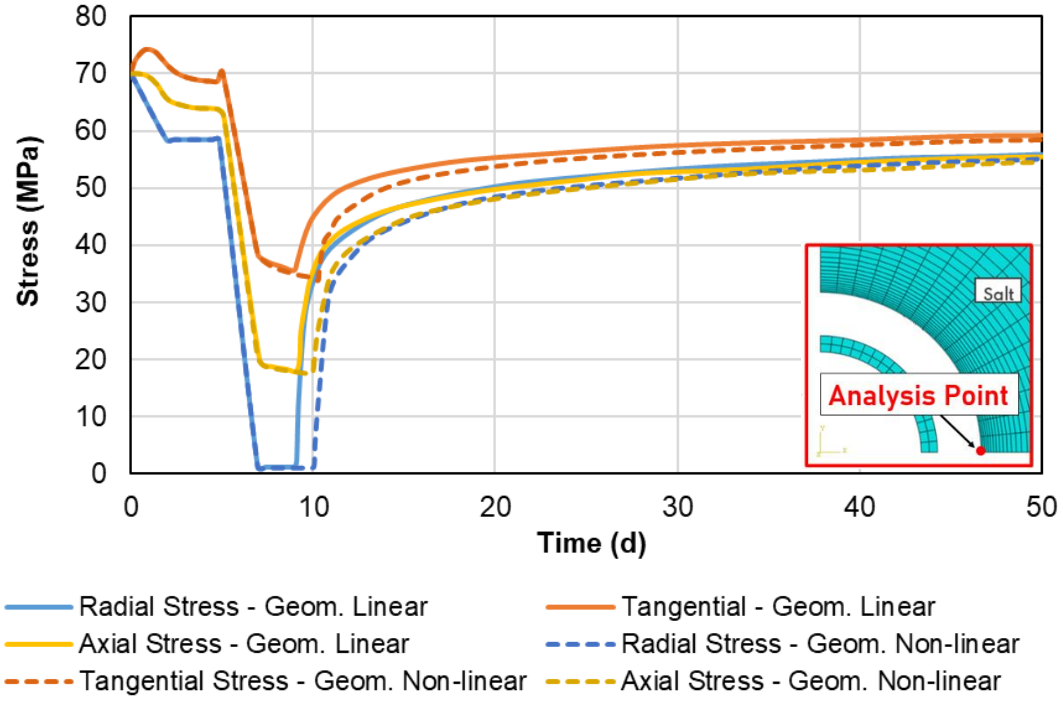

Figure 4.23 – Plane Strain Model – Stress behavior throughout the time simulation at depth 3100 m, considering the new geometry in case Zwd (base case).

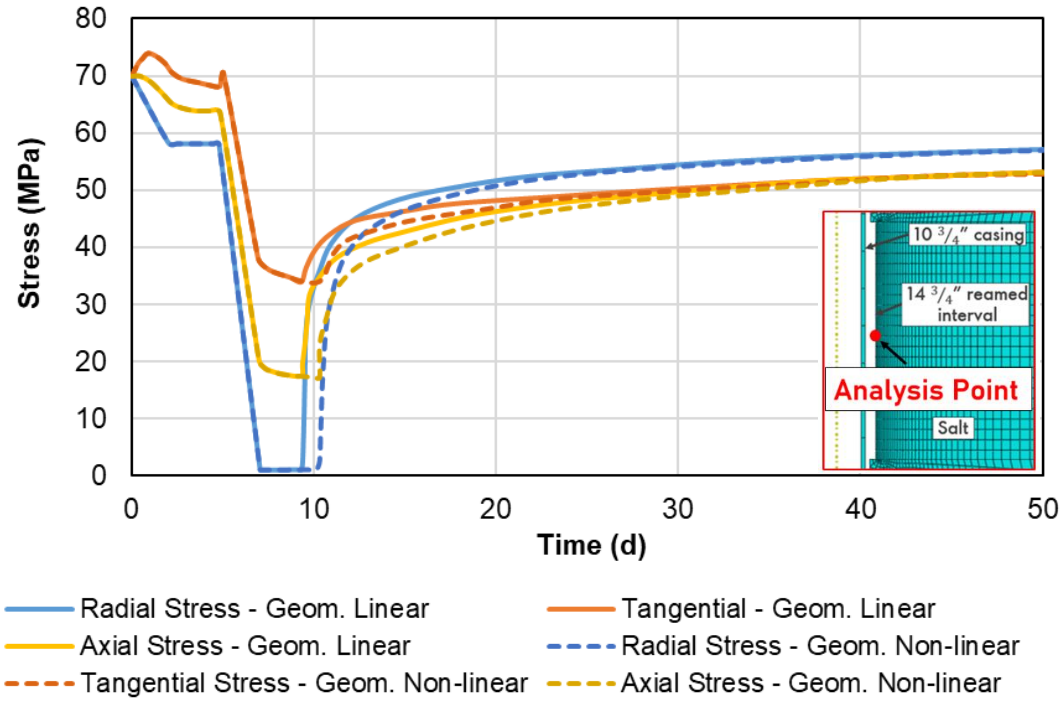

Figure 4.24 – Axisymmetric Model – Stress behavior throughout the simulation at depth 3100 m, considering the new geometry in case Zwd (base case).

It is possible to notice that both linear and nonlinear geometric solutions have similar behavior and the models do not present numerical instabilities along the creep deformation, following the imposed stresses as input data. Furthermore, the behavior of the stresses after contact is also stable and does not peak or exceed in-situ stress levels.

Such results are obtained because, with the reduction of the annular space, the deformation of the element is smaller as well as its distortion during the analysis. In this way, the solution is more stable and converges satisfactorily, leading to physically acceptable results, before and after contact, in both solutions.

It is interesting to verify that the stresses obtained after contact for the original and new geometry are similar and are between 50 and 60 MPa, approximately 10 MPa below the in-situ stresses, with the same upward convergence trend for the values of in-situ stress.

In addition, the concern with the stresses after contact that reach values above the in-situ stresses, which could cause fractures that would not guarantee the tightness of the barrier, is resolved with the results obtained by the new geometry, which indicate that the stress values peak values obtained previously are due to numerical instabilities of the simulation and do not represent the stress state behavior of the rock.

These results contribute to the proposition that, over time, the rock will reach the initial stress value, before disturbance due to drilling, returning to act as a natural seal for the reservoir.

4.9.2 Displacement analysis

Figure 4.25 and Figure 4.26 present the borehole closure along the time with the new geometry for the plane strain and axisymmetric models. As it was presented before, the caption *Nlgeom* refers to the activation or non-activation of the geometric nonlinearity of the solution. Thus, the results with nonlinear geometric solution are represented by *Nlgeom on* and the results obtained by linear geometric solution by *Nlgeom off*.

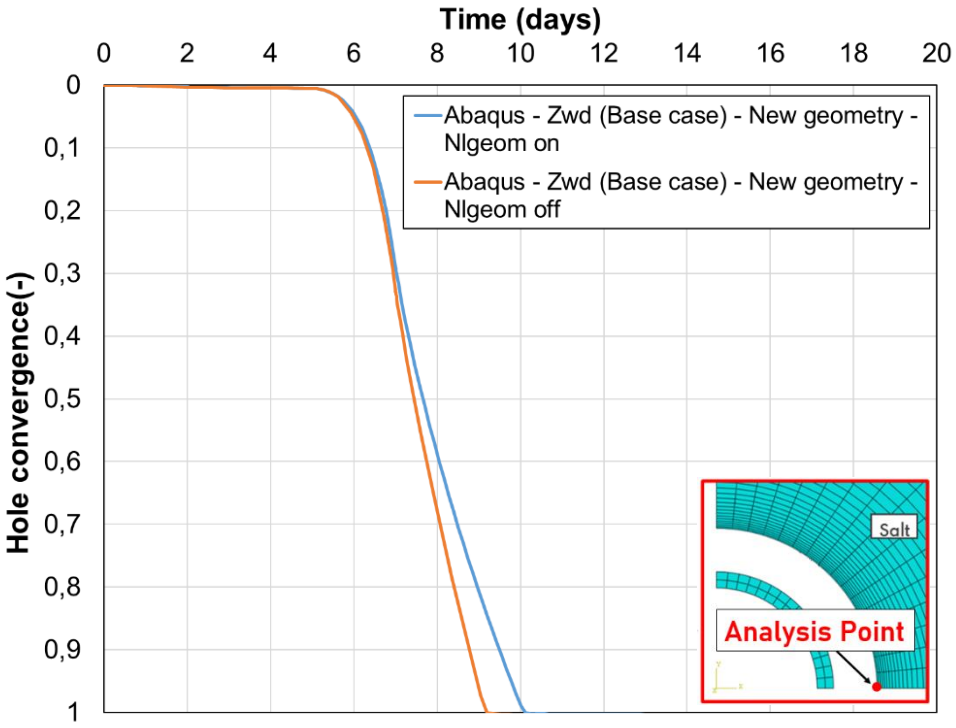

Figure 4.25 – Plane Strain Model – Displacements obtained by the simulations in the plane strain model with new geometry at a depth of 3100 m in the Zwd (base case).

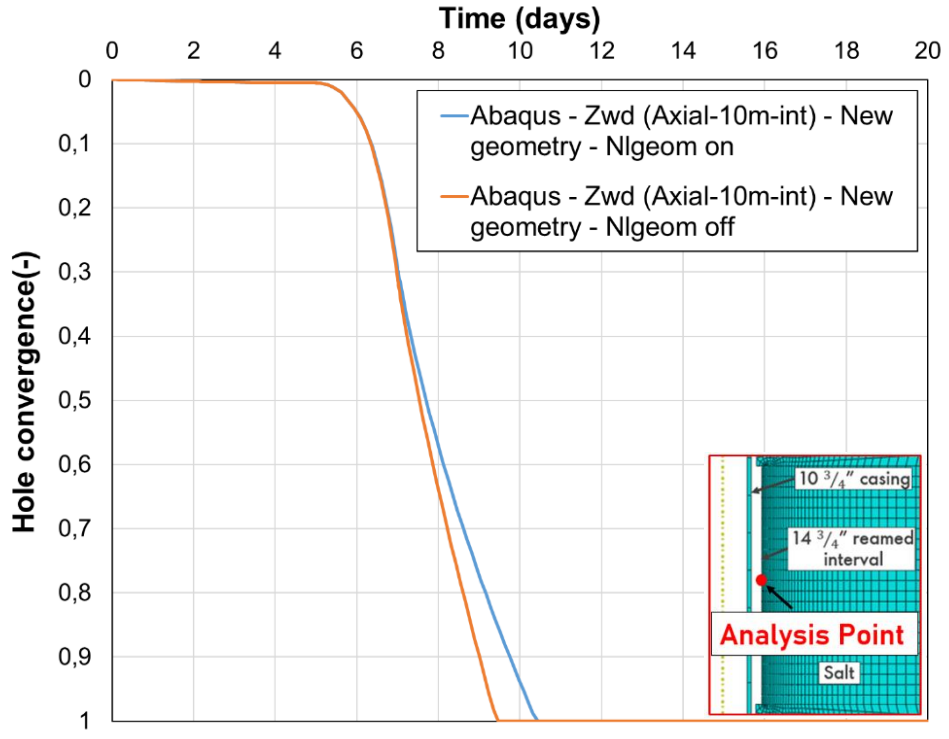

Figure 4.26 – Axisymmetric Model – Displacements obtained by the simulations in the axisymmetric model with new geometry around the 10 m-long reamed interval at a depth of 3100 m in the Zwd (base case).

Due to the change of geometry, the times of the annular closure are not

comparable with those presented by Orlic et al. (2019). Therefore, as a result obtained by simulations with the new geometry, the estimated closure times of the open-hole section in rock salt at a depth of 3100 m are in the range of:

- 9-10 days for the plane strain model (Figure 4.25);
- 9-11 days for the axisymmetric model (Figure 4.26).

It is observed that the difference between the annular closure time between the models and types of analysis is up to, approximately, 1 day. Therefore, as the model has greater numerical stability, the difference between a linear or nonlinear geometric consideration is less significant, thus being able to indicate results with a higher degree of confidence.

However, it is noteworthy that the models that consider the geometric nonlinearity have longer closure times than the models that consider the geometric linearity. Such divergence, even if in small magnitude, corroborates the fact that the linear model does not capture the drop in the creep strain rate of the salt over time, being a relevant aspect for the analysis of the formation of natural barriers.

5
Annular closure analysis in a syntetic scenario

5.1 Introduction

Based on the analyses carried out previously, numerical simulations are conducted in the finite element simulator ABAQUS to evaluate a wellbore closure of synthetic scenario, considering conditions such as stress and temperature in situ, material properties, geometry and fluid weight more realistic for the Brazilian pre-salt wells.

The well under analysis is considered vertical and one section at 3600 m of depth is studied, located in halite layers of approximately 50 m, representing potential candidates for the formation of external natural barriers, that is, annular barriers.

Numerical geomechanical simulations are conducted to assess the displacement of a wellbore wall in salt formations due to induced creep. Therefore, the analyses are made in two-dimensional models of cross-section and longitudinal section of the wellbore normal to the axis of the well, plane strain and axisymmetric models, respectively.

Effects related to temperature changes during the construction and production of the well, as well as heat exchanges between the formation and the annular fluid are added to this analysis.

All the analyses in this case consider the large deformation mode of ABAQUS. Therefore, the analyses consider the geometric nonlinearity due to the large deformations present in the problem.

The ABAQUS finite element simulator is used to build geomechanical structural models of the well and run simulations. In addition, a subroutine is implemented to the model through the FORTRAN program, in order to implement the constitutive law of double mechanism of deformation used in the analyses to predict the viscoelastic behavior of salt.

5.2 Initial data

In this analysis, the type of saline rock used is halite, the main saline mineral in the salt layers, present in several hydrocarbon basins around the world, including Brazilian pre-salt.

The constitutive law adopted to reproduce the creep behavior of halite is the double mechanism of deformation, described in item 3.3.3.2 of this work together with the creep properties of halite. This constituvive law is widely used in Brazil and the creep parameters of the main Brazilian saline rocks were calibrated in the last decades during an important experimental program. The implementation of this model in ABAQUS was carried out with the help of the FORTRAN program through a subroutine described in Appendix A of this work.

The input data for the simulations takes into account in-situ stress and temperature conditions characteristics of the Campos Basin in Brazil, shown in Table 5.1.

Table 5.1 – Input data for simulation scenario

Depth (m)	In-situ isotropic stress (MPa)	In-situ temperature (°C)
3600	52	58

The simulations are performed by activating the large deformation mode available in ABAQUS. This implies conditioning the solution to geometric nonlinearity.

Physical and elastic properties of halite are reported by Poiate (2012) and are the same in all simulations: density $\rho = 2170$ kg/m³, Young's modulus $E = 20.97$ GPa and Poisson's coefficient $\nu = 0.3$. As thermal properties of halite, there is thermal conductivity $k = 4.33$ W/m.K and the specific heat $c = 916.79$ J/kg.K (Urquhart & Bauer, 2014).

Casing is modeled as a steel, purely elastic with Young's modulus $E = 200$ GPa and Poisson's ratio $\nu = 0.27$ and density equal to $\rho = 7860$ kg/m³. Thermal properties of conductivity $k = 52$ W/m.K and the specific heat $c = 502.42$ J/kg.K are considered.

The type of fluid used in the drilling phase has a density equal to 1130 kg/m³ and the pressure applied in the wellbore wall corresponds to 8.5 ppg, which leads to pressure of 36 MPa at the analysis depth of 3600 m. The temperature of the fluid in the annular is considered equal to $T = 60$ °C in the well construction stage, named drilling, and $T = 120$ °C in the production stage phase until the end of the useful life of the well, named annular closure. The thermal properties adopted for

the annular fluid refer to brine, such as conductivity $k = 0.70$ W/m.K and specific heat $c = 4186$ J/kg.K.

5.3 Model pre-processing

5.3.1 Plane strain model

A plane strain model is developed along a horizontal cross-section normal to the shaft of the well at depth of 3600 m. The geometry of the model consists of the casing and the rock formation, with the outer limit having a radius of 30 m. The diameter of the wellbore is 37.5 cm ($14^3/_4$ inches) and the inside and outside diameter of the casing is 23.5 cm ($9^1/_4$ inches) and 27.3 cm ($10^3/_4$ inches), respectively, constituting an annular space of approximately 5 cm.

Plane strain elements are used to allow the formulation of full three-dimensional stress in salt. The mesh is formed by quadratic quadrilateral elements of eight nodes, with intermediate nodes, and reduced integration. The elements have thermal coupling for the analysis of thermal effects during creep.

As in the models reported by the previous chapter, in order to avoid distortion of the element, the dimension of the element was reduced in the radial direction, making it more elongated in the tangential direction of the well. Thus, with the greater deformation in the radial direction of the element throughout the simulation, the difference between the size of the element faces tends to disappear, decreasing the distortion. Figure 5.1 presents the numerical model and mesh distribution.

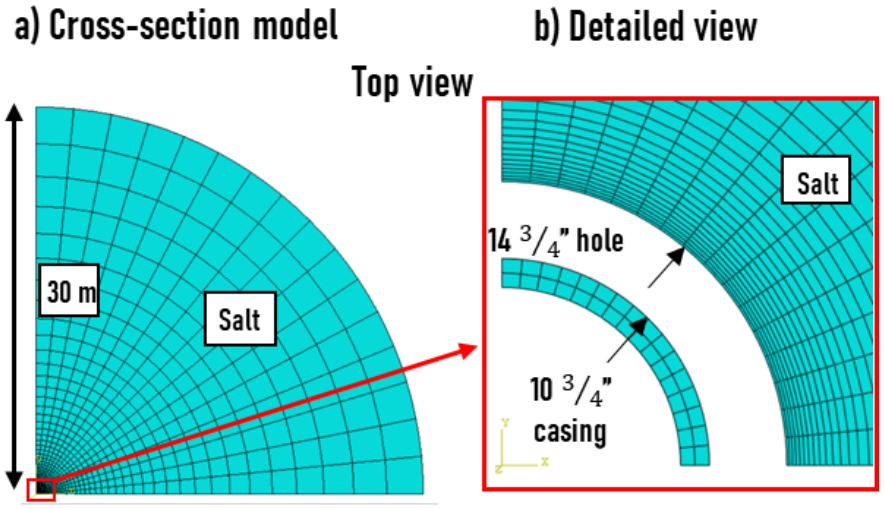

Figure 5.1 – (a) Mesh for a plane strain model of cross-section of the wellbore normal to the well axis, located in the middle of the creep interval and (b) detailed view of the same model around the wellbore.

5.3.2 Axisymmetric model

Axisymmetric model of the area close to the wellbore is developed around the vertical axis of the well, modeling a longitudinal section that crosses a layer of salt.

The geometry of the model is composed of a cylinder with a height of 50 m and a radius of 10 m, the outer boundary of the model being defined at the same radial distance adopted for the model of the cross-section of the wellbore.

A section is modeled where the depth of the cross-section model is located in the center of the axisymmetric model. The casing follows the dimensions of the plane strain model and extends over the entire depth, that is, the wellbore diameter is 37.5 cm ($14^{3}/_{4}$ inches) and the casing inner and outer diameter is 23.5 cm ($9^{1}/_{4}$ inches) and 27.3 cm ($10^{3}/_{4}$ inches), respectively, constituting an annular space of approximately 5 cm.

The 50 m creep interval is adopted in order to verify the possible formation of a natural salt barrier in the wellbore annular, according to the specification of NORSOK D-010.

Axisymetric elements are used to allow the formulation of complete three-dimensional stresses in salt. Quadratic quadrilateral elements of eight nodes, with intermediate nodes, and reduced integration are used for the solution.

The model was reduced to half the area close to the wellbore due to considerations of symmetry to reduce computational costs. Figure 5.2 shows the numerical model, as well as its mesh.

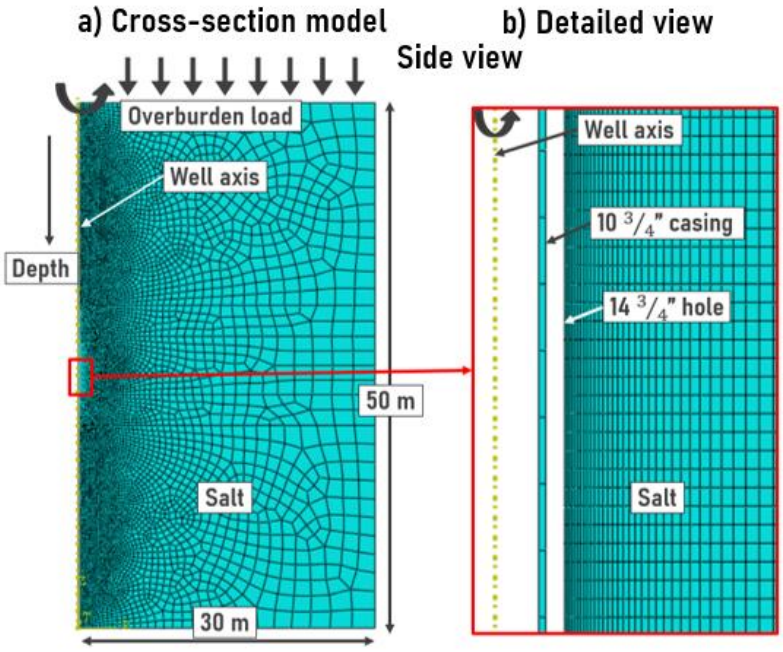

Figure 5.2 – (a) Mesh for an axisymmetric model around the axis of a wellbore and (b) detailed view of the creep interval of wellbore in the saline layer.

5.4 Model simulation stages

The stages of analysis are conducted and described in sequence: geostatic, drilling, completation and annular closure.

In the geostatic stage, the stress and temperature field conditions are inserted in the model. Boundary conditions are prescribed to restrict movement in the normal direction to the outer boundary of the models.

For the plane strain model, the wellbore wall and the outer boundary of the model are restricted on the x and y axes. In this way, the horizontal and vertical zero displacement is guaranteed in this step. Figure 5.3 shows the boundary conditions in the first stage of simulations in the plane strain model.

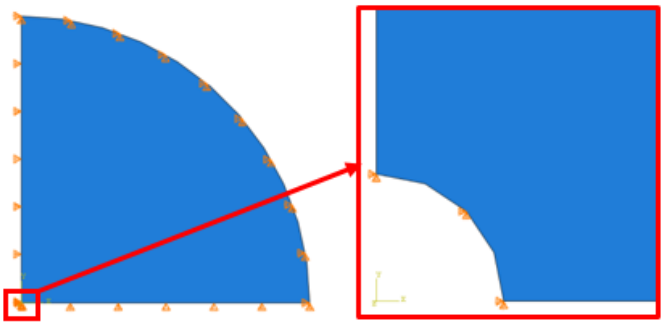

Figure 5.3 – Boundary conditions of the geostatic stage in the plane strain model.

The temperature and stresses in-situ are considered constant at each depth of analysis in the plane strain model for the geostatic stage of the simulation.

In the axisymmetric model, the boundary condition of the upper limit of the model is not made with displacement restriction, but by applying the load related to the layers superimposed on the top of the model. Figure 5.4 shows the boundary conditions at the first stage of simulations in the axisymmetric model.

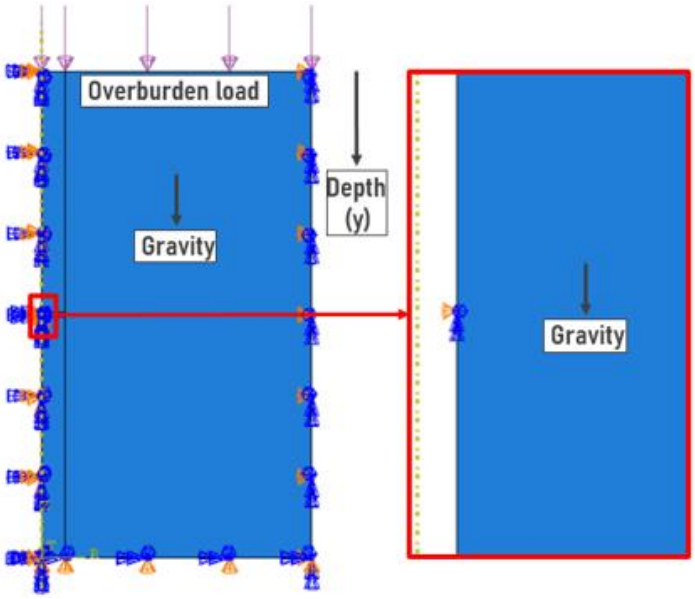

Figure 5.4 – Boundary conditions of the geostatic stage in the axisymmetric model.

As the axisymmetric model represents an interval along the depth, the temperature has a constant variation according to the height of the model, reaching at the depth of 3600 m the temperature informed in Table 5.1 at the depth 3600 m located in the center of the model. Figure 5.5 shows the temperature distribution of the axisymmetric model.

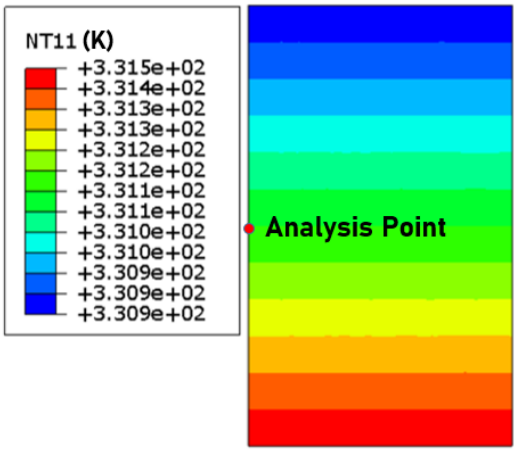

Figure 5.5 – Constant gradient of the in-situ temperature in the axisymmetric model.

In terms of isotropic tension in-situ, the procedure is given in a similar way to temperature, varying according to the multiplication of depth, halite density and gravity (g = 9.81 m/s²). Thus, the in-situ stress in the middle of the axisymmetric model is equal to the stress reported in Table 5.1 at the depth of 3600 m. Figure 5.6 shows the stress distribution of the axisymmetric model.

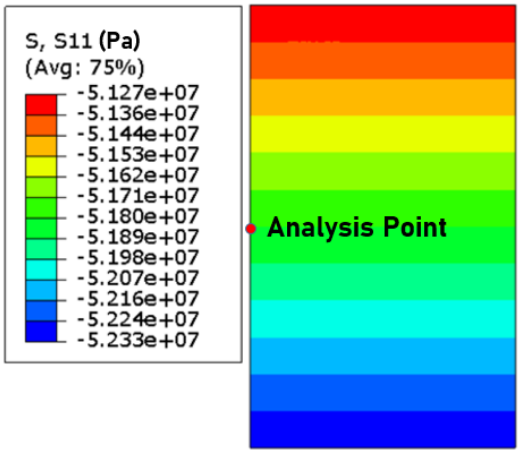

Figure 5.6 – Constant gradient of in-situ isotropic stress in the axisymmetric model.

In the drilling phase, the excavation of the well is simulated by removing the restrictions from the wellbore wall and applying pressure caused by the weight of the drilling fluid. Thus, a disturbance is caused by a stress redistribution due to the differential stress imposed between the in-situ stress of the formation and the pressure of the drilling fluid that cause the creep displacements.

The drilling phase considers a drilling speed of 2,10 m/h, thus having a stage time of 86400 s or 1 day.

In the plane strain model, the pressure caused by the fluid weight is constant, since this model represents only a depth of analysis. In the axisymmetric model, the pressure due to the weight of the fluid is distributed along the depth, with values similar to those of the plane strain model in the depth of analysis located in the middle of the axisymmetric model. In addition, the temperature during the construction of the well, defined in this work as the drilling stage, is considered equal to T = 60 °C.

Figure 5.7 and Figure 5.8 present the boundary conditions in the drilling phase of the simulations in the plane strain and axisymmetric models, respectively.

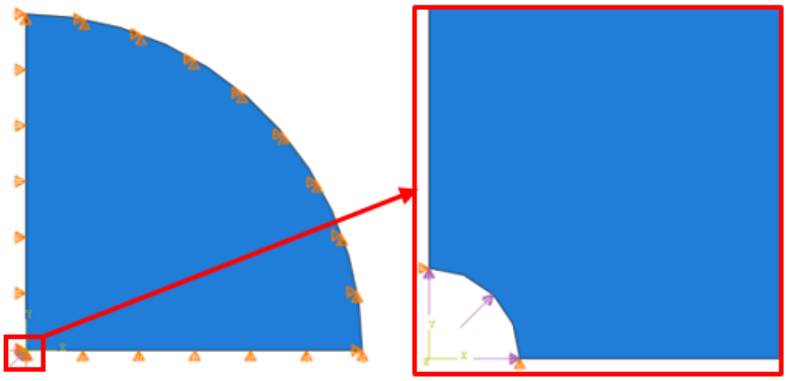

Figure 5.7 – Boundary conditions of the drilling phase in the plane strain model.

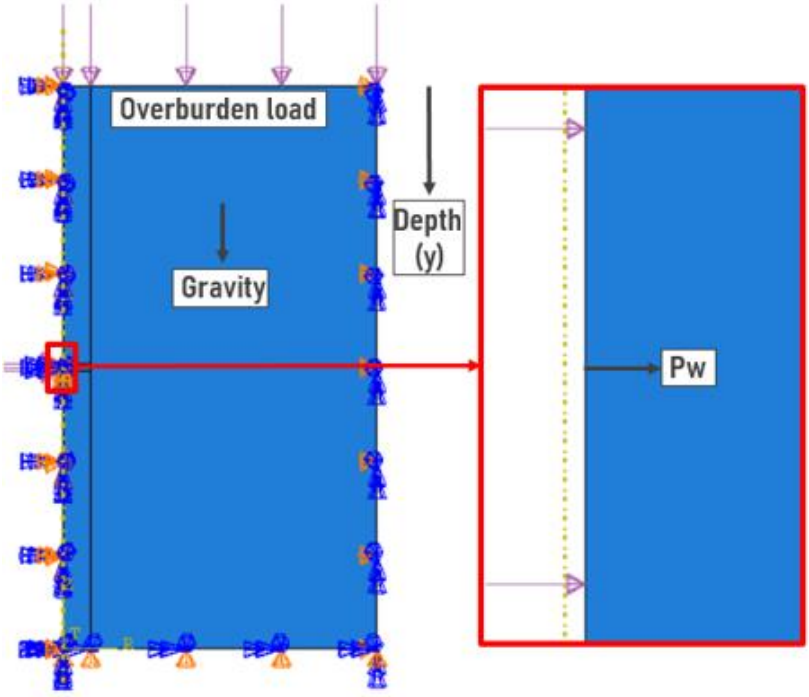

Figure 5.8 – Boundary conditions of the drilling phase in the axisymmetric model.

The completion stage is the time of well preparation before oil production, considered as 100 days in this simulation. Boundary conditions of the rock salt remain the same that in the drilling stage. Casing is inserted and the fluid pressure is the same of the rock salt and it applyed internally and externally to the casing.

The final stage of simulation is called annular closure, which considers the increase in rock temperature due to oil production. Temperature is inserted in the inner wall of the casing with a magnitude of 120°C, initiating the heat exchange between the system formed by the casing, annular fluid and salt, which increases the temperature of the rock in the vicinity of the wellbore wall.

The annular closure stage has the same boundary conditions and fluid

pressure as the completion stage and the simulation time considers the useful life of the well, being adopted as 30 years for this case.

Figure 5.9 and Figure 5.10 present the boundary conditions in the completation and annular closure stages of the simulation in the plane strain and axisymmetric models, respectively.

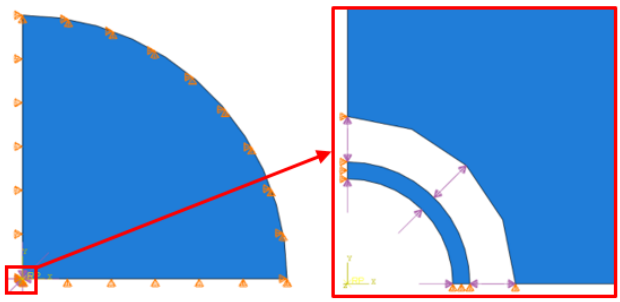

Figure 5.9 – Boundary conditions of the completation and annular closure stages in the plane strain model.

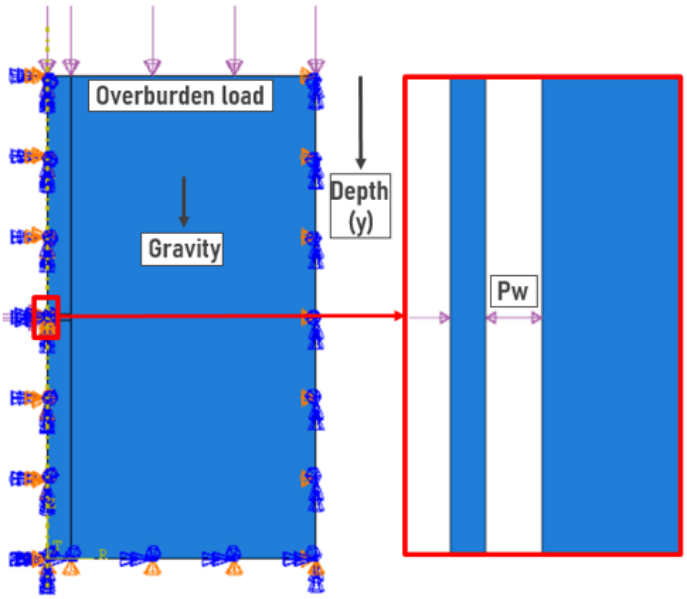

Figure 5.10 – Boundary conditions of the completation and annular closure stagea in the axisymmetric model.

5.5 Results analysis

Figure 5.11 and Figure 5.12 present the analysis points of the plane strain and axisymmetric models, respectively, which were used to obtain the results.

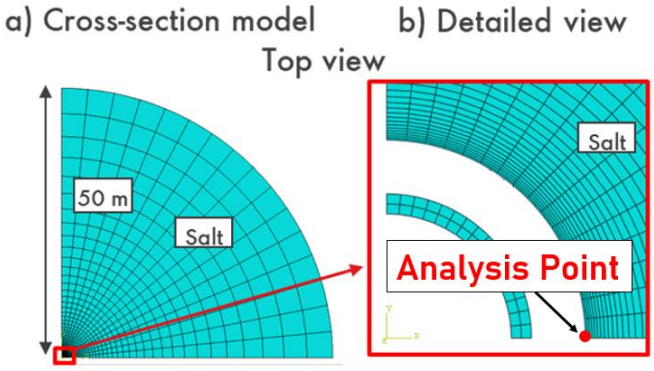

Figure 5.11 – Plane Strain Model – Analysis Point

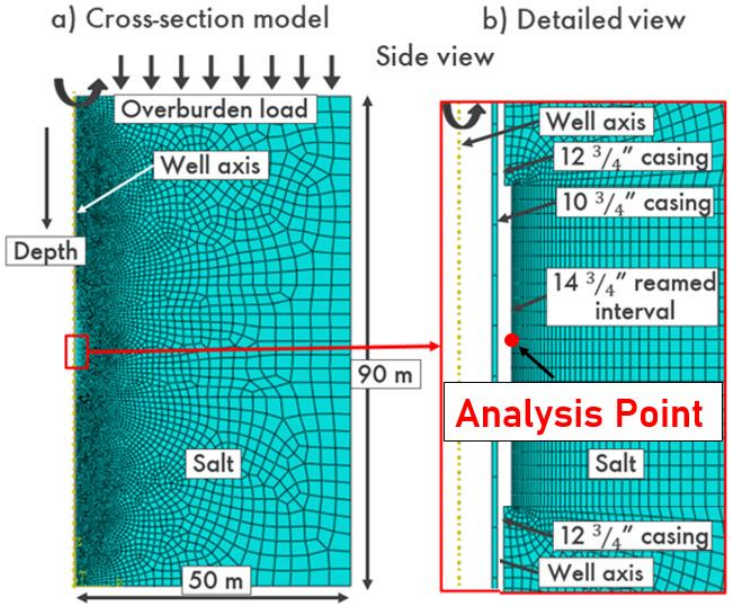

Figure 5.12 – Axisymmetric Model – Analysis point.

5.5.1 Stress analysis

As in the previous chapter, the analysis of stresses before contact is made by checking whether values applied as input data in the various simulation steps are being followed by the model. After contact, the stresses are analyzed through the tendency of stress increase over time and the difference between the in-situ stress value and the value reached by the model until the end of the analysis. In both analyses, numerical instabilities of the model that generate fluctuations or inadequate behavior of the stresses are analyzed in order to generate more reliable results.

Figure 5.13 shows the behavior of the stresses over time until the closure of wellbore wall at depth of 3600 m for the Brazilian halite in the plane strain model compared to the axisymmetric model.

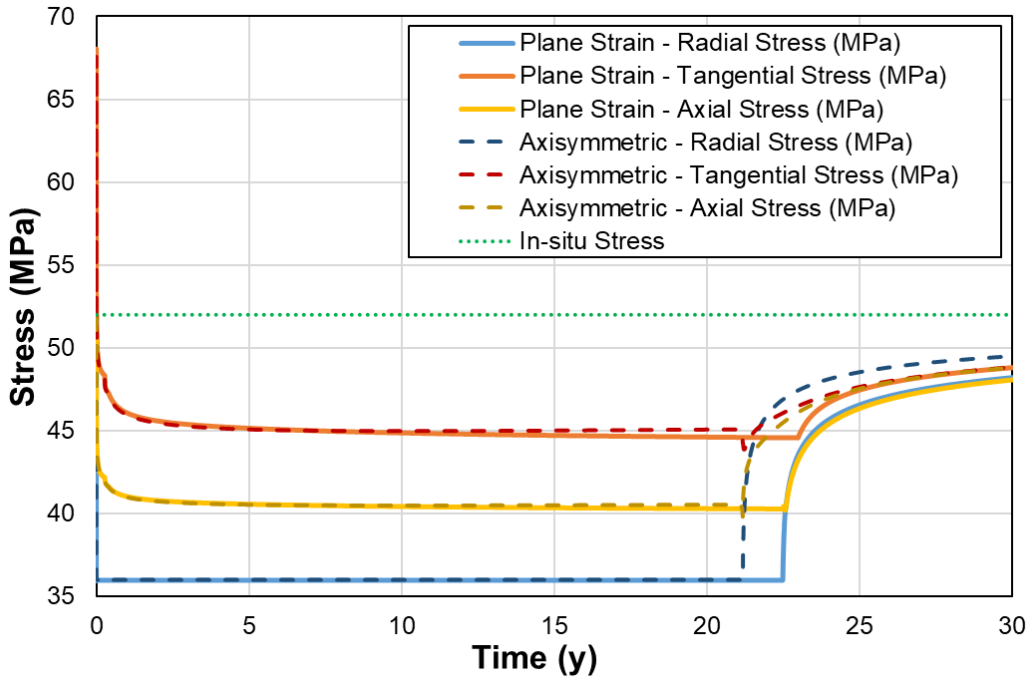

Figure 5.13 – Stress behavior throughout the time of simulation.

From the above, it is possible to notice that in both models the radial stress is congruent with the stress imposed as input data until the contact between the casing and the salt. Furthermore, an abrupt increase in tangential stress is observed in response to a reduction in radial stress by 16 MPa when drilling is simulated and fluid pressure is applied to the wellbore wall.

Then, the stresses have an approximately constant distribution until the annular closure, showing no signs of numerical instability in both models.

It is observed that the tangential and axial stresses of the plane strain model and the axisymmetric model are compatible throughout the simulation. However, it is possible to observe greater stresses in the axisymmetric model than in the plane strain model, which has a slight downward trend in tangential and axial stresses. Such difference is evidenced after 15 years of well operation, causing the deviatoric stress to be reduced and, consequently, to decrease the creep strain rate over time in the cross-section in relation to the logitudinal section.

After contact, the stresses converge to similar values in both models, ending the simulation with stresses between 48 MPa and 50 MPa, about 92 to 96% of the magnitude of the in-situ stress.

In addition, the slight upward trajectory of stresses in the final years of the simulation is pointed out, indicating the tendency of the rock to converge to its natural state of equilibrium before the disturbance due to drilling, returning to act as a natural seal for the reservoir and, therefore, forming a natural salt barrier.

5.5.2 Displacement analysis

As a result obtained by the synthetic scenario simulations at a depth of 3600 m, the estimated annular closure times for the plane deformation and axisymmetric model varied by about 1 year, taking about 22.5 years for annular closure in cross-section and 21.20 years in longitudinal section.

It is possible to observe that the annular closing times presented by the axisymmetric model is smaller than that estimated by the plane strain model. However, the difference of the order of one year found by the two models is considered small in relation to the total simulation time.

From the point of view of the formation of a natural barrier, it is possible to affirm that the annular closure time is satisfactory since it occurs during the production phase, speculating that the barrier is formed in the permanent abandonment stage, that is, when end of well life.

Figure 5.14 presents the annular closure along the time in the plane strain and axisymmetric models, respectively.

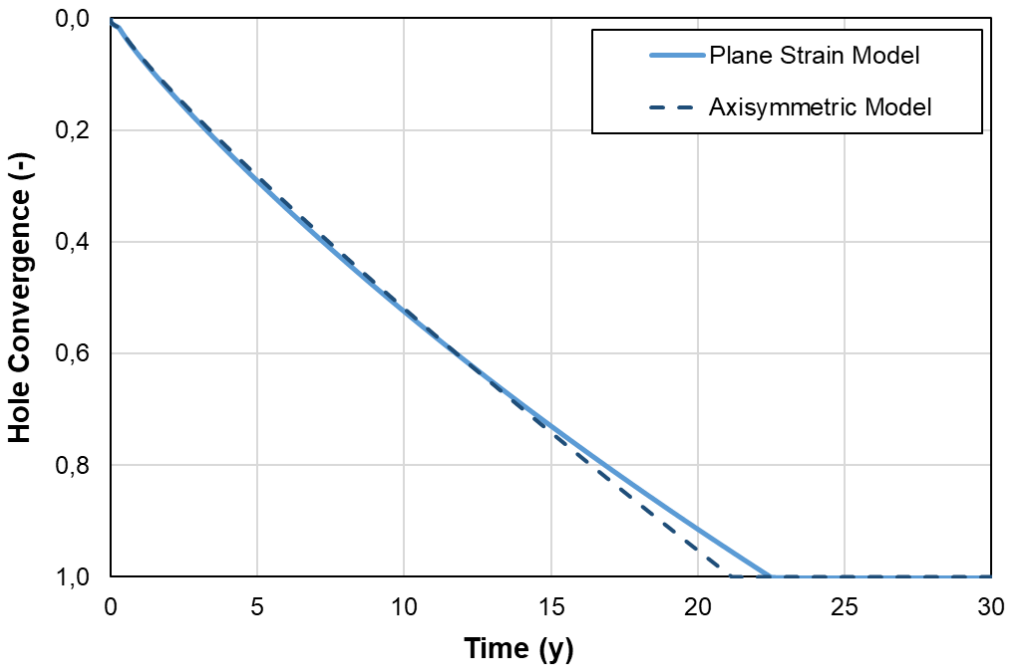

Figure 5.14 – Displacements obtained by the simulations of the synthetic scenario.

6
Conclusions and suggestion for future work

6.1 Conclusions of numerical simulation of wellbore closure

This work contributes to the advancement of research being carried out in Brazil that includes salt as a sealing material for operations of permanent plug and abandonment of oil and gas wells. For this, a computational methodology was tested and discussed in order to simulate a synthetic scenario that encompasses characteristics of the Brazilian Pre-Salt and attest to the potential for the formation of natural barrier in saline layers in this context.

In this way, it was possible to conclude that the simulation protocol was efficient to reproduce results published in the literature, obtaining results that respect the imposed stresses and boundary conditions. Furthermore, through the computational methodology used, an analysis of the stresses and displacements generated over time was carried out, generating greater reliability in the results obtained through a series of discussions and improvements applied to the model.

The differences between the analyses considering the small- and large-deformation mode are closely linked to the critical condition imposed by the simulation that generates a high strain rate combined with an enlarged annular of about 10 cm, causing a series of numerical instabilities in the model due to distortion of the wellbore wall elements throughout the simulation.

This instability is verified after contact between casing and salt in both types of analysis, geometrically linear and nonlinear. However, the model that considers the geometric nonlinearity needs more iterations to reach convergence, due to the deformation of the mesh throughout the simulation, which does not happen when the geometric linearity is considered, where the analysis are using the original nodal coordinates.

The analyses carry out with the new geometry show that for a smaller annular of approximately 5 cm, which is a more realistic scenario, the elements suffer less distortion and the solution does not present numerical instabilities. Therefore, the difference in results between considering the small- or large deformation mode of ABAQUS is not as significant as for the case presented in the

reference work.

Although the results are not compatible with the displacements presented in Orlic et al. (2019), it is believed that the solution obtained with the large deformation mode is the most appropriate. This is because the geometrically nonlinear analysis allows the mesh to adapt to large strains, generating a more realistic stress redistribution over time, even capturing the reduction in creep strain rate that the rock can present over time, which is a relevant feature for the study of annular closure and formation of natural barriers.

From that, for a synthetic scenario defined with the creep properties of the Brazilian Halite adopted in the literature, in addition to in-situ conditions and geometry of a hypothetical scenario of the Brazilian pre-salt, it is possible to verify that the annular closure of the well occurs in approximately 22 years after drilling.

Considering that the average useful life of a well is equal to 30 years, it can be seen that the closure time is adequate, as it occurs during the production stage.

Furthermore, from the point of view of stresses, at the end of the useful life adopted for this case, the stresses reached values in the order of 92 to 94% of the in-situ stress.

It is speculated that due to the tendency of constant increase in stresses after contact, over time such stresses will converge to the in-situ stress value, reestablishing the natural seal that operated before the well drilling.

Thus, it is concluded that the results presented are indicative of the potential for the formation of natural barriers in saline layers for permanent plug and abandonment operations.

6.2 Suggestion for future research

The simulation of drilling and closure the well was performed considering a synthetic scenario where there are no data quality limitations. A suggestion would be to carry out a study with applications to a real case and to a model induced in the laboratory.

It is noteworthy that the study carried out configures the initial step in the verification of the formation of natural barriers in salt for permanent abandonment operations. Thus, to fully achieve the objective, further studies will be needed on the quality of the contact between salt and casing, verifying the adherence of salt to the casing and formations in its surroundings.

In this context, studies related to the watertightness of the generated barrier must also be carried out to verify if the Brazilian pre-salt meets the requirements

defined by the ANP regarding isolation and resistance to fluids and loads.

REFERENCES

ABAQUS. (2017). *ABAQUS User's Manual.* Simulia Corporation ABAQUS vs. 2017. Providence, Rohde Island, USA: Dessault Systèmes.

ANP. (2016). *Resolução ANP N° 46, de 1°.11.2016 - dou 3.11.2016 – Retificado dou 7.11.2016.* Retrieved from http://legislacao.anp.gov.br/?path=legislacao-anp/resol-anp/2016/novembro&item=ranp-46--2016

Baar, C. (1977). *Applied salt-rock mechanics.* Amsterdam: Ensevier Scientific Publishing Company.

Benitz, M. A. (2012). *Simulations of non-contact creep in regimes of mixed dominance.* University of Massachusetts, Master's Thesis – Mechanical and Industrial Engineering, Amherst.

Bérest, P., & Brouard, B. (2003). Safety of salt caverns used for underground storage. *Oil & Gas Science and Technology – Rev. IFP, 58*(No. 3), pp. 361-384.

Botelho, F. V. (2008). *Análise numérica do comportamento mecânico do sal em poços de petróleo.* Pontifícia Universidade Católica do Rio de Janeiro, Dissertação de Mestrado – Departamento de Engenharia Civil, Rio de Janeiro.

Costa, A., & Poiate, E. (2009). Rocha salina na indústria do petróleo: aspectos relacionados a reologia e a perfuração de rochas salinas. In *Sal: Geologia e Tectonica* (2a ed., pp. 362-385). Editora Beca.

Costa, A., Poiate, E., Amaral, C., Gonçalves, C., Falcão, J., & Pereira, A. (2010). Geomechanics applied to the well design through salt layers in Brazil: A history of success. *44th US Rock Mechanics Symposium and 5th US-Canada Rock Mechanics Symposium.* Salt Lake City: American Rock Mechanics Association (ARMA).

Costa, A., Poiate, E., Falcão, J., & Coelho, L. (2005). Triaxial creep tests in salt applied in drilling through thick salt layers in Campos Basin - Brazil. *SPE/IADC Drilling Conference.* Amsterdam: Society of Petroleum Engineers Inc. (SPE). doi:10.2118/92629-MS

DIANA FEA. (2018). *Finite element program and users documentation*, 10.1. Retrieved from https://dianafea.com/

Dowling, N. E. (2012). *Mechanical Behavior of Materials, Engineering Methods for Deformation, Fracture, and Fatigue* (4th ed.). Pearson Education.

Dusseault, M. B. (1989). Saltrock behavior as an analogue to the behavior of rock as greath depth. (M. &. Fourmaintraux, Ed.) *Rock at Great Depth*, pp. 11-17.

Dusseault, M. B., Rothenburg, L., & Mraz, D. Z. (1987). The design of openings in salt rock using a multiple mechanism viscoplastic law. *28th US Symposium on Rock Mechanis*, pp. 633-642.

Dusseault, M., & Fordham, C. (1995). Time-dependent behavior of rocks. In *Comprehensive Rock Engineering – Principles, Practices and Projects* (pp. 119-149). Pergamon Press.

Firme, P. A. (2013). *Modelagem constitutiva e análise probabilística aplicadas a poços em zonas de sal.* Pontifícia Universidade Católica do Rio de Janeiro, Dissertação de Mestrado – Departamento de Engenharia Civil, Rio de Janeiro.

Firme, P. A., Brandão, N., Roehl, D., & Romanel, C. (2018). Enhanced double-mechanism creep laws for salt rocks. *Acta Geotechnica*. doi:10.1007/s11440-018-0689-7

Fjær, E., Folstad, J., & Li, L. (2016). How creeping shale may form a sealing barrier around a well. *50th US Rock Mechanics / Geomechanics Symposium (ARMA)*. Retrieved from http://www.onepetro.org/conference-paper/ARMA-2016-482

Fossum, A., & Fredrich, J. (2002). *Salt mechanics primer for near-salt and subsalt deepwater Gulf of Mexico field developments.* Technical Report, Sandia National Laboratories. doi:10.2172/801384

Fredagsvik, K. (2017). *Formation as barrier for plug and abandonment of wells.* University of Stavanger, Masther Thesis – Departament of Petroleum Technology, Stavanger.

Goodman, R. (1989). *Introduction to rock mechanics - Second edition.* New York: John Wiley & Sons.

Gravina, C. (1997). *Simulação numérica do comportamento mecânico do sal em poços de petróleo.* Universidade Estadual de Compinas (UNICAMP)., Dissertação de Mestrado – Departamento de Engenharia do Petróleo, Campinas.

Hallak, T. V. (2017). *Plugging & abandonment techniques of offshore wells.* Universidade Federal do Rio de Janeiro, Departamento de Engenharia do Petróleo, Rio de Janeiro.

Hou, Z., Wundram, L., Meyer, R., Schmidt, M., Schmitz, S., & Were, P. (2012). Development of a long-term wellbore sealing concept based on numerical simulations and in situ-testing in the Altmark natural gas field. *Enviromental Earth Sciences*(67), pp. 395-409. doi:10.1007/s12665-012-1670-7

IBP. (2017). *Caderno de boas práticas de E&P: Diretrizes para abandono de poços.* Rio de Janeiro, Brasil.

Jeremic, M. L. (1994). *Rock Mechanics in Salt Mining.* Rotterdam: A.A. Balkema Publishers.

Khalifeh, M., & Saasen, A. (2020). *Introduction to permanent plug and abandonment of wells.* Springer Open. doi:10.1007/978-3-030-39970-2

Lomenick, T., & Bradshaw, R. (1969). Deformation of rock salt in openings mined for the disposal of radioactive wastes. In *Rock Mechanics* (pp. 5-30).

Mackay, F. (2011). *Análise geomecânica na perfuração e cimentação de poços de petróleo em zonas de sal.* Pontifícia Universidade Católica do Rio de Janeiro, Tese de Doutorado – Departamento de Engenharia Civil, Rio de Janeiro.

Miura, K. (2004). *Um estudo sobre a segurança operacional na construção e reparo de poços marítimos petróleo.* Universidade Estadual de Campinas, Tese de Doutorado – Departamento de Engenharia do Petróleo, Campinas.

Munson, D., & Dawson, P. (1979). *Constitutive model for the low temperature creep of salt (with application to WIPP).* Albuquerque: Sandia National Laboratories.

Munson, D., & DeVries, K. (1991). Development and validation of a predictive technology for creep closure of underground rooms in salt. *7th ISRM Congress.* Aachen: International Society for Rock Mechanics and Rock Engineering.

NORSOK Standard D-010. (2013). *Well integrity in drilling and well operations* (4 ed.). Norway.

Norton, F. (1929). *The creep of steel at high temperature* (1st ed.). New York: McGraw-Hill Book Company, Inc.

Oil & Gas UK. (2015). *Guidelines for the abandonment of Wells* (5 ed.). London, United Kingdom.

Øksnes, A. L. (2017). *Permanent Plugging and Abandonment – An identification and discussion of technologies and differences in UKCS and NCS regulations.* University of Stavanger, Master's Thesis – Faculty of Science and Technology, Stavanger.

Oliveira, J., Idagawa, L., & Nogueira, E. (1985). *Evaporitos na Bacia de Campos, aspectos geológicos e problemas de perfuração.* Rio de Janeiro: PETROBRAS/CENPES-475.

Orlic, B., & Buijze, L. (2014). Numerical modeling of wellbore closure by the creep of rock salt caprocks. *48th US Rock Mechanics / Geomechanics Symposium (ARMA).* Minneapolis.

Orlic, B., Wollenweber, J., Geel, C., Vandeweijer, V., Meekes, J., Heerens, G., & TerHeege, J. (2019). Formation of a sealing well barrier by the creep of rock salt: numerical investigations. *53rd US Rock Mechanics/Geomechanics Symposium (ARMA).* New York.

Poiate, E. (2012). *Mecânica das rochas e mecânica computacional para projeto de poços de petróleo em zonas de sal.* Pontifícia Universidade Católica do Rio de Janeiro, Tese de Doutorado – Departamento de Engenharia Civil, Rio de Janeiro.

Silva, R. S., & Mainier, F. B. (2008). Descomissionamento de sistemas de produção offshore de petróleo. *IV Congresso Nacional de Excelência em Gestão.* Niterói.

Skjerve, K. M. (2013). *Evaluation os shale formations as barrier element for permanent plug and abandonment of wells.* Norwegian University of Science and Technology, Master's Thesis – Department of Petroleum Enginnering and Applied Geophysics, Trondheim.

Teraoka, L. Y. (2017). *Análise comparativa entre as diretrizes das principais associações da indústria de petróleo e agências reguladoras para abandono permanente de poços.* Universidade Federal Fluminense, Departamento de Engenharia Química e de Petróleo, Niterói.

Turcotte, D., & Schubert, G. (1982). *Geodynamics* (2nd ed.). Cambridge: Cambridge University Press.

Urquhart, A., & Bauer, S. (2014). *Experimental determination of single-crystal halite thermal conductivity, diffusivity and specific heat from - 75°C to 300°C.* Sandia National Laboratories, Albuquerque, New Mexico.

Vrålstad, T., Saasen, A., Fjær, E., Øia, T., David, J., & Khalifeh, M. (2019). Plug & abandonment of offshore wells: Ensuring long-term well integrity and cost-efficiency. *Journal of Petroleum Science and Engineering*, 478-491. doi:10.1016/j.petrol.2018.10.049

Williams, S. M., Carlsen, T., Constable, K. C., & Guldahl, A. C. (2009). Identification and qualification of shale annular barriers using wireline logs during plug and abandonment operations. *SPE/IADC Drilling Conference and Exhibition.* Amsterdam. doi:10.2118/119321-MS

Yao, H.-T., Xuan, F.-Z., Wang, Z., & Tu, S.-T. (2007). *A review of creep analysis and design under multi axial stress states.* Nuclear Engineering and Design 237.

Appendix A

A.1 Constitutive creep model used in the ABAQUS program, through the subroutine of FORTRAN program

For the simulations of this work, the constitutive model of Double Mechanism of deformation is adopted, since, according to Costa & Poiate (2009), the constitutive laws of creep based on deformation mechanisms are recommended by the international technical literature because they represent the intrinsic behavior of the material.

Thus, this law is implemented in ABAQUS through a subroutine by the FORTRAN program, and the constitutive equation of Double Mechanism, given by Equation (3.20), must have the equivalent deformation increment for the explicit solution and for the implicit solution. The constitutive model based on the Double Mechanism of deformation is expressed by Equation (A.1).

$$\dot{\varepsilon} = \dot{\varepsilon}_0 \left(\frac{\sigma_{eq}}{\sigma_0}\right)^n \exp\frac{Q}{R}\left(\frac{1}{T_0} - \frac{1}{T}\right) \rightarrow \varepsilon = \dot{\varepsilon}_0 \left(\frac{\sigma_{eq}}{\sigma_0}\right)^n \exp\frac{Q}{R}\left(\frac{1}{T_0} - \frac{1}{T}\right) t \tag{A.1}$$

For the explicit algorithm, the increase in uniaxial creep equivalent deformation is presented by Equation (A.2) and Equation (A.3).

$$\Delta\bar{\varepsilon}^{cr} = \dot{\varepsilon}_0 \left(\frac{\sigma_{eq}}{\sigma_0}\right)^n \exp\frac{Q}{R}\left(\frac{1}{T_0} - \frac{1}{T}\right)((t + \Delta t) - t) \tag{A.2}$$

$$\Delta\bar{\varepsilon}^{cr} = \dot{\varepsilon}_0 \left(\frac{\sigma_{eq}}{\sigma_0}\right)^n \exp\frac{Q}{R}\left(\frac{1}{T_0} - \frac{1}{T}\right)\Delta t \tag{A.3}$$

In the case of the implicit algorithm, the increment of creep equivalent deformation is presented by Equation (A.4).

$$\frac{\partial\Delta\bar{\varepsilon}^{cr}}{\partial\sigma_{eq}} = n\,\dot{\varepsilon}_0 \left(\frac{\sigma_{eq}}{\sigma_0}\right)^n {\sigma_{eq}}^{-1} \exp\frac{Q}{R}\left(\frac{1}{T_0} - \frac{1}{T}\right)\Delta t \tag{A.4}$$

Where, $\Delta\bar{\varepsilon}^{cr}$ is the equivalent strain increment, σ_{eq} is the equivalent stress of Tresca ($\sigma_{eq} = \max(|\sigma_1 - \sigma_2|, |\sigma_2 - \sigma_3|, |\sigma_3 - \sigma_1|)$, σ_1, σ_2 and σ_3 are the principal stresses, $\dot{\varepsilon}_0$ is the reference creep rate, σ_0 is the reference deviatoric stress, Q is the activation energy, R is the universal gas constant, T_0 is the reference temperature, T is the absolute temperature of the rock at the analyzed depth, n is the stress exponent and Δt is the time interval.

A.2 Verification of the subroutine implementation

The Double Mechanism model is not part of the ABAQUS library and it is inserted through a subroutine of the FORTRAN software. In this way, a validation of the model must be carried out in order to assess the representativeness of the constitutive model and the parameters reported in the literature based on experimental results of laboratory tests.

The model is validated by simulating a triaxial creep test reported in Costa et al. (2005). In this case, the presented triaxial creep test is performed on halite samples from the Muribeca formation, in Sergipe, Brazil.

A.3 Computational simulation of triaxial creep test

The numerically simulated triaxial creep test uses halite from Brazil (Muribeca Formation, Sergipe) in cylindrical samples with a proportionality ratio of 2, according to the ISRM test specifications.

The test is simulated using a two-dimensional axisymmetric model. The model was reduced to one quarter of the specimen due to transversal and axial symmetry considerations to reduces computational costs.

The numerical simulation aims to measure the displacement in the direction of axial loading where the deviatoric stress is applied, which removes the body from the initial stress state. In this way, measurements of axial displacement (δ_{ax}) are made as presented by the Figure A.1.

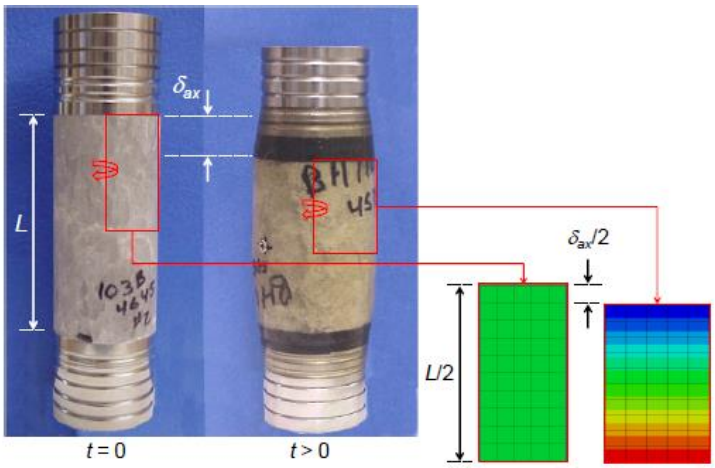

Figure A.1 – Scheme for calculating axial strain of the specimen (Modified from Lee et al., 2004 apud Firme, 2013).

Equation (A.5) shows the axial strain of the test. Thus, the creep curve is modeled from displacement and time readings.

$$\varepsilon_{ax} = \frac{\delta_{ax}}{L} \tag{A.5}$$

Where, ε_{ax} is the axial strain, δ_{ax} is the axial displacement and L is the specimen length.

For analysis on Brazilian halites, the test specimens are 7.0 inches (17.6 cm) long and 3.5 inches (8.8 cm) in diameter (Poiate, 2012). In the numerical simulation, considering the axisymmetry and the symmetry in relation to the half height, the specimens are 8.8 cm long and 4.4 cm in radius. Finite element models of 181 nodes and 50 CAX8R elements were generated, as shown in Figure A.2.

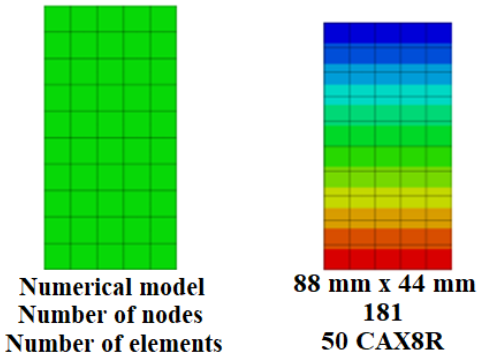

Figure A.2 – Mesh specifications of the model in the Brazilian halite sample.

The simulation steps are analogous to the actual test following confinement, axial loading and creep over time. Figure A.3 presents the simulation stages.

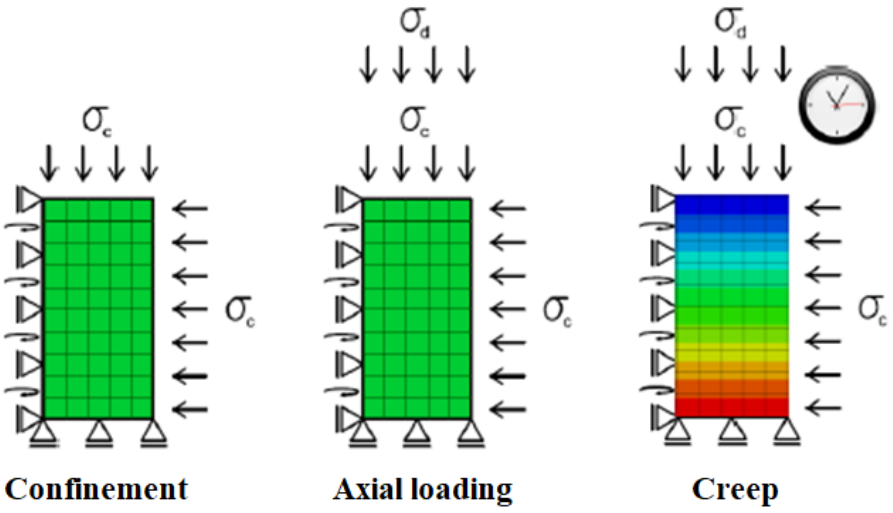

Figure A.3 – Simulation stages of triaxial creep test (Firme, 2013).

The boundary conditions of the model are simple supports, restricting vertical displacements at the base of the model and horizontal on the left side, corresponding to the axes of symmetry of the real sample.

In the confinement stage, the confinement stress (10 MPa) is applied to the top and side of the model and is equivalent to geostatic loading, simulating the state of in-situ stress of the salt. In this step, the initial displacements are null. Proceeding to the axial loading stage, the deviatoric stress (14 MPa) is added to the confining and applied to the top of the model, imposing the change in the stress state instantly. Finally, in the creep stage, the deviatoric stress is kept constant for 1000 hours, starting the creep of the model. The test is carried out under a constant temperature of 86 ° C.

Figure A.4 shows the stresses of the horizontal and vertical confinement of the sample in the confinement stage, the deviatoric stress in the axial loading stage and the axial displacement at the end of the test.

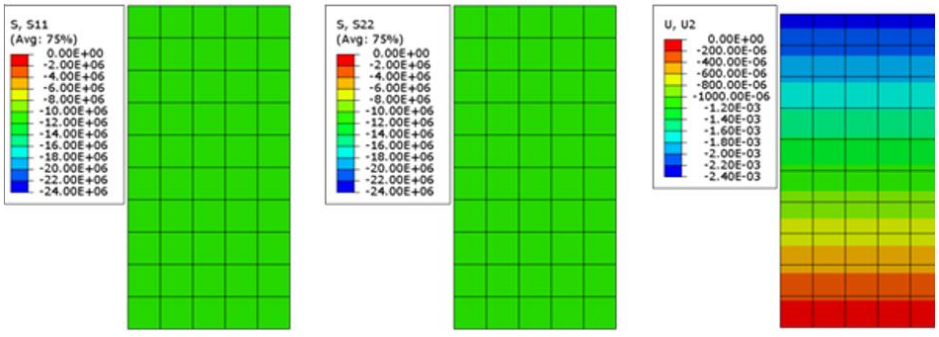

Figure A.4 – Results of the simulation stage of the triaxial test on Brazilian halite.

Figure A.5 presents the creep curves of triaxial creep test in Brazilian halite. Experimental points and simulations performed by the ANVEC program and by the author of this dissertation using ABAQUS are presented.

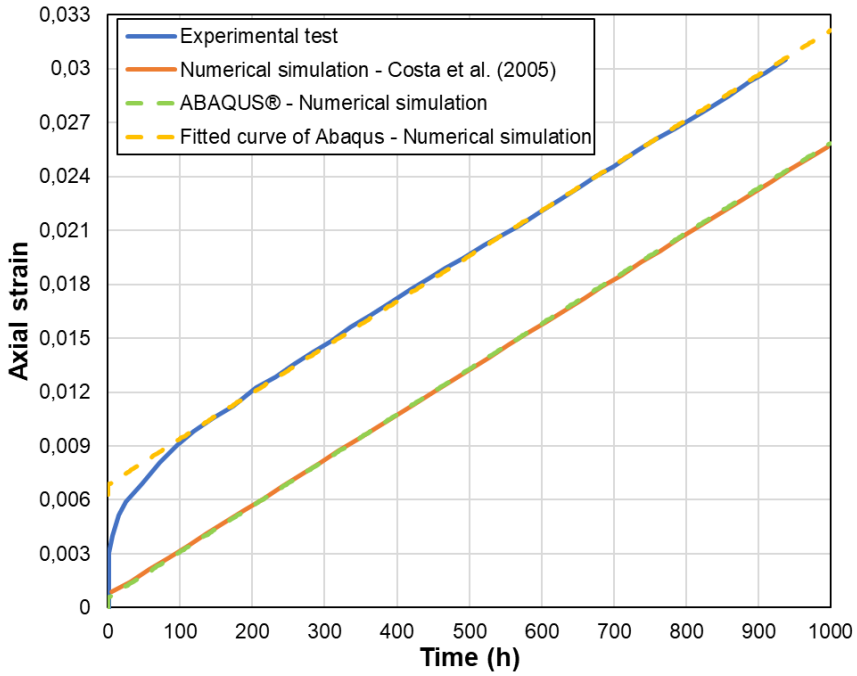

Figure A.5 – Displacement obtained of triaxial creep test in Brazilian halite.

The final deformation estimated by ANVEC is 0.025899, against 0.025851 obtained by ABAQUS, resulting in a relative difference of 0.18% in 1000 hours of simulation. The difference in slope between the line obtained with ABAQUS and that presented by the ANVEC program may be due to differences between solver's.

Therefore, it appears that the creep deformation rate in steady state obtained by numerical simulation accurately reproduces the experimental results, with a relative difference of less than 0.5%, validating the application of the Double Mechanism model and the numerical simulation performed.